CHARACTERIZATION OF POWDER WETTABILITY USING CAPILLARY RISE IN A CLOSED COLUMN

By

MINGLU LI

A dissertation submitted to the

School of Graduate Studies

Rutgers, The State University of New Jersey

In partial fulfillment of the requirements

For the degree of Doctor of Philosophy

Graduate Program in Chemical and Biochemical Engineering

Written under the direction of

German Drazer and Gerardo Callegari

And approved by

_____

_____

_____

_____

New Brunswick, New Jersey

OCTOBER 2020

ABSTRACT OF THE DISSERTATION

CHARACTERIZATION OF POWDER WETTABILITY USING CAPILLARY RISE IN A CLOSED COLUMN

by MINGLU LI

Dissertation

Director:

German Drazer

Gerardo Callegari

The wettability of powders plays a critical role in various industrial manufacturing processes and products. In particular, in the pharmaceutical industry, examples include wet granulation and the dissolution performance of solid doses obtained by powder compression. This study aims to develop a characterization method to study the wetting properties of powders, and finely divided solids in general, using a closed column packed with the material of interest. Using a closed column in contact with a liquid allows us to i)

study both the advancing and receding process as the liquid penetrates and is later displaced from the column, ii) to characterize the powder composing the porous media inside the column in both static and dynamic ways for a wide range of powder-liquid systems, and iii) to control (reduce) the characteristic time of the experiments by changing the experimental (column height).

The advancing, receding and bubbling pressure are defined to characterize the system in a static way. Analytical solutions are provided to study the dynamics during the capillary rise process. The explicit solutions are obtained in terms of the pressure differential and the liquid mass, two independent variables in the system that can be measured directly in the experiments. The hydrostatic effects and the non-linear pressure dependence on the penetration height are considered in the solutions without any approximations. Therefore, the solutions are general and can be used to characterize a wide range of solid-liquid systems, especially for systems with large capillary pressure. Two non-dimensional parameters governing the system are identified: the capillary pressure and the initial pressure in the closed column, both normalized by the hydrostatic pressure corresponding to the effective column height. The non-dimensional description provides valuable information on how to optimize the experimental setup depending on the application. As an important example we discuss how to reduce the equilibrium time.

Experiments were performed using two sets of glass beads, $10\,\mu m$ and $45\,\mu m$ with Polydimenthysiloxane (PDMS) as the model system. The experimental data are fitted with the analytical solutions to study different imbibition regimes and obtain the effective capillary pressure and permeability. Three imbibition regimes are determined: the early/Washburn imbibition, the intermediate and the late imbibition. It is shown that the

intermediate imbibition stage is the preferred region to obtain the effective capillary pressure and permeability values from fitting. The importance of these different stages and their importance to characterize systems presenting a relatively large heterogeneity of pore sizes is discussed. After validating the characterization method with the model system, it is applied to other solid-liquid systems with larger heterogeneity, including the larger glass beads and Deionized water, as well as pharmaceutical powders such as lactose, Microcrystalline cellulose (MCC) and alumina. In cases of highly heterogeneous system such as lactose and MCC, a spontaneous bubbling process is observed and thus the advancing pressure cannot be measured. The contact angle is estimated using the effective pressure obtained from the fitting with the analytical solutions. Different column heights were used in the experiments with lactose and a reduced time to reach the same completion factor is achieved by a shorter column. Performing shorter experiments was shown crucial when working with a powder (lactose) that is soluble in the penetrating liquid (water).

Acknowledgement

This journey over the past five years has been a life-changing experience for me and it would not have been possible without all the guidance and help from many people.

First and foremost, I want to thank my advisors, Prof. German Drazer and Prof. Gerardo Callegari. They have been guiding me since the first day I joined the group, with their endless patience and insightful advice. I am extremely grateful for their contributions of time and ideas to my dissertation throughout the years. Giving presentations to the public used to be one of my biggest fears, however, after countless practices with them and the confidence they expressed in me, I overcame the fear that I would never believe I can. In addition to advising me on my research, they are also the role models and inspirations for me in life. They are always willing to listen to students' needs and offer the best help they can. Their dedications to work have inspired me to become a professional like them. When I was writing this thesis during the days of the pandemic, they not only provided me support on academic research, they were also keeping me stay strong during this challenging time. The lessons I learned from them have helped me through the tough times in the past five years and will constantly benefit me in my future life. I simply cannot imagine a better advisor.

I would like to extend my sincere thanks to members in the Mechanical and Aerospace Engineering department who helped me machining the parts of my experimental setup. I wish to thank Mr. John Petrowski, Mr. David Cunningham and Mr. Yanjun Wang for providing me advice on the setup design and offering me help in the machine shop to bring the design to life.

I am also grateful to the Engineering Research Center for Structured Organic Particulate Systems (ERC-SOPS) for providing all kinds of resources and facilities for my research. I would like to thank Dr. Sara Moghtadernejad who inspired to become an enthusiastic professional with her knowledge and passion for research. I wish to thank Mr. Zhanjie Liu for his guidance on the lab equipment in ERC.

I would like to thank my committee members Prof. Nina Shapley and Prof. Marcial Gonzalez for devoting their time to my dissertation and providing valuable feedback.

The members in my research group have contributed immensely to my time at Rutgers. They are a source of research advices as well as friendship and encouragement. I am indebted to you all: Dr. Siqi Du, Dr. Tianya Yin and Mr. Erdi Kurtyigit, thank you all for enriching my work and life.

Finally, I want to thank my parents for always being there to support me with their unconditional love.

I would like to acknowledge that the chapter four of this dissertation is adapted from our previous publication titled “Capillary rise in a closed column: Application to the characterization of powders” [1], it was published in *Colloids and Surfaces A* in 2020.

Table of Contents

List of Tables

List of Illustrations

1. Introduction

1.1 Motivation and thesis overview

The wetting of powders plays a critical part in the manufacturing processes of various industries, such as food processing [2]–[4], water infiltration [5]–[7], mineral handling [8]–[10], and especially in pharmaceutical technology [11]. The wettability of both the active pharmaceutical ingredient and the excipients provides valuable information to process development and product quality control. For example, during the wet granulation process, the preferential wettability of one ingredient particle with the liquid binder can cause non-uniformity in the granules [12]. When blending powders, the shear strain can affect the hydrophobicity of the blend and thus impact the dissolution rate of tablets made from that blend [13]. The importance of the powder wettability in diverse industries generates constant interest for researchers to develop appropriate methods to understand it from a fundamental perspective and to be able to characterize the wettability of different powders and finely divided solids in general.

In this thesis, we focus on characterizing the wetting process of powders by capillary rise in a closed column. One of the benefits of using a closed column is that both the advancing and the receding process can be studied. Also important is that the dynamics during the imbibition process can be investigated, and the experimental data can be interpreted with analytical solutions, providing fundamental understanding on the dimensionless variables that determine the behavior of the system.

The thesis is divided into seven chapters. The first chapter summarizes some background information, including the motivation behind our work and some basic concepts of wetting

and contact angle, followed by an overview of the existing approaches to study the contact angle in liquid-solid-gas systems, with special focus on those available to characterize the wettability of finely divided solids.

Chapter two provides details on the experimental system design, including the experimental setup, material characterization, sample preparation and experimental procedures. The description of the experimental procedures explains how the advancing and receding processes are investigated with the setup used in our work.

Chapter three provides analytical solutions for the imbibition process in a closed column. The solutions are obtained in terms of liquid mass and the pressure differential as a function of time. The hydrostatic effects and a non-linear pressure dependence on the penetration front are considered in the solution. Therefore, the solutions presented here are more general than those available in the literature and can be used for a wider range of capillary pressures than before. A simplified solution is also obtained for the initial stage of the imbibition process and it will be compared with the general solution in later chapters.

The dimensionless form of the analytical solutions is presented in chapter four. Two non-dimensional parameters governing the evolution of the system are identified. Based on the dimensionless analysis, means to optimize the experimental setup and conditions are provided.

The experimental results are presented and discussed in chapter five, six and seven, each chapter focuses on a different solid-liquid system. Chapter five addresses the interaction of our model systems (glass beads) with the liquid used as reference (Polydimethylsiloxane (PDMS)). Chapter six compares the result between the reference liquid (PDMS) with the testing liquid (Deionized water). Both static and dynamic ways are used to characterize the

system in terms of contact angle, characteristic pore size and permeability. Additionally, different stages of the imbibition process are studied, depending on the initial dynamic characterization results. In chapter seven, a characterization protocol is summarized based on the results presented in chapters five and six. This protocol is then applied to pharmaceutical powders and the preliminary characterization results are discussed. A final discussion of the results and conclusions obtained in the thesis is presented in chapter eight.

1.2 Basic concepts: surface energy, wettability and contact angle

In this section, we introduce some fundamental concepts commonly used to describe wetting. Wetting is a phenomenon that manifests the existence of the attractive forces between molecules. When two phases are in contact, for example, solid-liquid or gas-liquid, surface tension is a measure of the force per unit length or the energy per unit surface, acting on the boundary between the two phases. The surface energy is the work needed to separate the two phases [14]. An extensive discussion on the physical meaning of surface tension is provided in the book by Defay and Prigogine [15].

An indication of the interactions between the solid and two immiscible fluid phases is wettability. We are restricting our discussion here to the fluids being a liquid and the liquid's vapor. In this context, the wettability is characterized in terms of the solid-liquid-vapor contact angle θ [16]. The contact angle captures the equilibrium balance between adhesive and cohesive forces in a three phase system [17]. The work of adhesion is the energy needed to separate two different phases while the work of cohesion is the energy to separate one phase into two [18], [19]. When the three phase system is in equilibrium, illustrated in figure 1.1, contact angle is related to three different interfacial tensions by the classical Young's equation [20].

$$cos\theta = \frac{\gamma_{SV} - \gamma_{SL}}{\gamma_{LV}} \quad (1.1)$$

These three interfacial tensions are the solid-vapor surface tension γ_{SV}, the solid-liquid surface tension γ_{SL}, and the liquid-vapor surface tension γ_{LV}. The line in which the three phases meet is called the *triple contact line* [21], [22]. The case when $\gamma_{SV} \geq \gamma_{SL} + \gamma_{LV}$ is called *complete* or *perfect wetting* and is manifested by a film coating the solid surface ($\theta = 0°$). The case when $0° < \theta < 90°$ is called *partial wetting*, and cases where $\theta \geq 90°$ are called *nonwetting* [23]. A small contact angle of a solid with water ($0° < \theta < 90°$) indicates a *hydrophilic* solid surface while a large contact angle ($\theta \geq 90°$) indicates that the solid is *hydrophobic*.

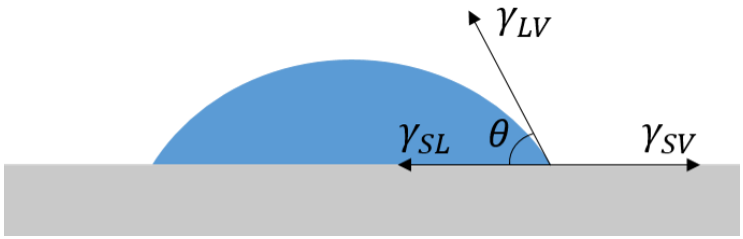

Figure 1.1 A schematic drawing of a liquid droplet on a solid surface showing quantities in the Young equation.

The Young equation predicts a single contact angle for each material system assuming a smooth, homogeneous, ideal surface. This contact angle is usually referred to as the *thermodynamic equilibrium contact angle*, or, *static contact angle*. In reality, however, surfaces are rough and heterogeneous, and liquids will show a range of contact angles on such surfaces. When the contact line is moving, the contact angle will, in general, be different from the static angle [24]. The movement of an interface in a porous media can be divided into two processes: imbibition and drainage. The process in which the wetting phase displaces a nonwetting phase is referred as the imbibition, the minimum contact angle that can be obtained during this process is the advancing contact angle. Conversely,

the drainage refers to the process when the nonwetting phase displaces the wetting phase. Correspondingly, the maximum contact angle that can be obtained during this process is referred as the receding contact angle [25].

The difference between the advancing and receding contact angles gives the contact angle hysteresis:

$$\Delta\theta_{\mathrm{hyst}} = \theta_{\mathrm{A}} - \theta_{\mathrm{R}} \tag{1.2}$$

Major sources causing contact angle hysteresis are surface roughness [26]–[30] and chemical heterogeneities [31]–[37]. Contact angle hysteresis can also exist in homogeneous surface due to liquid retention or sorption [38]–[40], or disjoining and conjoining pressure that acts in the vicinity of the three phase contact line and causes deformation of an elastic solid substrate [41]–[43].

Since we are interested in the wetting process inside a porous media, we shall now introduce the concept of capillarity. Capillarity is used to describe the process when liquid penetrates in a porous material or a capillary tube. The interfacial forces acting on the contact line inside a capillary force the interface to curve, and a difference in the pressure (p_{c}) between the two phases is given by the Laplace equation:

$$p_{\mathrm{c}} = \frac{2\gamma cos\theta}{r}, \tag{1.3}$$

where γ is the surface tension, r is the radius of the capillary tube, and θ is the contact angle. This pressure differential exerts a net force on the triple contact line that may makes it move.

When the triple contact line is in motion, the contact angle becomes dependent on the velocity of the moving contact line. This contact angle is referred to as the dynamic contact angle (larger than the advancing in an imbibition process and smaller than the receding in a drainage process). The relation between the dynamic contact angle and the contact line velocity has been studied in simple geometries in many different works both experimentally [44], [45] and theoretically [46]–[49]. In synthesis, due to the hydrodynamic stress applied to a moving contact line, an effective macroscopic (dynamic) contact angle develops [50], [51]. This dynamic contact angle is related to the velocity of the contact line (v) through the the capillary number [44], $\mathrm{Ca} = \mu v/\gamma$ where μ is the viscosity of the liquid. The capillary number is the ratio between the "macroscopic" viscous and the interfacial forces acting on the interface. It is worthy to mention that due to its definition, the scale of the capillary number is shifted and a value of 10^{-4} is considered large as the effects on the dynamic contact angle are considerable [44], [52]. On the other hand, a values in the order of 10^{-6} and lower, were experimentally found to be negligible [44].This effect of liquid velocity on the dynamic contact angle is found to be magnified by surface heterogeneity [53], including surface roughness and any impurities in the system [54].

1.3 Capillary hysteresis and pore geometry

In section 1.1 it is mentioned that using a closed column allows us to study both the advancing and the receding process for a given solid-liquid system. In particular, we will determine the difference in pressure between the end of the advancing process and the beginning of the receding one. This difference between the advancing pressure and the

receding pressure can be a result of the contact angle hysteresis, or the heterogeneity of the porous media. The existence of a different advancing and receding capillary pressure for each pore or capillary tube is straightforward when there is hysteresis in the contact angle. However, there are other sources that can contribute to the differences in the capillary pressure in a porous media and, in particular, we need to consider the pore geometry. First, let us consider the case of a capillary tube. For a single capillary tube, or a bundle of capillary tubes with the same radius, this difference in capillary pressure is a result of the contact angle hysteresis. However, in practical cases the pore media is heterogeneous, in the sense that there is a distribution of pore sizes (Note that we will refer to heterogeneous porous media as those porous media in which the pores are not monodisperse). The difference in the advancing and receding capillary pressure can be a result of the combination of the contact angle hysteresis and the heterogeneity of the pores. Let us then consider two models for heterogeneous porous media where there are bundles of parallel capillary tubes. In the first case, each of the capillary tubes is a cylinder with uniform radius but the capillary tubes are of different radii (figure 1.2a). In the other case, the radius is changing within each capillary tube (figure 1.2b). The top of the capillary tubes are all connected together and therefore have a common air pressure. We will refer to this pressure as the *pressure differential*.

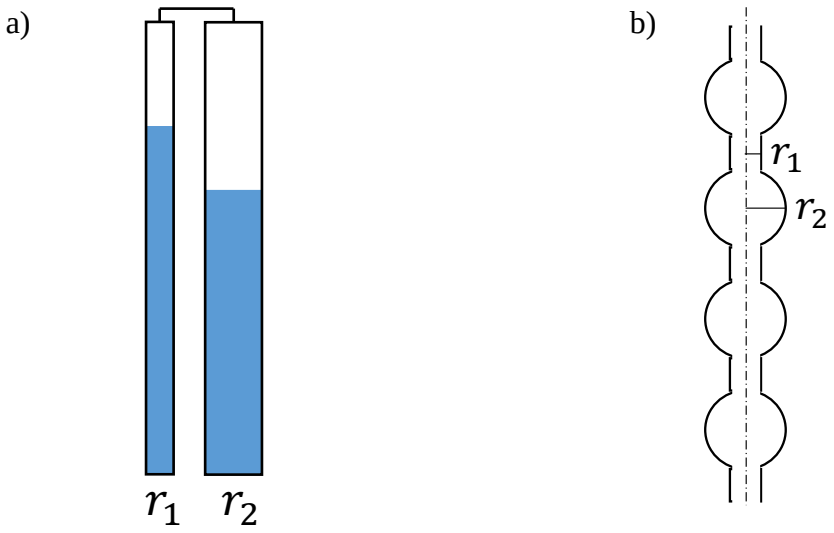

Figure 1.2 Different types of the parallel capillary tubes. (a): The capillary tube is a cylinder that has a uniform radius, the radius varies from each tube/cylinder. (b): The radius varies in each of the capillary tubes.

According to the Laplace equation, smaller pores correspond to a higher capillary pressure while larger pores correspond to a lower capillary pressure. During the imbibition process in both cases shown in figure 1.2, the pressure differential inside the tube increases as the liquid penetrates into the capillaries and air is compressed. In both cases, the pressure will continue increasing and eventually reach the advancing capillary pressure of the large pores. After reaching this capillary pressure, the result is different depending on the geometry. In the first case shown in figure 1.2a, the liquid will stop advancing in the large capillaries, representing large pores (r_2), while it still advances in the small capillaries, representing small pores (r_1), because the pressure differential is lower than the advancing pressure of the small pores. Since the top of the capillaries are connected, the liquid may recede in some of the tubes when the pressure differential reaches the receding pressure for a given tube radius. For capillaries with an open top, such receding process will not happen. In the case shown in figure 1.2b, the liquid cannot advance further into the next small pore after reaching the advancing pressure for large pores, because the next small pore is only

connected through a large pore. In this case, the spontaneous imbibition process stops at the capillary pressure of the large pores. In this work we focus on the closed systems where the pores are interconnected on the top. In this case the pressure differential can be further increased after the liquid stops advancing by injecting air into the common air reservoir with a syringe.

In the first case, after reaching the advancing pressure of large pores, since the capillaries are connected on the top, the pressure differential still increases as the liquid continues to advance in the small pores. Eventually the pressure will reach the receding pressure of the larger pores and the liquid will evacuate from them. Depending on the size of the pores, this moment can happen before or after reaching the advancing pressure of the smaller pores. Figure 1.3 shows the different scenarios of the receding and advancing pressures for different pore sizes. We consider there are two sizes of the pores r_1 and r_2, with $r_1 < r_2$. In the case shown in figure 1.3a, the receding pressure of r_2 (p_{R2}) is higher than the advancing pressure of r_1 (p_{A1}). After filling r_2, the pressure will first reach the advancing pressure of r_1 and fill in the smaller pores. At this point, the spontaneous imbibition process will stop. If the pressure differential is further increased, for example using a syringe pump, the pressure will reach the receding pressure of r_2 and the large pores will be emptied. The smaller pores will be emptied later when the pressure reaches its corresponding receding pressure p_{R1}. In this example, however, this is not possible, as air will escape through the large tube and the pressure differential will vanish. In the other example, presented in figure 1.3b, the receding pressure of r_2 is lower than the advancing pressure of r_1 ($p_{\mathrm{R2}} < p_{\mathrm{A1}}$). After reaching p_{A2}, the pressure will first reach the receding pressure p_{R2} and the large pores will be emptied before the pressure reaches the advancing pressure of the smaller

pores. This scenario is more likely to happen when the porous media is highly heterogeneous.

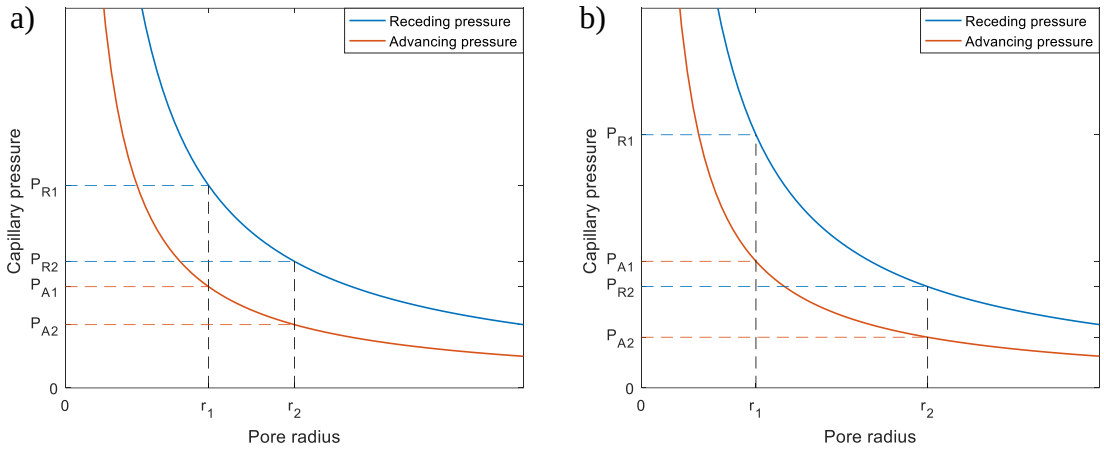

Figure 1.3 Different scenarios of the advancing and receding pressure for two pore sizes. (a): The receding pressure of large pores is higher than the advancing pressure of the small pores, $p_{\mathrm{R2}} > p_{\mathrm{A1}}$ Large pores will be emptied after the liquid fills in the small pores. (b): The receding pressure of the large pores is lower than the advancing pressure of the small pores, $p_{\mathrm{R2}} < p_{\mathrm{A1}}$. Large pores will be emptied before reaching the advancing pressure of the small pores.

For the case shown in figure 1.2b, after reaching the advancing pressure of large pores, liquid will stop advancing. The receding pressure can be reached by externally increasing the pressure differential using a syringe pump, and the liquid will recede from the entire capillary after reaching the receding pressure p_{R2} of the large pores. A more detailed discussion on this geometry is provided in this work by Dullien and Batra [55].

A more complicated model geometry for the porous media is presented in figure 1.4. The pores are irregularly shaped (although represented by circles to demonstrate the effective pore size), randomly distributed and interconnected along the porous media. The pores filled with liquid are colored, the color represents the size (orange, grey and blue are the small, medium and large pores respectively), the size of the empty pores is represented by the color of their border following the same rule. In the example considered in figure 1.4,

initially all the pores are filled. As the liquid penetrates in the porous media, a cluster of large pores formed a layer (represented by the red solid circles in the figure). This layer blocks the liquid from advancing further in the porous media in the same way as in the case shown in figure 1.2b before. If the liquid were to continue advancing, it can only go through the small pores (orange). If there are no small pores that go through the barrier formed by the large pores shown in red in figure 1.4, liquid cannot advance further. Any pores larger than this radius can form the layer to block the liquid penetration. On the other hand, the receding pressure is the pressure at which the liquid first starts to recede from the porous media. Since large pores correspond to a lower receding pressure, liquid will evacuate through the connected large pores. Therefore, the receding pressure corresponds to the smallest pore needed to form this connection. Any pores larger than this can form a channel for the liquid to recede. To conclude, the pore geometry is very complicated in practical cases. Accordingly, the hysteresis in capillary pressure is a result of the combination of contact angle hysteresis and porous media heterogeneity, the latter includes pore size variation and the connectivity of the pores.

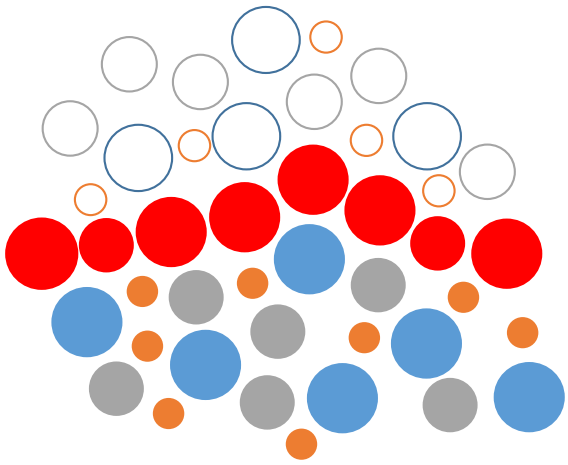

Figure 1.4 An example of the randomly distributed pores in the porous media. The solid circles are filled with liquid. The empty circles have not been filled.

1.4 Methods to determine contact angle

Over the years, researchers have developed various methods to study contact angle and wettability. A direct measurement of the contact angle is the sessile drop method. As shown in Fig 1.5a, a liquid droplet is placed on a solid surface and the contact angle is then measured directly at the triple contact line. Because of its simplicity, it is one of the most common methods to measure contact angle. However, this commonly used method is not practical in the case of porous materials because it requires a flat, smooth and nonporous solid surface for direct measurement. For powder samples, to create a flat, smooth surface, they are compacted into a disc or pellet under very high pressure. For pharmaceutical powders, the compaction pressure can be up to 210MPa [56]. One concern is that high compaction pressure may change the surface properties of the powder, for example, by changing to a different molecular orientation [57], or change the surface structure by plastic deformation [58]. Hence the contact angle of the compacted disc may not be representative of the powder. These problems make it challenging to use the sessile drop method.

To avoid compacting the powders, an alternative method to prepare the powder sample is by packing them inside a column and tap it repeatedly until a homogeneous porosity is obtained. Using a packed column allows us to indirectly measure the contact angle through the capillary rise process. Using a column, the contact angle can be studied in a static or a dynamic way.

According to Jurin's law [59], the maximum height of a liquid rising in a vertical capillary is reached when the hydrostatics balances the capillary pressure p_c:

$$h = \frac{p_c}{\rho g} \tag{1.4}$$

From the Laplace equation $p_c = 2\gamma cos\theta / r$, the contact angle can be obtained by measuring the maximum height of liquid penetration inside an open column. One limitation for this static method is that, when the capillary pressure is too high, a very long column is required to reach the maximum height. For example, a 10m column (and several days if not months) is needed to reach the equilibrium in the capillary imbibition of water in a wetting material with one-micron size pores!

An alternative method is to study the dynamics during the imbibition process. In 1921, Washburn demonstrated that for an open column, at short times, the square of the penetration height is linearly dependent on the penetration time [60]

$$h^2 = \frac{\gamma cos\theta r}{2\eta} t \tag{1.5}$$

The contact angle can be extrapolated from the slope of h^2 vs t. A reference liquid is used to determine the effective radius r. Since the hydrostatic pressure is neglected in this equation, only the very early stages of the penetration can be used to plot h^2 vs t. During this time, however, the liquid penetrates very fast and dynamic contact angle effects are dominant, as a result, the contact angle is dependent on the penetration velocity [61]–[64] as discussed in 1.2. Inertia effects are responsible for additional deviations from the Washburn equation during the initial imbibition [65]–[68]. Another limitation for the open column is that only the advancing contact angle can be studied, the receding process cannot be achieved with an open column.

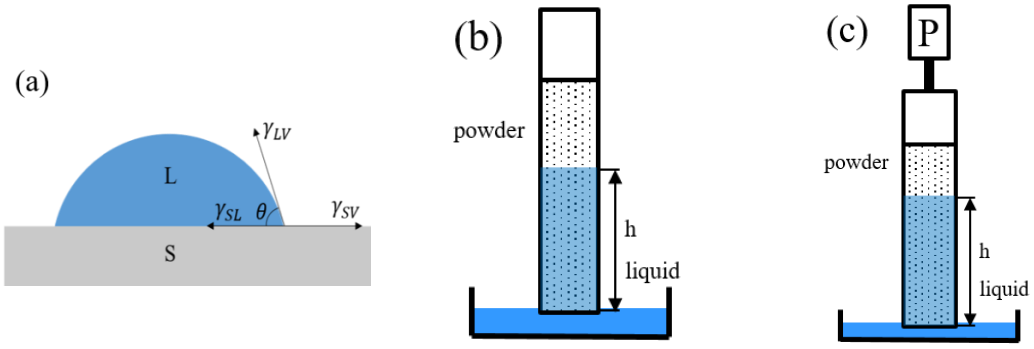

Figure 1.5 Common methods to determine contact angles: (a) sessile drop method, (b) open column method, (c) closed column method.

Modifications have been made on the open column method simply by closing the top to be able to measure the pressure inside the column. Therefore, closing the top of the column offers an additional measurement, the pressure differential inside the column. In 1927, Bartell proposed a closed column method in which the column pressure is monitored by a pressure sensor [69], [70]. The capillary pressure is obtained through the measurement of the static pressure at which the liquid stops penetrating. Dunstan and White studied both the advancing and the receding process using a closed column [71]. The receding process is studied by increasing the column pressure after reaching the advancing static pressure, as a result, the liquid front is forced to recede. Stevens and Ralston also studied the receding process, they suggested calculating the capillary retention to obtain the receding contact angle [72]. Depalo and Santomaso looked into the dynamics of the capillary rise inside a closed column by integrating the column pressure over time [73]. They focused on the initial imbibition and during this time overpressure is approximately linearly dependent on the height of the liquid rise. This approximation, however, is only valid when the overpressure is significantly smaller than atmospheric pressure. In the case of very small particles, capillary pressures of the order of the atmospheric pressure is not unusual, and

the linear approximation is no longer valid. In addition, the solutions are numerical calculations and the analytical solution to the problem was not provided.

In this work, we will present the analytical solutions for the imbibition process in porous media inside a closed column. The solution will include the hydrostatic effects and consider the non-linear pressure dependence on the penetration height. Compared to the previous solutions, this solution is more general and can therefore be applied to smaller particles. Using the analytical solutions, we can characterize the porous media dynamically by fitting the solution with the experimental data. We are able to determine the effective capillary pressure and permeability during different stages of the imbibition.

2. Methodology

2.1 Experiment set up

A schematic representation of the experimental system is shown in Figure 2.1. The powder sample is packed in an acrylic cylindrical column (height=12.70cm, inner diameter=1.27cm) vertically held by clamps and a metal stand. A filter paper and a porous disc are used at the bottom to prevent powders from falling out of the column. The top of the column is closed by a seal plug with O-rings and then connected to a four-way connector. The other three ends of the connector are connected to a syringe (Becton Dickinson, 3mL), a pressure sensor (Omega PX409, range: 0-103.4kPa) and the ambient air inside the setup with tubes (ETFE tubing from IDEX Health and Science LLC, ID=0.0254cm). An effort was made to reduce the dead volume in tubes and connectors in order to reduce the total empty volume of the setup and eventually decrease the time to reach equilibrium, as we will discuss later in section 7.3. Valves (IDEX shut off valve) are used to control the connection to the outside atmosphere (valve 1 in the figure) and the syringe (valve 2 in the figure). Pressure change inside the system is monitored by pressure sensor connected to a computer. The column containing the powder sample is brought into contact with a reservoir of the liquid of interest at the beginning of each experiment. To this end, we use a relatively large plastic plate container (diameter=5 inch) to create the liquid reservoir. The objective of using a large reservoir is to avoid any significant change in the liquid height during the liquid penetration into the column. The plate is placed on a scale (Ohaus NV212) to measure the liquid weight in the reservoir. The liquid reservoir and the plate were placed on a lift platform. They were lifted up by the platform until the surface of the liquid gets in touch with the bottom of the column. A syringe pump (Harvard

Apparatus, 703007) is connected to the syringe. It will be used to control the pumping rate of the syringe during the receding process.

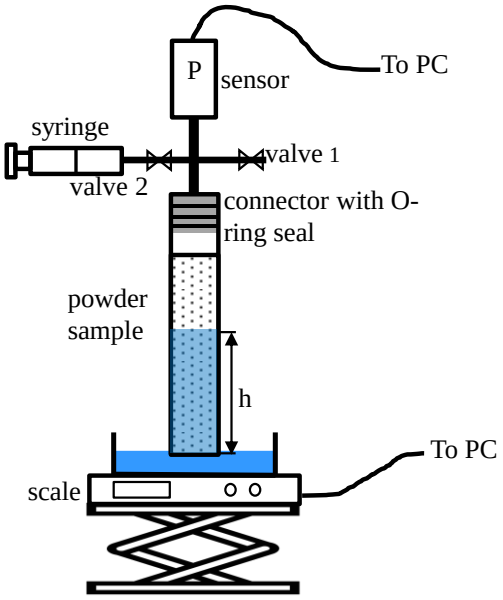

Figure 2.1 A schematic view of the experimental setup.

2.2 Experiment materials: particles and liquids

The particles used to prepare the porous media were 10μm and 45μm glass beads, lactose and microcrystalline cellulose (MCC). The liquids used to wet the particles were polydimethylsiloxane (PDMS) and deionized water (DI water). Here we present the characterizations of these materials.

2.2.1 Model System

For the model system we use glass beads to perform initial experiments and to validate our proposed method. The glass beads were chosen as the model system because of their simplicity: they are spherical, not porous, and they will not swell or dissolve in water. Their particle size distributions were measured by a laser-diffraction analyzer with a Tornado Dry Powder System (LS-13320, Beckmann-Coulter) and shown in Table 2.1 and Figure

2.2. The 9-13μm glass beads were purchased from Sigma-Aldrich. We will refer to them as *10μm glass bead*s in future discussions. The 45-50μm glass beads were purchased from Polysciences, Inc. Originally the glass beads were 30-50μm, they were separated by sieves (Dual Manufacturing, mesh #325, mesh opening =45μm) to obtain powders with a narrow particle size distribution.

Particle	d_{10} (μm)	d_{50} (μm)	d_{90} (μm)	d_{32} (μm)
9-13μm glass beads	4.39	11.03	22.67	8.46

Table 2.1 Particle size distribution of glass beads. (d_{32} is the Sauter mean diameter).

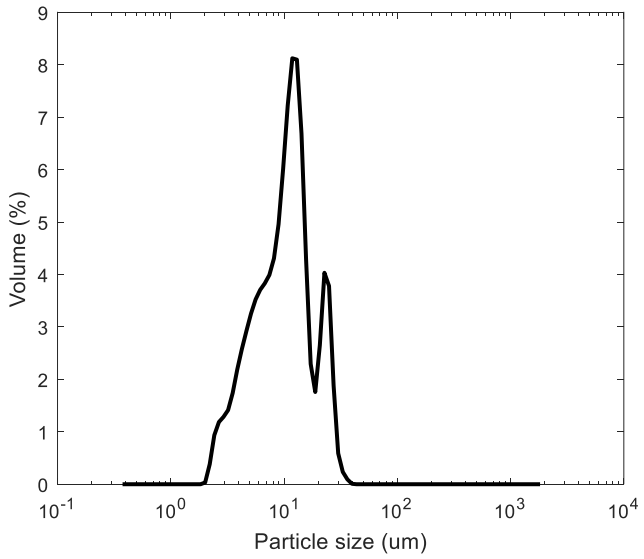

Figure 2.2 Particle size distribution of 10μm glass beads.

2.2.2 Pharmaceutical powders

The model system represents the ideal case. After validating the solutions with the model system, we also want to extend this model to study the pharmaceutical powders. We chose lactose and MCC because they represent two different material properties we may encounter in practical scenarios. Lactose will dissolve in water, we will use a saturated solution as the wetting liquid. MCC can swell after wetted, as a result, the structure of the porous media can change. Their particle size distributions were presented in Table 2.2 and Figure 2.3.

Particle	$d_{10}\ (\mu m)$	$d_{50}\ (\mu m)$	$d_{90}\ (\mu m)$	$d_{32}\ (\mu m)$
Lactose	10.73	63.00	118.67	15.80
Microcrystalline Cellulose (MCC)	24.1	73.5	167.3	52.4

Table 2.2 Particle size distribution of lactose and MCC (d_{32} is the Sauter mean diameter).

a) b)

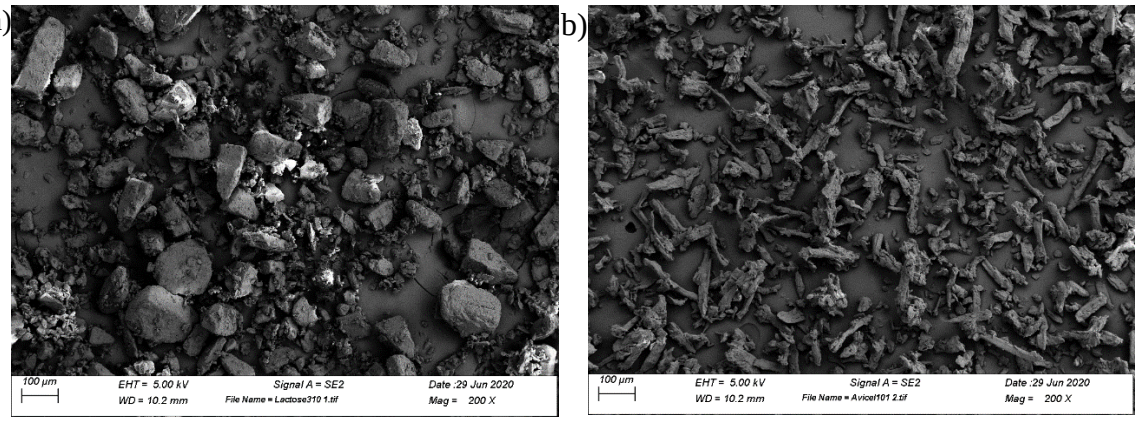

Figure 2.3 SEM images of a) lactose, b) MCC (Avicel 101).

2.2.3 Wetting liquids

Polydimethylsiloxane (PDMS) and deionized water (DI water) are used as wetting liquids. Because of its low surface tension, PDMS is chosen as a reference liquid. It is assumed that particles have zero contact angle when wetted by PDMS, the $cos\theta_{\mathrm{PDMS}} = 1$. The PDMS used in experiments was obtained from Gelest. Inc (DMS-T11). DI water is obtained from Direct-Q 3 UV Water Purification System (MilliporeSigma). Their properties are listed in Table 2.3.

Wetting liquid	Density (kg/m^3)	Viscosity (m$Pa \cdot s$)	Surface tension (mN/m)
PDMS	935	9.35	20.1
DI water	1000	1.00	72.8
Lactose Saturated solution	1071	1.10	71.6

Table 2.3 Properties of wetting liquids at 20˚C, values for lactose saturated solution were taken from [73].

2.3 Sample preparation and experimental procedure

Before packing the glass beads in a column, they are cleaned in the ultrasonic cleaner to remove any impurities or contaminants attached to the surface. They are cleaned first by acetone, followed by water, and then dried in the oven. The glass beads were packed in a

column by adding them incrementally and compressing with a plastic rod until a desired packing porosity φ is achieved. Then, the column is closed by the plug with an O-ring seal discussed before. The packed and sealed column is then placed on the metal stand through the clamps and connected to the pressure sensor. At this time, valve 2 is closed for the advancing process while valve 1 is open. The column is thus open to atmosphere. Before staring the experiment, we pre-wet the porous disc with the same liquid that will penetrate into the column. Experiments start by lifting the liquid container until the bottom of the column makes contact with the liquid. After a short time, when the liquid penetrated approximately 5mm into the powder sample, the column is closed. Pressure change is then recorded every second using software USBH Application (OMEGA Engineering, Inc.). Liquid weight change is recorded using MATLAB (Mathworks, Inc.).

The objective of the pre-wetting procedure before the liquid penetration is to prevent the formation of bubbles escaping at the bottom of the column. In some of our experiments we noticed there was bubble forming at the bottom of the column after it was brought into contact with the liquid. This phenomenon was also observed by Iveson et al [74]. They reported that a sudden pressure increase inside the column would cause the air to flow through the support at the bottom. In our case, we use porous discs with pore openings of $40\mu m$, which is larger than the pore sizes of the porous media. When the liquid is penetrating very fast in the beginning, it may leave some air pockets in the porous media. These air pockets will be emptied later when the column pressure builds up, bringing noises in the pressure and liquid weight measurement. To avoid this problem, we first estimate the amount of liquid to completely wet the porous disc. Then before putting column bottom into contact with the liquid, we would use that amount of liquid to wet the porous disc so

that we make sure there are no air pockets left in it. After implementing this pre-wetting procedure, no more bubbles were observed at the beginning of the experiment.

As the liquid penetrates into the column, the air pressure in the dry part of the column increases. The expected curves of the pressure differential (blue curve) and the liquid weight (red curve) left in the container is plotted in figure 2.4a. Eventually the pressure inside the column reaches equilibrium, the advancing process has finished. The pressure differential measured at the end of the advancing process is the *advancing pressure*. Then, we open valve 2 and use the syringe pump to start injecting air into the column. As the syringe compresses the air in the column, the overhead pressure will increase again. The expected curves of the receding process is presented in figure 2.4b. At a certain pressure, the liquid begins to recede from the column. Pressure at this point corresponds to the *receding pressure*. As the syringe continues injecting air into the column and the pressure continues to increase, more liquid would leave the column. At some point the emptied pores form a connected path from the top of the column to the bottom, and air would be released from the bottom of the column. This process can be observed as bubbles start forming and releasing from the bottom of the column and into the liquid reservoir. Pressure drops drastically as bubbles are released. The highest pressure reached just before the first bubble is released is the *bubbling pressure*.

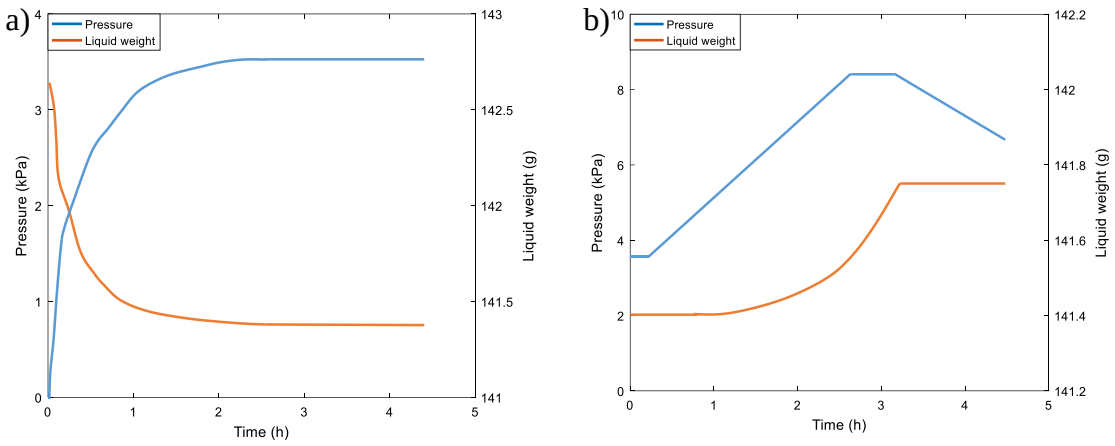

Figure 2.4 Expected curves for the pressure and liquid weight during a) advancing process, b) receding process.

After finishing the experiments, the powder sample is emptied from the column, they are then discarded in a waste container for powders or cleaned for reuse. If reusing them, they will be collected in a container and together with the porous discs to be cleaned following the same cleaning procedures mentioned in the beginning of this section. The 45μm glass beads are the only particles that are being reused because they are a lot more expensive than any other particles used in this project. Once they are dried in the oven, they are sieved again by the sieve with mesh opening of 45μm before they are ready to use in the next experiments. The columns are wiped by paper towels to remove any leftover particles and liquids. They are then air dried in the drying rack in the lab. We use two different sets of columns and porous discs for PDMS and DI water so that the liquid will not get mixed up.

3. Analytical Solutions

In this chapter, we derive the analytical solutions for the capillary rise in a porous media. We start with the governing equation for this process, followed by discussing a linear approximation used to relate the pressure differential with the penetration front. Then we solve the differential equation to obtain a *full solution* in terms of the liquid uptake and the pressure differential. In this full solution, the hydrostatic effects are included, as well as the non-linear pressure dependence on the penetration front. Finally, we will discuss a simplified case for the beginning stage of the capillary rise, which we call the *modified Washburn solution* Equations governing capillary rise.

3.1 Equations governing the capillary rise

To derive the analytical solution of capillary rise in a closed column, we start with Darcy's law[75]. In 1856, Darcy proposed that when a fluid with viscosity μ is passing through a porous media, the flow discharge is proportional to the pressure drop over a certain distance in the porous media,

$$q = -\frac{\kappa}{\mu}\nabla p \tag{3.1}$$

where κ is the *permeability* of the porous media, according to the Kozeny-Carman equation, the permeability is related to the physical properties of the materials used [76]–[78]. q is the *specific discharge* or discharge per unit area, often referred to as the Darcy velocity. This velocity, however, is not the velocity at which the fluid is advancing or moving through the porous media. This velocity is also called the *superficial velocity* u_s, and is a

hypothetical flow velocity calculated as if there is only, without taking into account the presence of porous medium,

$$u_s = \frac{Q}{S} \tag{3.2}$$

Where Q is the volume flow rate of the fluid and S is the cross sectional area. We assume the porous media is completely saturated by the fluid and there is on air trapping in the porous media, Darcy velocity is related to the fluid velocity dh/dt by porosity φ:

$$\frac{dh}{dt} = \frac{q}{\varphi} \tag{3.3}$$

Note that we will neglect the inertia effects that might happen in the beginning of the capillary rise process [79]–[82]. We also assume that the powder bed is homogeneous and isotropic, under this assumption, the permeability across the porous media is uniform, the liquid advancing process can be treated as a one-dimensional transport problem.

The schematic drawing of the experiments is presented in figure 3.1. A cylindrical column with closed top is vertically packed with powder sample. This packed column has a length H and porosity φ. The column bottom is in contact with a wetting liquid, and the length of the column immersed in the liquid is Δl. There will be a gauge pressure p_l at the bottom of the column that is different from the atmospheric pressure p_0 at the interface of liquid-air. For simplicity, we will neglect this gauge pressure because Δl is only a few millimeters in all experiments and the resulting gauge pressure is relatively small. As we discussed, initially, the column top is open to atmosphere. When the liquid reaches a certain height h_0, the column is closed (figure 3.1a). This is the initial time $t = 0$. After it is closed for time t, liquid height reaches h (figure 3.1b).

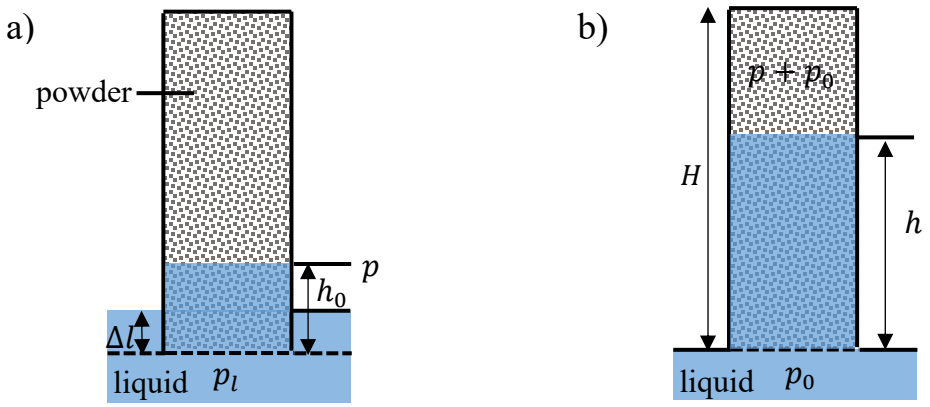

Figure 3.1 Sketch of pressure and volume change when liquid penetrates in a closed column packed with powders. a): initial condition, the column is closed to the outside when the liquid penetrates to height h_0, the initial pressure inside the column is p_0. b): the liquid front reaches height h, the pressure of the dry part inside the column is $p + p_0$.

According to Washburn's work on the dynamics of capillary flow [60], the total driving force for the liquid penetration inside the porous media consists of three separate pressures: the unbalanced atmospheric pressure, which is the air pressure difference between the advancing and stationary interfaces. In our case, this is the pressure differential p measured by the pressure sensor. The second component of the driving force is the hydrostatic pressure $p_{\mathrm{h}} = \rho g(h + h_0)$, where ρ is the density of the wetting liquid and g is the gravitational acceleration. We assume that the pressure drop over the dry part of the column is negligible, due to the significant difference in the viscosity and density between the wetting liquids and the air. The last pressure term contributing to the driving force is the capillary pressure p_{c}. As mentioned in section 1.2, the capillary pressure is the pressure difference between the liquid and air and is represented by the Laplace equation. In this work we consider this capillary pressure is independent of the position of the liquid front and the advancing velocity [83], [84]. Adding these three pressures we obtain the total driving force for the liquid penetration process inside a closed column: $\Sigma p = p_{\mathrm{c}} - p -$

$\rho g(h + h_0)$. Combining this driving force with Darcy's law and replace the Darcy velocity with the fluid velocity dh/dt:

$$\varphi \frac{dh}{dt} = \frac{\kappa}{\mu} \frac{p_c - p - \rho g(h + h_0)}{h + h_0} \tag{3.4}$$

Equation 3.4 is the governing equation of the liquid penetration process in the porous media in terms of the pressure differential p and the penetration height h. In order to find the dynamics of liquid penetration, we need to find the relation between the penetration height and the pressure differential. In the schematic drawing in figure 3.1, when the column is closed, the pressure above the liquid front is in equilibrium with the outside and it is therefore equal to the atmospheric pressure p_0. The initial volume of the air in the column is $\varphi(H - h_0)S$. After the liquid penetrates to height h, the pressure of the dry part in the column above the advancing front is now larger due to compression. This pressure is $p_0 + p$ and the air volume becomes $\varphi(H - h_0 - h)S$. Assuming that the air behaves as an ideal gas at constant temperature, this is an approximation for typical capillary pressures in powder systems [85]. we can use the ideal gas law to relate the pressure increase to the penetration height,

$$\varphi p_0(H - h_0)S = \varphi(p_0 + p)(H - h_0 - h)S \tag{3.5}$$

Where S is the cross section area of the column. From equation 3.1 we can obtain:

$$h = (H - h_0)\frac{p}{p + p_0} \tag{3.6}$$

H is an effective height of a powder column, it represents the total empty space inside the column $V_0 = \varphi SH$. In the most ideal case, as shown in figure 3.1, when the entire column

is fully filled with powders and no extra empty space is introduced, the effective height H equals to the physical height of the powder column. In the experiments, however, the column is not completely filled with powders and there is also empty space in the connections, tubes and any other dead volume that comes with the setup. As a result, H will be higher than the physical height of the powders packed in the column. In section 5.3 we will provide methods to estimate this effective height.

When p is very small comparing to p_0, then $p_0 + p$ can be approximated by p_0 and the liquid height h can be approximated to depend linearly on the pressure differential p. In fact, in this case equation 3.6 can be written as $h = Kp$ where K is a constant $K = (H - h_0)/p_0$. We will refer this approximation as the "*linear approximation*" in future discussions. This approximation is valid at the beginning of the capillary rise or at all times if p_c is also significantly small compared to p_0. This linear approximation was used by Wei [86] and Santomaso [73] to solve the problem numerically. In their experiments, the pressure differential is small and they focused on the beginning part of the capillary rise process, where this approximation is valid. In this chapter, we will derive implicit analytical solutions for this process and we will include the full pressure dependence in the solutions so that it can be used in cases when the pressure differential is large.

3.2 Liquid mass uptake solution

In the governing equation (3.4) there are two variables, liquid front h and the pressure differential p. In order to obtain a solution to it we need to obtain a differential equation for one of them above. In general, during the experiments it can be difficult to determine the position of the liquid front by optical observation because of its fuzzy appearance.

Instead people usually use the liquid uptake m in the porous media to calculate the liquid front h, under the assumption that the liquid can fully fill all the available pores of the powder column. Liquid front h and mass m are related through the density ρ of the liquid, the cross sectional area S of the column and the porosity φ of the packed powder,

$$h = \frac{m}{\varphi \rho S}. \tag{3.7}$$

Combining Equation (3.7) with (3.6) we obtain the equation relating liquid uptake with the pressure differential:

$$p = \frac{m p_0}{M - m_0 - m}, \tag{3.8}$$

Where m_0 is the initial liquid uptake when the column is open to atmosphere. $M = \rho V_0 = \varphi \rho S H$ is the amount of liquid that can fill in all the empty space in the experiment setup. We then replace h and p in equation 3.4 with Equation 3.7 and 3.8, to obtain a governing equation in terms of liquid uptake:

$$\frac{dm}{dt} = \frac{\kappa \varphi \rho^2 S^2}{\mu} \left(\frac{p_c - \frac{m p_0}{M - m_0 - m}}{m + m_0} - \frac{g}{\varphi S} \right) \tag{3.9}$$

To solve Equation 3.9, we first separate the variables:

$$\frac{(m_0 + m)(M - m_0 - m)}{[p_c \varphi S - g(m + m_0)](M - m_0 - m) - p_0 \varphi S m} dm = \frac{\kappa \rho^2 S}{\mu} dt \tag{3.10}$$

Then we write the left hand side using partial fractions decompositions, to obtain:

$$\left[\frac{A_1 m}{g(m_1 - m)} + \frac{B_1 m + C_1}{(m_2 - m)}\right] dm = \frac{\kappa \rho^2 S}{\mu} dt \tag{3.11}$$

Where m_1, m_2 are roots of the denominator in the left hand side of Equation 3.10 and $m_1 < m_2$, m_1 is the amount of liquid uptake when it reaches equilibrium. Integrating both sides on equation 3.11, assuming that p_c is constant (as discussed in section 1.2 and section 3.1, this can be done for capillary numbers $O(10^{-6})$) and using the initial condition that $m(t = 0) = 0$, we obtain the solution to equation 3.9:

$$-\left(\frac{A_1}{g} + B_1\right) m + \frac{A_1 m_1}{g} \ln \frac{m_1}{m_1 - m} + (C_1 + B_1 m_2) \ln \frac{m_2}{m_2 - m} = \frac{\kappa \rho^2 S}{\mu} t \tag{3.12}$$

The constants are in terms of m_0, m_1 and m_2:

$$A_1 = \frac{m_1(M - 2m_0 - m_1) + m_0(M - m_0)}{m_1(m_2 - m_1)} \tag{3.13}$$

$$B_3 = \frac{m_1(M - 2m_0 - m_2) + m_0(M - m_0)}{g m_1(m_1 - m_2)} \tag{3.14}$$

$$C_3 = \frac{m_0(M - m_0)}{g m_1} \tag{3.15}$$

Equation 3.12 is the implicit analytical solutions for the liquid uptake as a function of time in the most general case. The hydrostatics and the effect of the pressure differential in the closed column were both included. In the experiments we record the liquid weight change over time, the unknown parameters in Equation 3.12 are the permeability κ of the porous media and the capillary pressure p_c. We can fit the experiment using this solution to determine the permeability and the capillary pressure. In Chapter 5 we will show the results of these fittings.

3.3 Pressure solution

One of the advantages of using a closed column is that we are now able to monitor the pressure differential as an additional direct measurement. In some cases, when the total liquid uptake is so small, e.g. less than 1g, but the scale resolution is only 0.01g and the resolution is not enough. However, using pressure will provide higher resolution because the column pressure can increase to thousands of pascals. To derive a solution in terms of pressure, we also start with the governing equation obtained in section 3.2, then replace h by p using equation 3.6. By taking the derivatives on both sides of equation 3.6 we also obtain:

$$\frac{dh}{dt} = \frac{(H - h_0)p_0}{(p_0 + p)^2}\frac{dp}{dt} \tag{3.16}$$

After replacing h, dh/dt in equation 3.4 with (3.6) and (3.16) we obtain:

$$\frac{dp}{dt} = \frac{\kappa(p_0 + p)^2}{\varphi\mu p_0(H - h_0)}\left[\frac{(p_c - p)(p_0 + p)}{pH + p_0h_0} - \rho g\right] \tag{3.17}$$

Using separation of variables, equation 3.17 can be written as:

$$\frac{(h_0p_0 + Hp)}{(p_0 + p)^2[(p_c - p)(p_0 + p) - \rho g(h_0p_0 + Hp)]}dp = \frac{\kappa}{\varphi\mu p_0(H - h_0)}dt \tag{3.18}$$

The procedures to solve this equation is similar to the weight solutions, where we also assumed that p_c is constant. We write the LHS of equation 3.18 using partial fraction decomposition to obtain:

$$\left[\frac{A_2p}{(p_0 + p)^2} + \frac{B_2p}{p_1 - p} + \frac{C_2p + D_2}{p_2 - p}\right]dp = \frac{\kappa}{\varphi\mu p_0(H - h_0)}dt \tag{3.19}$$

Where $p_1,\ p_2$ are the roots of denominator on the LHS of equation 3.18

$$p_{1,2} = \frac{1}{2}[(p_c - p_0 - \rho g H) \pm \sqrt{(p_c - p_0 - \rho g H)^2 - 4(\rho g h_0 p_0 - p_c p_0)}] \quad (3.20)$$

Given that $p_1 < 0, p_2 > 0$ is the equilibrium pressure reached in experiments. Integrate both sides of equation 3.19 and using the initial condition that $p(t = 0) = 0$, we obtain the solution to equation 3.19:

$$\begin{aligned} A_2 \ln\frac{p_0}{p_0 + p} + \frac{A_2 p}{p_0 + p} - C_2 p_1 \ln(1 - \frac{p}{p_1}) + (C_2 p_2 + D_2)\ln(1 - \frac{p}{p_2}) \\ = \frac{\kappa}{\mu\varphi p_0 (H - h_0)} t \end{aligned} \quad (3.21)$$

A_2, B_2, C_2 and D_2 are constants:

$$A_2 = \frac{H - 2h_0}{p_1 p_2 - {p_0}^2} \quad (3.22)$$

$$B_2 = -C_2 \quad (3.23)$$

$$C_2 = \frac{h_0(p_1 p_2 - {p_0}^2) - p_0 p_1 (H - 2h_0)}{p_0 p_1 (p_1 p_2 - {p_0}^2)(p_1 - p_2)} \quad (3.24)$$

$$C_2 = \frac{h_0}{p_0 p_1} \quad (3.25)$$

Equation 3.21 is the implicit solution for the liquid penetration process in terms of the pressure differential as a function of time in general case. In the experiments we record the pressure differential data over time, then we fit the experimental data using this solution to obtain the permeability κ and the capillary pressure p_c of different solid-liquid systems. In

Chapter 5, 6 and 7 we will fit these solutions to the experimental data and discuss the fittings.

3.4 Modified Washburn solution

In this section, we will derive solutions for the initial stage of the capillary rise in a closed column. In the beginning of the capillary rise, the hydrostatic effects are negligible because the penetration height is very small. The same goes for Washburn equation where the hydrostatic effects are neglected. Since we are using a closed column, we will refer to the solutions as the *modified Washburn solution*.

For capillary rise in an open column, the pressure differential is zero. After neglecting the hydrostatic effects, the only term contributing to the driving force is the capillary pressure. Consider a case where $h_0 = 0$, we then write the governing equation from equation 3.4:

$$h\frac{dh}{dt} = \frac{\kappa p_c}{\mu\varphi} \tag{3.26}$$

Solving equation 3.26 and enforcing the initial condition $h(t = 0) = 0$ we obtain Washburn Equation [60]:

$$h^2 = \frac{2\kappa p_c}{\mu\varphi}t \tag{3.27}$$

According to Washburn equation, the penetration height is proportional to the square root of the penetrating time. This equation applies to the initial stage of the capillary rise process in an open column where the hydrostatic pressure is negligible.

To obtain the modified Washburn solution for a closed column, we first write the governing equation. In closed columns the pressure differential is no longer zero. After neglecting the hydrostatic effects we obtain the governing equation:

$$\varphi \frac{dh}{dt} = \frac{\kappa}{\mu} \frac{p_c - p}{h + h_0} \tag{3.28}$$

In Equation 3.28 there are two variables: the penetration height h and the pressure differential p as we are assuming that p_c is a constant (as previously discussed). In closed columns we have the pressure differential as a measurement in addition to the penetration front/liquid uptake, we will write this modified Washburn solution in terms of pressure. Although the pressure differential is not zero in a closed column, in the beginning stage, it is still very small comparing to the atmospheric pressure. Therefore we can use the linear approximation discussed in section 3.1 and write equation 3.6 as $h = Kp$, where K is a constant $K = (H - h_0)/p_0$. We replace h with p in the equation 3.28 and write it in terms of pressure:

$$\varphi \frac{dp}{dt} = \frac{\kappa}{\mu} \frac{p_c - p}{Kp + h_0} \tag{3.29}$$

During the initial stage, when the pressure differential is significantly smaller than the capillary pressure p_c, we can also neglect it on the right-hand-side of equation 3.29. Solving it and enforcing the initial condition $p(t = 0) = 0$ we obtain the modified Washburn solution for a closed column:

$$\frac{h_0}{K} p + \frac{p^2}{2} = \frac{\kappa p_c}{\mu \varphi K^2} t \tag{3.30}$$

The pressure term $(\frac{h_0}{K}p + \frac{p^2}{2})$ is proportional to the penetration time. In cases when $h_0 = 0$, then the constant $K = H/p_0$, and the solution becomes:

$$p^2 = \frac{2\kappa p_c}{\mu\varphi K^2}t \tag{3.31}$$

Similar to the original Washburn equation, the pressure differential depends linearly on the square root of the penetration time. Remember that this equation is only valid for the initial stage of the capillary rise. In Figure 3.2 we plot the entire capillary rise duration using this modified Washburn solution (equation 3.30) together with the full solution in terms of pressure (equation 3.21), using the same parameters (κ, H, h_0, p_c, p_0, μ, φ):

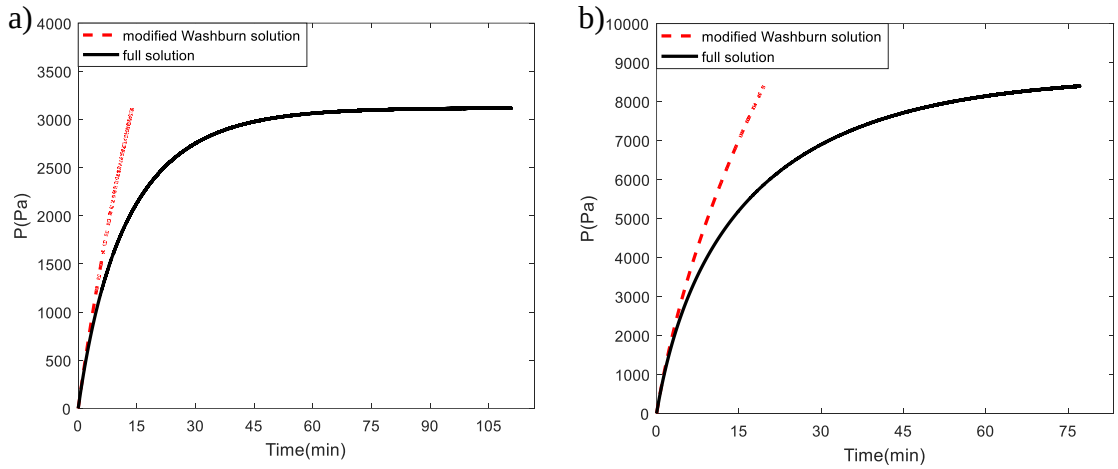

Figure 3.2 Plot the two solutions in terms of pressure as a function of time. The red dashed line represents the modified Washburn solution. The black solid line represents the full solution. a) 45μm glass beads with PDMS; b) 45μm glass beads with DI water.

It is easy to tell from figure 3.2 that the differences between the two solutions are very small when the pressure differential is small. As it builds up in the column, the assumptions we made to obtain the modified Washburn solution are not valid. The height of the penetration front is not proportional to the pressure differential. The pressure differential becomes significant and cannot be neglected on the right-hand-side of equation 3.29. In

figure 3.2, as the pressure differential increases, the curve representing the full solution deviates from the modified Washburn solution and eventually saturates at certain pressure. The reason for the separations of the two solutions at large pressure can be the significance of the hydrostatic effects, or the increase of the pressure differential in the column. In the next chapter, we will give a more detailed discussion on the dimensionless parameters governing the evolution of the capillary rise experiments. We will also discuss the significative contributions coming from the hydrostatic effects and the pressure differential. In Chapter 5, we will use this modified Washburn solution to fit with the initial stage of the experiments and compare the fitting results with the full solution.

4. Dimensionless discussion

In Chapter 3 we derived the analytical solutions in terms of liquid uptake and pressure differential for the capillary rise process in a closed column. The solutions will later be used to fit with experiments in Chapter 5. In this chapter, we will write the equations in dimensionless forms and identify the dimensionless parameters that are responsible for the dynamics of the capillary rise process with different liquids on a given particle system. We will also discuss how these dimensionless parameters can be monitored in the experiment setup to optimize the capillary rise experiments, especially by reducing the saturation time.

4.1 Nondimensional equation and implicit solutions in an open column

In Chapter 3.1 we obtained the governing equation in terms of liquid front when liquid is penetrating into the porous media:

$$\varphi \frac{dh}{dt} = \frac{\kappa}{\mu} \frac{p_c - p - \rho g(h + h_0)}{h + h_0} \tag{3.4}$$

Note that in this chapter of dimensionless discussion, we will consider the case when $h_0 = 0$ for simplicity. When the column is open to atmosphere, the pressure differential $p = 0$, and the initial pressure p_0 is no longer included in the equations. We then choose the capillary pressure p_c to characterize the system. For an open column, the capillary rise stops when the capillary pressure is balanced by the hydrostatics. This equilibrium height h_g^e is also known as the Jurin's length [59] it can be obtained as:

$$p_c = \rho g h_g^e \tag{4.1}$$

Using h_g^e as the characteristic length we obtain the governing equation for an open column in the dimensionless form:

$$\lambda' \frac{d\lambda'}{d\tau'} = 1 - \lambda' \tag{4.2}$$

Where $\lambda' = h/h_g^e$ is the dimensionless height and $\tau' = t/t_g$ is the dimensionless time. For an open column, the characteristic time is given by $t_g = (\varphi\eta(h_g^e)^2)/(\kappa p_c) = (\varphi\eta p_c)/(\kappa(\rho g)^2)$.

It should be noted that in Equation 4.2 there is no dimensionless parameters present, therefore, the solution to this equation is universal, it does not depend on the fluid or the porous media. Washburn derived an implicit solution for an open capillary [60], Green and Ampt also obtained the solution independently in their work on the soil infiltration [82]:

$$-\lambda' - \ln(1 - \lambda') = \tau' \tag{4.3}$$

A different approach is to write the solutions with the Lambert function W, discussed by Barry [87], [88] and more recently, Fries and Dreyer [79], [89]:

$$\lambda'(\tau') = (1 + W(-e^{-1-\tau'})) \tag{4.4}$$

Where the Lambert function W is defined by $W(x)e^{W(x)} = x$ [90].

4.2 Nondimensional equation and implicit solutions in a closed column

In the case of a closed column, the pressure differential p is no longer zero. It is related to the initial pressure p_0 and the effective length H. This initial pressure can be monitored by putting the experiment setup inside a closed chamber. In our experiments, it is equal to the atmospheric pressure. We will use this initial pressure to derive an independent dimensionless pressure $\pi_0 = p_0/\rho g H$, we refer to it as the normalized initial pressure.

Recall in Chapter 3.1, H is an effective length representing the empty space of the experiment setup. $\rho g H$ represents the hydrostatic pressure when the column of a length H

is fully filled with liquid. We can then use H to obtain another dimensionless number $\pi_c = p_c/\rho g H = h_g^e/H$, it is the ratio of the capillary pressure to the hydrostatic pressure. We refer to it as the normalized capillary pressure. It is also the reverse of the Bond number. In cases where the Bond number is small, the hydrostatic effects can be neglected.

Now we can use the characteristic length H and the characteristic pressure $\rho g H$ to nondimensionalize the governing equation 3.4:

$$\lambda \frac{d\lambda}{d\tau} = \pi_c - \pi - \lambda \tag{4.5}$$

Where the new dimensionless height $\lambda = h/H$, the new dimensionless pressure $\pi = p/\rho g H$, and the dimensionless time $\tau = t/t_c$, with $t_c = (\varphi \eta H)/(k \rho g)$.

Similarly, Equation 3.6 which relates h and p can also be written in dimensionless form following the same dimensionless parameters λ and π:

$$\pi = \pi_0 \frac{\lambda}{1-\lambda} \tag{4.6}$$

Then we replace π in the governing equation to obtain a differential equation in terms of the penetration height:

$$\lambda \frac{d\lambda}{d\tau} = \pi_c - \pi_0 \frac{\lambda}{1-\lambda} - \lambda \tag{4.7}$$

After separation of variables:

$$\frac{\lambda(1-\lambda)}{\lambda^2 - (1 + \pi_c + \pi_0)\lambda + \pi_c} d\lambda = d\tau \tag{4.8}$$

To solve Equation 4.8, we write the left hand side using partial fraction decomposition, to obtain:

$$[\left(\frac{\lambda_1 - 1}{\lambda_1 - \lambda_2}\right)\left(\frac{\lambda}{\lambda_1 - \lambda}\right) + \left(\frac{1 - \lambda_2}{\lambda_1 - \lambda_2}\right)\left(\frac{\lambda}{\lambda_2 - \lambda}\right)]d\lambda = d\tau \tag{4.9}$$

Where λ_1 and λ_2 are roots of the denominator on the left hand side of Equation 4.8:

$$\lambda_{1,2} = \frac{1}{2}[(1 + \pi_c + \pi_0) \pm \sqrt{(1 + \pi_c + \pi_0)^2 - 4\pi_c}] \tag{4.10}$$

The physical meaning of λ_1 and λ_2 is the possible dimensionless equilibrium heights that can be reached in experiments. Considering that they satisfy $\lambda_1 > \lambda_2$, it can also be proven that $\lambda_1 > 1$ and $\lambda_2 < 1$. The equilibrium height in a closed column h_g^e can then be obtained as $h_c^e = \lambda_2 H$. It can also be proven that λ_2 is bounded by

$$\lambda_2 = \frac{h_g^e}{H} < \min\{1, \frac{\pi_c}{1 + \pi_0}\} \tag{4.11}$$

Integrating both sides on Equation 4.9 and using the initial condition $\lambda(\tau = 0) = 0$ we obtain the implicit solution for the liquid front as a function of time in a closed column:

$$-\lambda - \left(\frac{\lambda_1 - 1}{\lambda_1 - \lambda_2}\right)\lambda_1 \ln\left(1 - \frac{\lambda}{\lambda_1}\right) - \left(\frac{1 - \lambda_2}{\lambda_1 - \lambda_2}\right)\lambda_2 \ln\left(1 - \frac{\lambda}{\lambda_2}\right) = \tau \tag{4.12}$$

This solution is a general solution that includes the hydrostatic effects and the pressure differential effects in a closed column.

Another measurement of the experiment is the pressure differential p. We can also obtain a dimensionless solution in terms of pressure following the same procedures we use for liquid front. The equation relating λ with π can be written as:

$$\lambda = \frac{\pi}{\pi_0 + \pi} \tag{4.13}$$

Replacing λ with Equation 4.13 in the governing equation we obtain the governing equation in terms of pressure:

$$\frac{\pi}{\pi_0+\pi}\frac{\pi_0}{(\pi_0+\pi)^2}\frac{d\pi}{d\tau}=\pi_c-\pi-\frac{\pi}{\pi_0+\pi} \tag{4.14}$$

After separation of variables:

$$\frac{-\pi_0\pi}{(\pi_0+\pi)^2[\pi^2+(1-\pi_c+\pi_0)\pi-\pi_c\pi_0]}d\pi=d\tau \tag{4.15}$$

Similar to the solutions for the height equation, the roots $\pi_1,\pi_2$to the denominator $\pi^2+(1-\pi_c+\pi_0)\pi-\pi_c\pi_0=0$ are possible equilibrium pressure for the capillary rise process.

$$\pi_{1,2}=\frac{1}{2}[-(1-\pi_c+\pi_0)\pm\sqrt{(1-\pi_c+\pi_0)^2+4\pi_c\pi_0}] \tag{4.16}$$

Given that $\pi_1>\pi_2$, it is obvious that $\pi_1>0$ and $\pi_2<0$. The equilibrium pressure during the capillary rise is equal to $p_D^e=\pi_1\rho gH$. The solution to Equation (4.15) can be found after writing the left hand side by partial fraction decomposition and then integrating both sides, the initial condition is $\pi(\tau=0)=0$.

$$\begin{aligned}-\frac{\pi}{\pi_0+\pi}+(\pi_c+\pi_0)\ln\left(1+\frac{\pi}{\pi_0}\right)-\frac{\pi_0\pi_1}{(\pi_1-\pi_2)(\pi_0+\pi_1)^2}\ln\left(1-\frac{\pi}{\pi_1}\right)\\+\frac{\pi_0\pi_2}{(\pi_1-\pi_2)(\pi_0+\pi_2)^2}\ln\left(1-\frac{\pi}{\pi_2}\right)=\tau\end{aligned} \tag{4.17}$$

Equation 4.17 is the implicit solution for the pressure differential as a function of time during the capillary rise process in a closed column. It is a general solution that includes the hydrostatic effects and the pressure differential effects.

Now that we have the implicit solutions for a closed column in terms of the liquid front (Equation 4.12) and the pressure differential (Equation 4.17), we can use them to obtain the characteristic time to reach equilibrium. The dimensionless equilibrium time τ_γ is defined as the time it takes for the liquid front to reach a certain completion fraction γ of the equilibrium height λ_2, or for the pressure differential to reach a certain completion fraction γ of the equilibrium pressure π_1.

For the case of using solution in terms of the liquid penetration height, at the given height $\gamma\lambda_2$, the equilibrium time τ_γ can be obtained by replacing λ by $\gamma\lambda_2$ in Equation 4.12:

$$\tau_\gamma = -\gamma\lambda_2 - \left(\frac{\lambda_1 - 1}{\lambda_1 - \lambda_2}\right)\lambda_1 \ln\left(1 - \frac{\gamma\lambda_2}{\lambda_1}\right) - \left(\frac{1 - \lambda_2}{\lambda_1 - \lambda_2}\right)\lambda_2 \ln(1 - \gamma) \tag{4.18}$$

For the case of using solution in terms of the pressure differential, at the given pressure $\gamma\pi_1$, the equilibrium time τ_γ can be obtained by replacing $\tilde{p}$ by $\gamma\pi_1$ in Equation 4.17:

$$\begin{aligned}\tau_\gamma = &-\frac{\gamma\pi_1}{\pi_0 + \gamma\pi_1} + (\pi_c + \pi_0)\ln\left(1 + \frac{\gamma\pi_1}{\pi_0}\right) \\ &- \frac{\pi_0\pi_1}{(\pi_1 - \pi_2)(\pi_0 + \pi_1)^2}\ln(1 - \gamma) \\ &+ \frac{\pi_0\pi_2}{(\pi_1 - \pi_2)(\pi_0 + \pi_2)^2}\ln\left(1 - \frac{\gamma\pi_1}{\pi_2}\right)\end{aligned} \tag{4.19}$$

Both Equation 4.18 and 4.19 can be used to study the effects of the dimensionless parameters have on the equilibrium time, we will discuss more details on this topic later.

4.3 Penetration dynamics depending on π_c and π_0

In this section, we will discuss how the dimensionless parameters affect the dynamics of the capillary rise experiments in a closed column. We will consider two different scenarios. Firstly, we fix the experiment setup and consider the effect of different values of the

capillary pressure on the penetration dynamics. In this case, the only parameter that is changing is the capillary pressure p_c. With a fixed experiment setup, p_0 and H are constants. Different values of the capillary pressure may be introduced by using particles of different contact angles but similar particle sizes, so the permeability of the porous media is similar. The second case is the opposite of the first one, we fix the capillary pressure p_c and study the effect of different values of p_0 and H. For this case, we will use a given solid and liquid system with different experiment setups where either p_0 or H is changing. The initial pressure p_0 can be monitored by putting the entire setup in a closed chamber. Different values of the effective length H can be achieved by changing the empty space of the setup, such as using a longer column. Note that when varying H, both π_0 and π_c are changing simultaneously, but the ratio α between them remains the same: $\pi_c = \alpha\pi_0$.

For the first case, since the setup is fixed, H is a constant, we will use the dimensionless variables discussed in section 4.2, which are $\{\lambda; \pi; \tau\}$. The corresponding characteristic scales used to obtain these dimensionless variables are $\{H, \rho g H, t_c\}$, recall that $t_c = (\varphi\eta H)/(k\rho g)$, they all remain constant and are independent of the only changing parameter p_c. In the second scenario, since p_c is fixed while p_0 and H are changing, we will use the dimensionless variables $\{\lambda'; \pi'; \tau'\}$ discussed in section 4.1. As in the open column case, the dynamics is also independent of the experiment setup. The corresponding characteristic scales $\{h_g^e, p_c, t_g\}$, with $t_g = (\varphi\eta p_c)/(\kappa(\rho g)^2)$, are independent of the changing parameters p_0 and H and will remain constant in this case. These two groups of dimensionless variables are related by the following equations: $\lambda = \pi_c\lambda'$, $\pi = \pi_c\pi'$ and $\tau = \pi_c\tau'$.

4.3.1 Penetration dynamics depending on p_c

We first look at the dynamics of the penetration height under different values of the capillary pressure p_c. We plot the evolution of penetration front over time in dimensionless forms: λ and τ. We consider two cases of different values of the normalized initial pressure π_0: $\pi_0 = 0.5 < 1$ (Figure 4.1a) and $\pi_0 = 2 > 1$ (Figure 4.1b). In both cases ($\pi_0 < 1$ and $\pi_0 > 1$), the equilibrium height increases with the capillary pressure and approaches the maximum height H ($\lambda_2 = 1$) asymptotically.

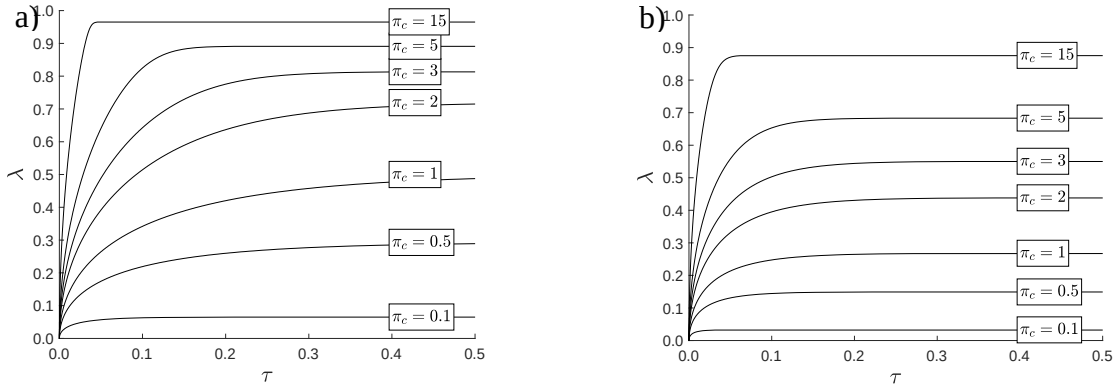

Figure 4.1 The evolution of the dimensionless penetration front over time under different values of the normalized capillary pressure. a): π_0=0.5 <1, b) π_0=2 >1.

Here we present the contour plot to show the complete behavior of the dimensionless equilibrium height as a function of π_0 and π_c, shown in Figure 4.2a. We notice the same trend as in Figure 4.1, that for a given initial pressure, a large capillary pressure will lead to a large value of the equilibrium height. This trend corresponds to the vertical lines in Figure 4.2a as well as each solid line in Figure 4.2b. In Figure 4.2b we plot the equilibrium height as a function of the capillary pressure π_c. The dashed line is the open column case and the solid lines represent different initial pressures.

On the other hand, the horizontal lines in Figure 4.2a corresponds to cases of a given π_c. It is obvious that in such cases, the equilibrium height decreases with the increasing value of

the initial pressure. The corresponding cases can be represented by the vertical lines in Figure 4.2b, where it is clear that increasing the value of π_0 results in a decreased equilibrium height. More details regarding this situation will be discussed in the following section where we explore the effects of p_0 and H.

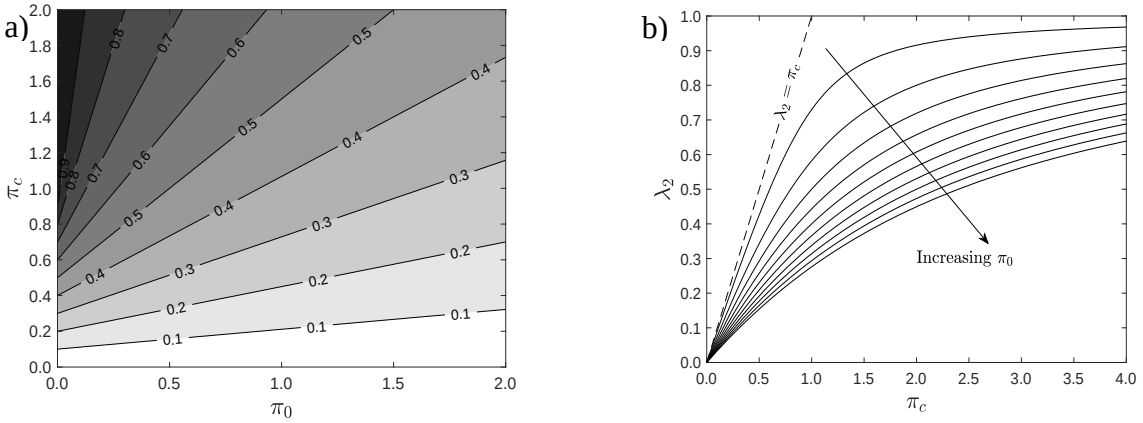

Figure 4.2 a) Contour plot of the dimensionless equilibrium height λ_2 as a function of the dimensionless parameters π_0 and π_c. b) Dimensionless equilibrium height λ_2 as a function of the dimensionless capillary pressure π_c. The dashed line represents the open column case, $\lambda_2 = \pi_c$ ($\lambda' = 1$). The solid lines are the closed column cases with initial pressure $\pi_0 = 0.1, 0.3, 0.5, 0.7, 0.9, 1.1, 1.3, 1.5, 1.7$ and 1.9.

We also notice in the early stage in Figure 4.2b, when the capillary pressure is very small, the equilibrium height is linearly dependent on π_c. At small values of π_c, the equilibrium height $\lambda_2 \approx \pi_c/(1+\pi_0)$. The equilibrium is a result of the capillary pressure balanced by the hydrostatics and the pressure differential effects. In the study by Wei [86] et al, they designed an experiment setup to obtain an equilibrium height $h_c^e \approx 1/2 h_g^e$. They connected an air bottle to their setup to introduce more empty space, consequently, the effective height in their experiments is large, $H \sim 10m$. The corresponding normalized initial pressure $\pi_0 = 1$. The capillary pressure generated by the particles used in their experiments is very low, $p \sim 100Pa$, which corresponds to $\pi_c \sim 0.001$. As a result, the equilibrium height is also very small, $\lambda_2 \sim O(10^{-3})$. Depalo and Santomaso [73] took a similar path by attaching

an air reservoir to include extra empty space in the setup. The effective height in their experiments with glass ballottini and calcium carbonate is $H \sim 5m$. The resulting normalized capillary pressure $\pi_c \sim O(10^{-2})$ and the equilibrium height $\lambda_2 \sim O(10^{-2})$ are both very small as expected.

In addition, it can be seen in Figure 4.2b that as the initial pressure decreases, the initial linear part is approaching the case of an open column. For which the $\lambda_2 \approx \pi_c$ or $p_c \approx \rho g h_g^e$, corroborating that the pressure differential is trivial in the experiments.

Next, we shall take a look at the evolution of the dimensionless pressure $\tilde{p}$ under different values of the capillary pressure p_c. In Figure 4.3a we plot the case when $\pi_0 = 2$. It is apparent that the dimensionless equilibrium pressure increases with the capillary pressure. The same trend is observed at different values of the initial pressure, similar to the case with the dimensionless equilibrium height presented in Figure 4.1.

We also plot the dimensionless equilibrium pressure π_1 as a function of π_0 and π_c in the contour plot in Figure 4.3b. We notice the same trend: for a given value of π_0, corresponding to a vertical line in Figure 4.3b, the equilibrium pressure is higher for cases in which the capillary pressure is large. In the other case, from the horizontal lines in Figure 4.3b, we observe that the dimensionless equilibrium pressure also increases with the normalized initial pressure. We will get back into details about this topic when we discuss the penetration dynamics depending on p_0 and H.

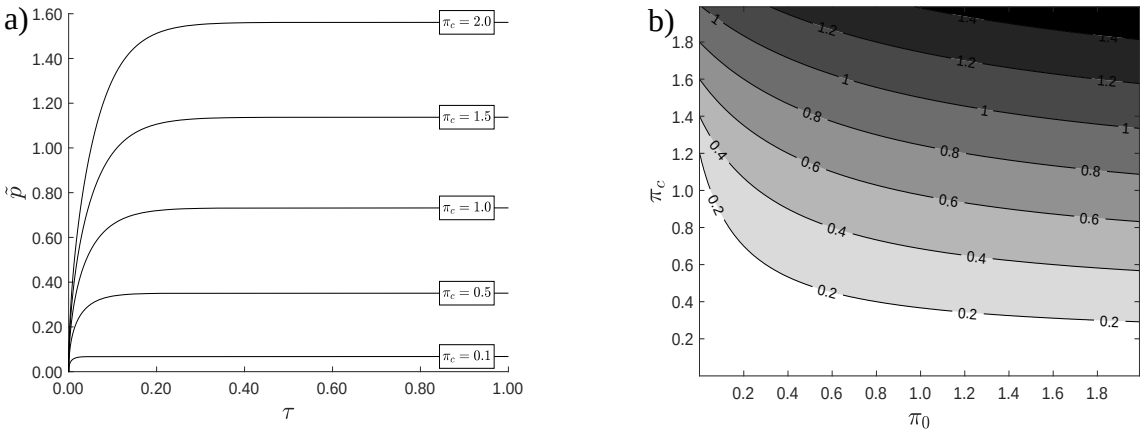

Figure 4.3 a) The evolution of the dimensionless pressure over time under different values of the normalized capillary pressure. The normalized initial pressure used for the plot is π_0=2. Similar trend is observed at different values of π_0. b) Contour plot of the dimensionless equilibrium pressure π_1 as a function of the dimensionless parameters π_c and π_0.

Finally, we study the effects of the capillary pressure on the equilibrium time. The dimensionless equilibrium time can be obtained by Equation 4.18. In Figure 4.4a we plot the dimensionless equilibrium time using $\gamma = 0.95$ in Equation 4.18.

$$\tau_{0.95} = -0.95\lambda_2 - \left(\frac{\lambda_1 - 1}{\lambda_1 - \lambda_2}\right)\lambda_1 \ln\left(1 - \frac{0.95\lambda_2}{\lambda_1}\right) - \left(\frac{1 - \lambda_2}{\lambda_1 - \lambda_2}\right)\lambda_2 \ln 0.05 \qquad (4.18)$$

Where λ_1, λ_2 are related to π_0, π_c. Therefore, the equilibrium time $\tau_{0.95}$ can be presented as a function of the dimensionless parameters π_0 and π_c, $\tau_{0.95} = \tau_{0.95}(\pi_0, \pi_c)$.

Apparently, the dimensionless equilibrium time is not monotonic with the capillary pressure. This trend is also presented in Figure 4.4b, where the equilibrium time as a function of the dimensionless capillary pressure is plotted for given values of π_0. When the capillary pressure is small, $\pi_c \ll 1$, both the pressure differential and hydrostatic effects are linearly dependent on the penetration height ($\lambda \ll 1$), and the equilibrium time increases with the capillary pressure. At this time, the dynamics is similar to that of an open column, except that there is a modified factor contributed by the pressure differential. This situation is observed in Wei's work [86] where we estimate their dimensionless equilibrium

time is $\tau_{0.95} \approx 0.001$. Using the other parameters in the experiments, we estimate their equilibrium time is $t_{0.95} \approx 40s$, which is consistent with the results reported by the authors (Figure 4 in [86]). In the opposite cases when there is a significantly large dimensionless capillary pressure, $\pi_c \gg 1$, the dimensionless equilibrium height approaches 1 as the liquid will need to compress most of the empty space to reach a higher pressure differential to balance the large capillary pressure. In this situation, the dynamics approaches the case when neglecting the hydrostatic effects, where the equilibrium time is inversely proportional to π_c.

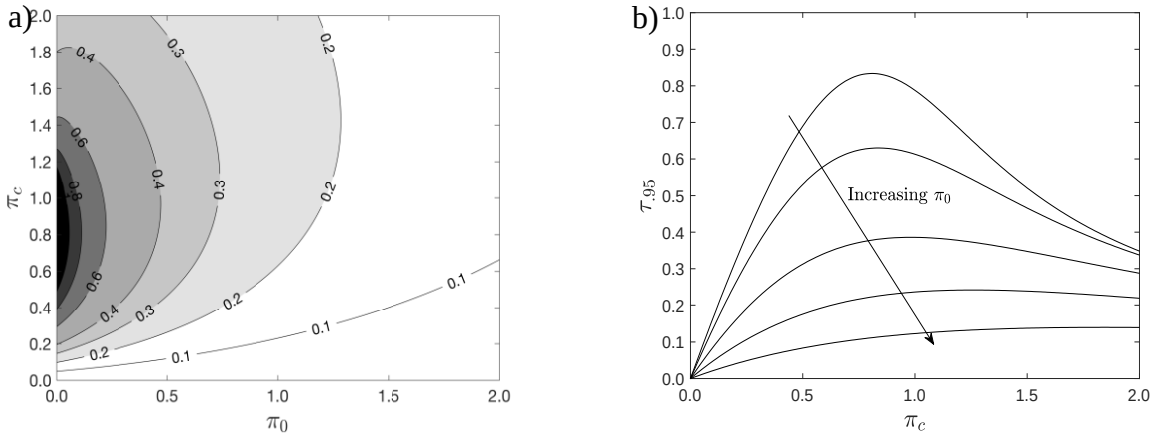

Figure 4.4 a) Contour plot of the dimensionless equilibrium time $\tau_{0.95}$ as a function of the dimensionless parameters π_c and π_0. b) The dimensionless equilibrium time $\tau_{0.95}$ as a function of the dimensionless capillary pressure π_c, at given values of the dimensionless initial pressure π_0.

4.3.2 Penetration dynamics depending on p_0 and H

In this section, out interest is in how the experimental conditions p_0 and H affect the penetration dynamics. Now that the p_c is constant while p_0 and H are changing, we use the dimensionless variables $\{\lambda', p', \tau'\}$ as discussed previously. In Figure 4.5 we plot the dimensionless height as a function of time using different values of the normalized initial pressure π_0. We consider two cases of different values of the normalized capillary pressure

π_c: $\pi_c = 0.5 < 1$ (Figure 4.5a) and $\pi_c = 2 > 1$ (Figure 4.1b). In both cases ($\pi_c < 1$ and $\pi_c > 1$), the equilibrium height decreases as the normalized initial pressure becomes larger. As one would expect, when the initial pressure is large, to reach the same capillary pressure, liquid do not need to compress as much of the empty volume, thus the penetration height is small. In contrast, when the initial pressure is small, liquid would need to compress a lot of the empty space to reach the same pressure differential value, consequently, the penetration height increases.

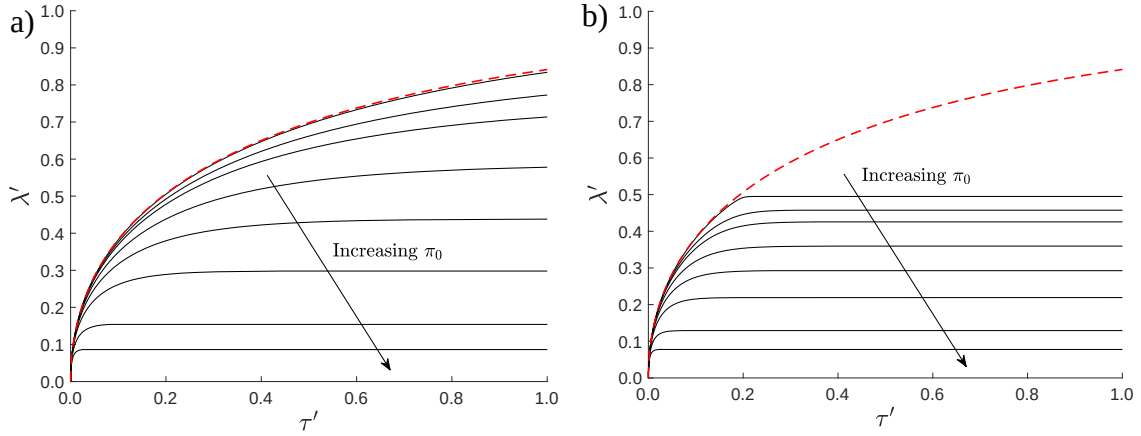

Figure 4.5 The evolution of the dimensionless height over time under different values of the normalized initial pressure. The dashed line represents the case for an open column, each solid line represents a case for closed column with different values of π_0, from top to bottom: $\pi_0 = 0.01, 0.1, 0.2, 0.5, 1, 5, 10$. a): $\pi_c = 0.5$, b) $\pi_c = 2$.

The dashed line in Figure 4.5 represents the solution for an open column. We observe that in the early times the closed column solution is very similar to the open column case, the dimensionless height evolution does not depend on the value of the initial pressure. We also notice in the case presented in Figure 4.5a, where the capillary pressure is small, $\pi_c < 1$, the solution is approaching the open column as the initial pressure decreases. This trend is not surprising since the initial pressure is very small, the pressure differential throughout the experiment will always be trivial, which is analogous to the open column case where the pressure differential $p = 0$. Besides, when $\pi_c < 1$, the capillary pressure can be

balanced by the hydrostatics alone. However, this case does not apply to a large value of π_c shown in Figure 4.5b. When $\pi_c > 1$, the hydrostatics cannot balance the capillary pressure, therefore the pressure differential will become dominant. It is obvious from the plot that the lines deviate from the open column. The equilibrium height will approaching $\lambda_2' = \lambda_2/\pi_c \approx 1/\pi_c$. While in the open column the equilibrium height is λ_2'.

In Figure 4.6a we consider a situation where we only change the effective length H. Accordingly, the normalized initial pressure and capillary pressure are also changing, but their ratio are kept at a constant α, such that $\pi_c = \alpha\pi_0$. The dashed line is the solution for an open column, each solid curve represents a different value of the effective length H. It is straightforward from the plot that, as the column length increases, both π_c and π_0 are decreasing, the curve is approaching the open column solution. In fact, the open column can be viewed as an extreme case for a closed column with an infinite length.

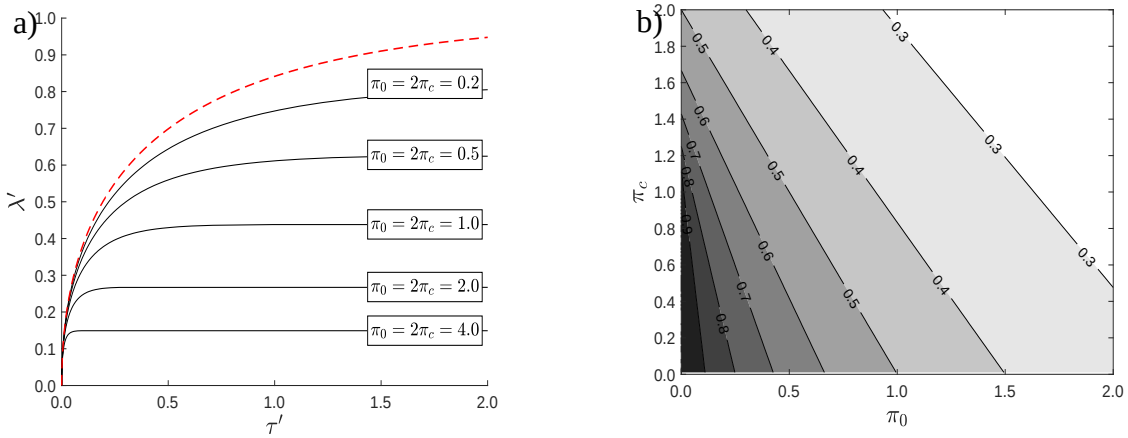

Figure 4.6 a) The evolution of the dimensionless height over time under different values of the effective column length H. The dashed line represents the case for an open column, each solid line represents a case for closed column with different values of H. b) Contour plot of the dimensionless equilibrium height λ_2' as a function of π_0 and π_c.

Next, we study the effects of the dimensionless parameters on the equilibrium height. The contour plot in Figure 4.6b presents the dimensionless equilibrium height λ_2' as a function

of the dimensionless parameters π_0 and π_c, $\lambda_2{}' = \lambda_2{}'(\pi_0, \pi_c)$. Apparently, as discussed before, increasing the normalized initial pressure $\pi_0$will result in a smaller equilibrium height, since compressing only a small portion of the empty space can cause a large pressure differential. This process can be achieved either by reducing the effective length H of the column or by enforcing a large initial pressure p_0.

We will now look at how the dimensionless parameters affect the equilibrium time $\tau'_{0.95}$. In Figure 4.7a we plot of the dimensionless equilibrium time $\tau'_{0.95}$ as a function of the dimensionless parameters π_c and π_0. The horizontal lines represent the case of a given π_c, the equilibrium time decreases as the normalized initial pressure increases. This trend is the same with the equilibrium height.

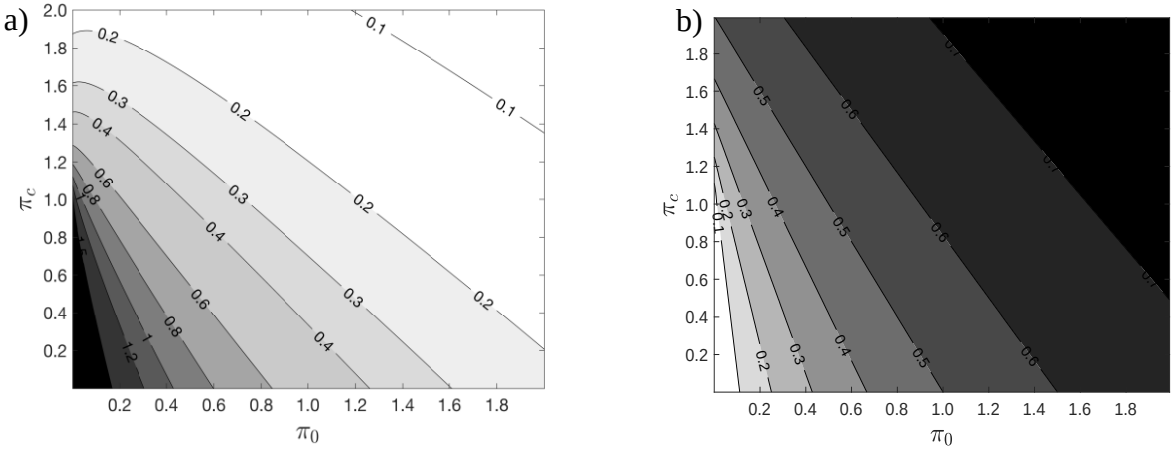

Figure 4.7 a) Contour plot of the dimensionless equilibrium time $\tau'_{0.95}$ as a function of the dimensionless parameters π_c and π_0. b) Contour plot of the dimensionless equilibrium pressure π'_1 as a function of the dimensionless parameters π_c and π_0.

The equilibrium time $\tau'_{.95}$ at large values of π_0 can be obtained:

$$\tau'_{.95} \approx [-\gamma - \ln(1-\gamma)]\frac{(\rho g H)^2}{p_0^2}. \tag{4.1}$$

It is clear from Equation 4.20 that the equilibrium time $\tau'_{.95}$ is inversely proportional to the square of π_0. Using a short column or increasing the initial pressure can both help reducing the equilibrium time.

5. Experimental Results with a Model System

In this chapter, we will discuss the experimental results with the model system considered in our work, that is a column packed with glass beads. Specifically, we will use either $10\mu m$ or $45\mu m$ glass beads to perform experiments. As mentioned in Chapter 2, glass beads are

chosen as a model material because they are spherical, non-porous and they do not dissolve or swell in contact with water. These properties make them an ideal model of finely divided solids to study the capillary rise in a packed column. In this chapter, we will use the model systems to study the imbibition process with PDMS. As discussed in Chapter 2, PDMS is chosen as a reference liquid because of its low surface tension, which makes it completely wet almost any solid surfaces, including glass. We will first present the experimental data of the advancing and receding processes, as well as the static characterization of the capillary pressure and pore radius using the advancing, receding and bubbling pressure. Finally, we will fit the advancing process with the analytical solutions derived in Chapter 3 to obtain the permeability and the effective capillary pressure of the packed columns.

5.1 Advancing, receding and bubbling pressure

There are two main stages in each experiment. The first part is called the advancing process, where liquid penetrates spontaneously into the column by capillarity. The second part is the receding process, which takes place after the pressure equilibrates and no additional liquid penetrates into the system in the advancing process. During the receding process, the liquid that penetrated into the column is forced to leave it by slowly increasing the pressure differential in the chamber. In order to increase the pressure differential, we use a syringe pump connected to the column, as described in Section 2.3. Both liquid weight and pressure differential are continuously measured and recorded during the entire experiment, including both advancing and receding stages. Representative curves for the advancing and receding processes in a model system are presented in Figure 5.1.

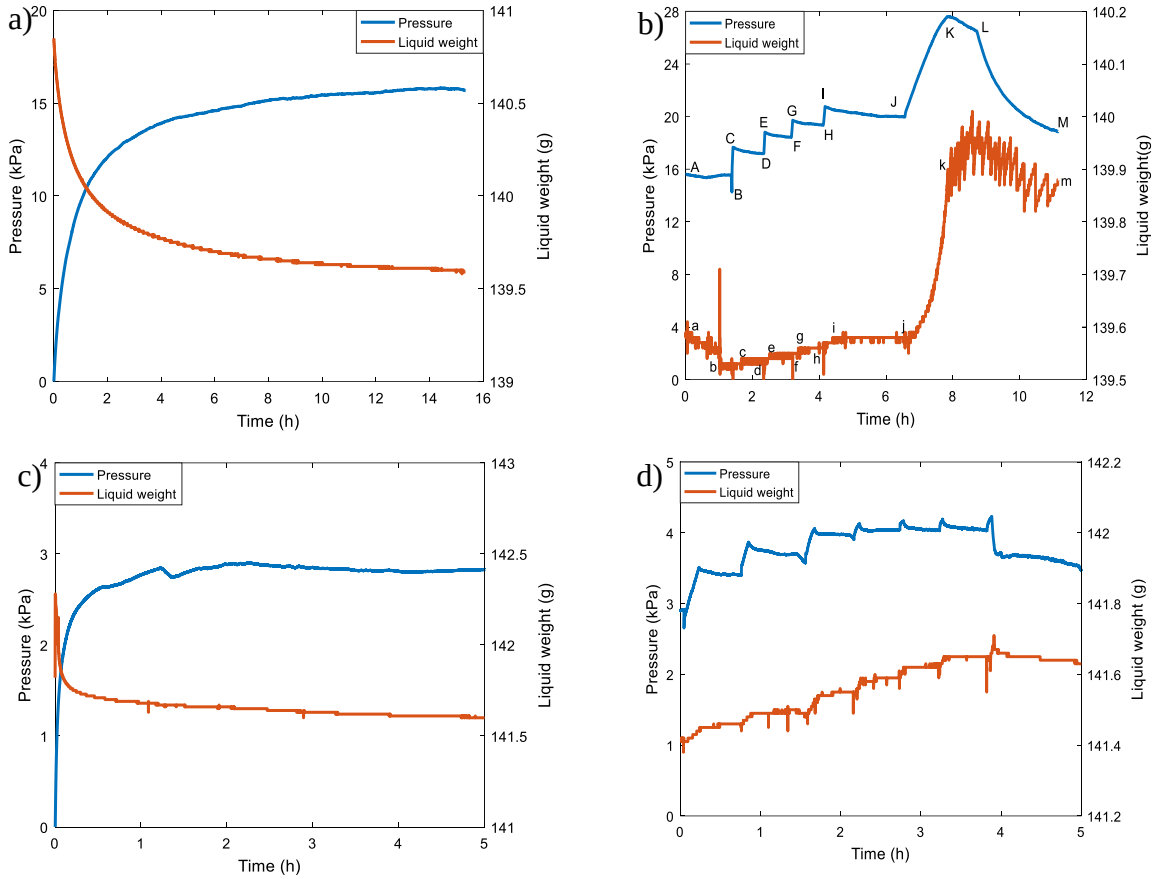

Figure 5.1 The development of the pressure and liquid weight over time for glass beads with PDMS. The blue curve is the pressure differential in the column and the red curve is the mass of the liquid left in the bottom container. (a) advancing process of 10μm glass beads, (b) receding process of 10μm glass beads, (c) advancing process of 45μm glass beads, (d) receding process of 45μm glass beads.

Figure 5.1a and c show the evolution of the pressure differential (blue curves) and the liquid weight (red curves) during the advancing process for PDMS. When the bottom of the column is in contact with a reservoir of the wetting liquid, the liquid will start to penetrate and occupy the empty spaces (*pores*) between the packed particles, due to capillary force. When the liquid advances inside the column, the amount of liquid left in the container decreases as observed in both plots. At the same time, when the column is closed to the outside atmosphere, the air inside the column is being compressed as liquid advances, leading to an increase in the pressure differential, also observed in both figures. This pressure differential, p, is monitored by a pressure sensor. The net driving force of the

advancing process is the pressure difference between the capillary pressure and the combination of the hydrostatic pressure and the pressure differential, that is $[p_c - p - \rho g(h + h_0)]$. Initially, both the pressure differential and the hydrostatic pressure are relatively small compared to the intermediate and late stages of liquid penetration. Accordingly, $[p_c - p - \rho g(h + h_0)]$ is large, and the liquid advances relatively fast compared to the intermediate and late times of the penetration process. As liquid advances, the pressure differential builds up in the column and the hydrostatic pressure also increases. As a result, the driving force is reduced and the liquid advancing rate decreases. Eventually, when $p_c - p - \rho g(h + h_0) = 0$, the driving force is zero. It should be noted that the driving force equals zero is an asymptotic situation. In reality, the driving force never actually reaches zero in theory. We consider it to be zero when there is no appreciable increase measured in the pressure differential. At this time, the pressure differential remains constant and no measurable amount of liquid is entering into the column. The system reaches an equilibrium and the advancing process finishes. The evolution of both the pressure and the liquid weight are observed to follow this trend in figure 5.1a and c. At the end of the advancing process, the pressure differential stops increasing, $p = p_c - \rho g(h + h_0)$. This is the maximum pressure reached in the advancing process, we call this pressure the *advancing pressure* p_A^{max}.

Figure 5.1b and d present the evolution of the pressure differential and liquid weight during the receding process. As we discussed, after the pressure differential reaches the maximum advancing pressure, liquid stops advancing, the system is in equilibrium and both the pressure differential and the liquid weight remain constant in time. At this point, we open the valve connecting the syringe pump to the top of the column and start injecting air. In

this way, we are able to further increase the pressure differential in a controllable manner. Notice that before connecting the syringe to the column, we compress the syringe by a prescribed amount such that the air in the syringe barrel has the same pressure as the pressure differential in the column. The objective of this procedure is to avoid a sudden change in the pressure differential as an extra empty volume is introduced into the system when the syringe is connected to the column. This compressed volume ΔV can be estimated using the following relationship that is based on the assumption that air behaves as an ideal gas: $p_0 V_0 = (p_0 + p_{\mathrm{A}}^{\max})(V_0 - \Delta V)$. Where V_0 is the initial volume of the syringe.

As the syringe injects air, at first, liquid weight remains constant, until a certain pressure is reached, at which time liquid will begin leaving the column. This moment can be detected with the scale as the liquid weight in the container increases (corresponding to point 'c' in the red curve in figure 5.1b). We call the magnitude of the pressure differential at which some of the liquid first begins to evacuate the column the *minimum receding pressure* $p_{\mathrm{R}}^{\min}$. In figure 5.1b, it should fall somewhere between point 'B' and point 'C' in the blue curve. However, it is not easy to determine an accurate value, because the initial change in the liquid weight might not be accurately captured by the scale due to its limited resolution. Especially in cases when the liquid starts to recede right after the pressure differential is increased by injecting air with the syringe.

In general, the value of the receding pressure is different from the advancing pressure. This difference could be a result of contact angle hysteresis, the heterogeneity of the porous media, or a combination of both. As mentioned in section 1.3, in the most ideal case when the porous media is homogeneous and all the pores are of the same size, any difference in advancing and receding capillary pressures is a result of contact angle hysteresis. However,

in practical cases, pores have different sizes so that pore size heterogeneity may play a role in any observed capillary pressure hysteresis. Pores of different sizes correspond to various capillary pressure values. More details of the pore size distribution and structure will be discussed in section 5.2 below.

During the receding process, air from the top of the column is replacing the liquid inside the porous media, this process can is also called a *drainage* process. In the experiments, when we notice an increase in the weight of the liquid in the reservoir, we stop injecting air and close the syringe valve (this corresponds to point C in the pressure curve shown in figure 5.1b). However, liquid continues to evacuate the column, resulting in more pores occupied by air. Therefore, air expands, and the pressure differential drops (corresponding to the segment 'CD' in the pressure curve in figure 5.1b). This process continues until no more pores can be emptied at the corresponding pressure. At this time, liquid weight will remain constant and a new equilibrium is reached (corresponding to the point 'd', 'f', 'h' and 'j' in the liquid weight curve in figure 5.1b). It should be pointed out that this new equilibrium is different from the previous one in the advancing process. During the advancing process, the system reaches equilibrium when the capillary pressure is balanced by the pressure differential and the hydrostatic pressure. The liquid stops penetrating into the porous media after reaching the equilibrium. In the receding process, the larger pores are emptied first. When the large pores are emptied, the system reaches equilibrium again. A higher pressure is required to continue evacuating the smaller pores. Therefore, we inject air again to further increase the pressure, until more liquid is pumped out of the column. Then, we stop injecting and wait until another equilibrium is established. This inject-stop-equilibrium-inject cycle is repeated several times. In figure 5.1b there is a "staircase-like

increase" in both the pressure (segment 'BCD'-'DEF'-'FGH'-'HIJ') and the liquid weight curve (segment 'bcd'-'def'-'fgh'-'hij'). The increase in the pressure indicates that every time it takes a higher pressure to empty smaller and smaller pores. From the "staircase-like increase" behavior we also learn that the pores in our porous media are not homogeneous.

As air injection continues, more and more of the liquid occupying the pores is replaced by air, that is, more pores are emptied and clusters of connected pores grow in size. At some pressure, a cluster of empty and connected pores will form a "channel" that goes from the top of the porous media all the way to the bottom. When this channel is formed, air from the top of the column will find its way through to the bottom of the column and bubbles will be created and released, as the pressure differential is greater than zero and the air in the top of the column is at a higher pressure than outside. The creation of such a channel is a *percolation process* [91], [92]. This moment can be easily identified in the pressure curve, as there is a sudden drop in the differential pressure (corresponding to point 'K' in the pressure curve in figure 5.1b). This bubbling phenomenon also creates significant noise levels in the measurement of the liquid weight, as can be seen between point 'k' and 'm' in the liquid weight curve in figure 5.1b. These changes in pressure and liquid weight are a result of the bubbles forming and detaching from the column. The pressure differential right before the first bubble is released is referred to as the *bubbling pressure* p_B^{max} (point 'K' in the pressure curve in figure 5.1b). It is also the highest pressure reached during the entire experiment.

5.2 Static characterization

In the previous section we introduced specific pressure definitions: the advancing pressure $p_{\mathrm{A}}^{\max}$, the receding pressure $p_{\mathrm{R}}^{\min}$ and the bubbling pressure $p_{\mathrm{B}}^{\max}$. As mentioned in Chapter 1, there are static and dynamic ways to study the liquid penetration process. In the static method, a specific pressure differential value, for example the pressure differential at which the spontaneous capillary rise stops is measured to calculate the capillary pressure [69], [70]. The three pressure terms $p_{\mathrm{A}}^{\max}$, $p_{\mathrm{R}}^{\min}$, and $p_{\mathrm{B}}^{\max}$ are static measurements. They can be used as a static characterization of the capillary pressure for the porous media. In this section we will discuss the characterization of the porous media created using the $10\,\mu m$ and $45\,\mu m$ glass beads using these three static pressures, with a focus on the characteristic pore size equivalent to these pressures.

The Laplace equation $p_{\mathrm{c}} = 2\gamma cos\theta / r$ is used for static characterization. Each of the capillary pressures can be interpreted by means of the Laplace equation as corresponding to a contact angle value and a certain pore size or radius r. The capillary pressure in the Laplace equation is the static pressure corrected by the hydrostatic contribution $p_{\mathrm{c}} = p + \rho g(h + h_0)$, where p is the corresponding advancing, receding and bubbling pressure measured in experiments. PDMS has very low surface tension and can completely wet the surfaces of glass beads. We will therefore assume that $\cos(\theta_{\mathrm{PDMS}}) = 1$ and obtain the effective pore size for each of the static pressure measurements. Note that since we assume that the contact angle of PDMS is zero, there is no contact angle hysteresis, and the differences between the capillary pressures are assumed to result from the heterogeneity of the porous media. Recall that the advancing pressure is the pressure when the system reaches an equilibrium in the advancing process, the receding pressure corresponds to the

pressure when liquid first begins to leave the column and the bubbling pressure is the pressure right before the first bubble is released. The pressure measurements with $10\mu m$ and $45\mu m$ glass beads are summarized in table 5.1.

Particle size (μm)	Advancing pressure (Pa)	Receding pressure (Pa)	Bubbling pressure
10	17000 ± 900	18800 ± 1700	27700 ± 2500
45	3000 ± 100	3500 ± 400	4300 ± 100

Table 5.1 Advancing, receding and bubbling pressure for $10\mu m$ and $45\mu m$ glass beads with PDMS.

We first characterize the system with $10\mu m$ particles. We corrected the pressure in table 5.1 by hydrostatics to obtain the corresponding capillary pressure. According to the t-statistics, there is no significant difference between the advancing pressure and the receding pressure since p>0.05 for both 10 and 45 microns systems. Then from the advancing capillary pressure we obtain a corresponding advancing radius $r_{\mathrm{A}}^{\min} = (2.4 \pm 0.1)\mu m$. The meaning of the advancing pressure is, if the liquid would continue to advance, it can only fill in those pores smaller than $r_{\mathrm{A}}^{\min}$. Analogously, the pore radius corresponding to the receding pressure and the bubbling pressure can be obtained as $r_{\mathrm{R}}^{\max} = (2.1 \pm 0.2)\mu m$ and $r_{\mathrm{B}}^{\min} = (1.4 \pm 0.1)\mu m$, respectively. The receding radius corresponds to the pores when we first observe the liquid receding from the change in liquid weight. However, as mentioned above, our measurements are not able to separate advancing and receding radii, as there is no statistically significant difference in the corresponding pressure values. The bubbling radius is smaller than the receding radius. It represents the smallest pores needed to create a channel from top to bottom so that the larger pores are connected and then emptied. This value will change from column to column depending on the pore size distribution and the structure of pore networks of that porous media. The difference between the advancing/receding and the bubbling radii once again suggests the heterogeneity of the porous media.

The porous media packed with $45\mu m$ glass beads generates a lower capillary pressure as expected. Since they have bigger particle size, the pore size of the packed powder bed will also be larger. We perform the same characterization on the pore radius as we did with the $10\mu m$ glass beads. Again, assuming the contact angle to be zero, we obtain the advancing radius for $45\mu m$ glass beads to be $(13.0 \pm 0.4)\mu m$ and the pore radius at the receding pressure and the bubbling pressure can then be obtained as $(11.2 \pm 1.2)\mu m$ and $(9.1 \pm 0.1)\mu m$, respectively.

Particle size (μm)	$r_{\mathrm{A}}^{\min}(\mu m)$	$r_{\mathrm{R}}^{\max}(\mu m)$	$r_{\mathrm{B}}^{\min}(\mu m)$
10	2.4 ± 0.1	2.1 ± 0.2	1.4 ± 0.1
45	13.0 ± 0.4	11.2 ± 1.2	9.1 ± 0.1

Table 5.2 The advancing, receding and bubbling pressure obtained for 10μm and 45μm glass beads with PDMS by assuming $\cos(\theta_{\mathrm{PDMS}}) = 1$.

The advancing, receding, and bubbling radii corresponding to the columns filled with $10\mu m$ and $45\mu m$ glass beads are summarized in Table 5.2. We notice that the ratio between the receding radius (5.3 ± 0.8) is similar to the ratio of particle sizes (4.3 ± 0.8). The ratio of the advancing radius is (5.4 ± 0.3), that is about 20% difference from the particle size ratio. The ratio in the bubbling radius between the two groups of particles is (6.5 ± 0.5), it is greater than the ratio of advancing and receding radii. This difference may be attributed to different shapes of the particle size distribution curves and different pore network structures of the porous media. Overall, however, the order of magnitude of these ratios are consistent with the ratio of particle sizes.

5.3 Effective column height, theoretical and estimated values

In section 5.2, we used the static measurements to characterize the porous media. We also want to characterize it dynamically using the analytical solutions derived in chapter 3. For this purpose, we first need to determine the effective column height H. As discussed in

section 3.1, the relation between the liquid front position and the pressure differential in a closed column is given by equation (3.6):

$$h = (H - h_0)\frac{p}{p + p_0} \tag{3.6}$$

Recall that H is the effective length of a column, that is a column fully packed at the same porosity φ that has the same void space V_0 as the entire column and the experimental setup connected to it. The effective height can be estimated from the measurements on the experimental setup, such as the length, porosity φ and cross section area S of the column, and dead volume in connectors, sensors and tubing. In the case when the column is completely filled with powders and there is no additional empty space in the setup, H is equal to the physical height of the powders inside the column. In practical cases, however, H will be greater than the physical height of the powders. We will demonstrate how to estimate it in the following section. This height is a theoretical estimate of the effective height, we refer to it as H_{th} . This value satisfies $V_0 = H_{\text{th}} S\varphi$.

5.3.1 Theoretical estimate for H

The total void space in the experiments is made up of two parts: the empty space in the setup, such as any empty portion of the column, the tubing, connectors and sensors (shown in Figure 5.2a), and the empty space that comes from the porous media. We first estimate the empty space in the setup.

The tubes connecting the column and the pressure sensor are cylindrical. Their inner diameter is $0.0254cm$ and their total length in the setup is $1m$, the void space in the tubes can be estimated as:

$$V_{\text{tube}} = \frac{\pi}{4} \times 0.0254^2 \times 100cm^3 = 0.051cm^3$$

The o-ring plug connector between the tubes and the column has a cylindrical opening in the center. There are two connectors used in experiments. Since the inner diameters of the columns are not consistent, we machined two connectors with a slightly different diameter to ensure a tight fit with all the columns. The void space for each connector can be calculated by the measurements:

Connector1: $V_{\text{connector}} = \frac{\pi}{4} \times 0.5263^2 \times 3.613 = 0.79cm^3$

Connector2: $V_{\text{connector}} = \frac{\pi}{4} \times 0.5567^2 \times 3.577 = 0.82cm^3$

Another source of void space comes from the chamber of the pressure sensor. According to the manufacturer, the volume of that chamber is $V_{\text{chamber}} = 0.1\ cubic\ inch = 1.64cm^3$.

These three empty spaces are independent of the packing of the powders, we add them together to obtain a total empty volume, or "dead volume" V_{dead} that is the same for all experiments.

$$V_{\text{dead}} = V_{\text{chamber}} + V_{\text{connector}} + V_{\text{tube}}$$

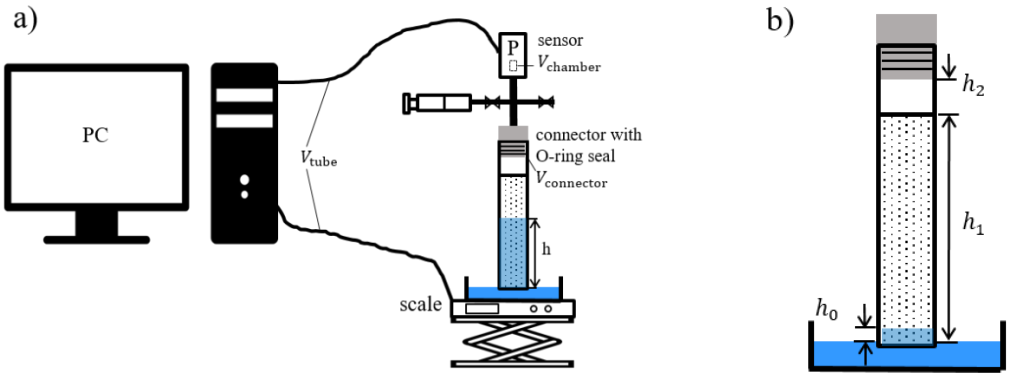

Figure 5.2 Schematic view of the empty space in the setup: a): "dead volume" in the experiment setup.$V_{dead} = V_{chamber} + V_{connector} + V_{tube}$. b): empty space in the packed column: the height of the packed powders is h_1, the length between the top of the packed powders and the connector is h_2, the initial height of liquid penetration is h_0.

The remaining of the empty space comes from the packing of the powders as shown schematically in Figure 5.2b. Consider that the packed bed forming the porous media has a total height h_1 and a cross section area of S, h_2 is the distance between the top of the porous media to the connector. Then the theoretical effective length H_{th} can be estimated using the following equation:

$$H_{th}\,\varphi S = h_1 \varphi S + h_2 S + V_{dead}$$

In addition to estimating the effective height theoretically, we can also obtain it from the experimental data. In the following section we will introduce this alternative method.

5.3.2 Experimental estimate for *H*

Recall that the liquid front is related to the pressure differential by equation (3.6). Thus the effective height H can be obtained by fitting the liquid front as a function of pressure differential. However, the direct measurement of the liquid front position is inaccurate because the wetting front is not flat. Here we use the liquid mass m instead to calculate an average position of the front. We rewrite equation (3.6) in terms of m:

$$\frac{m}{\rho S\varphi} = (H - \frac{m_0}{\rho S\varphi})\frac{p}{p + p_0} \tag{5.1}$$

In equation (5.1), ρ is the density of the liquid, S is the cross section area of the column, φ is the porosity of the porous media, m_0 is the liquid uptake before the column is closed while m is the amount of liquid that penetrates into the porous media after it is closed, and p is the pressure differential in the column. By fitting the liquid mass as a function of the pressure differential using Equation (5.1), we can estimate the effective height H, as the only fitting parameter in the equation.

In figure 5.3 we present an example of the fitting for an experiment with $10\mu m$ glass beads and PDMS. We use different ranges of the experiments in the fitting to evaluate a proper range to use. Specifically, we fit the data up to a pressure (from a) to d)): $0.25p_{\mathrm{A}}^{\max}$, $0.75p_{\mathrm{A}}^{\max}$, $0.9p_{\mathrm{A}}^{\max}$ and $p_{\mathrm{A}}^{\max}$. In figure 5.3a, b and c the experimental data and the equation agree very well. In figure 5.3d the entire experimental rang of pressure is fitted and the fit is not as good as in the previous three cases, with a smaller R^2value. We notice that at the end of the curve, there is a "tail" trend that is different from the rest of the curve. At the end of the advancing process, as the pressure differential is approaching the equilibrium value, the driving force $p_{\mathrm{c}} - p - \rho g(h + h_0)$ is small and the penetration rate slows down, only a very small amount of liquid is slowly entering the porous media. Since the resolution of the scale used in experiments is 0.01g, the changes in the mass during this period will be too small to be accurately measured. Meanwhile the pressure sensor can still measure the pressure change in the column. In figure 5.3d we see that p is still increasing while m is not changing. Therefore, we will not use the entire experimental range in the fitting. We

will fit the data points up to $0.9p_{\mathrm{A}}^{\max}$ because it contains more information comparing to $0.25p_{\mathrm{A}}^{\max}$ and $0.75p_{\mathrm{A}}^{\max}$.

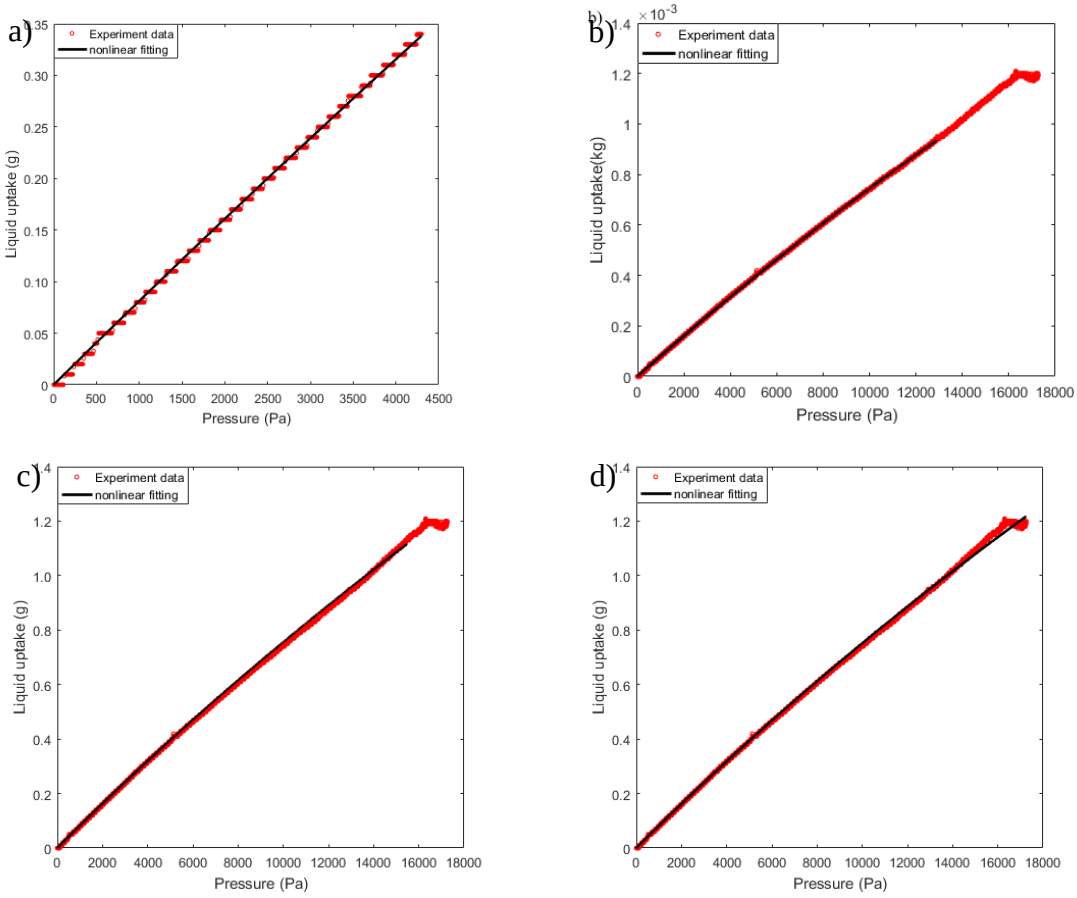

Figure 5.3 The fitting of liquid uptake m and pressure differential p at different ranges for an experiment with 10μm glass beads and PDMS. a): fit up to $0.25p_{\mathrm{A}}^{\max}$, the effective length $H = 0.178m$, $R^2 = 0.999$. b): fit up to $0.75p_{\mathrm{A}}^{\max}$, $H = 0.178m$, $R^2 = 0.999$. c): fit up to $0.9p_{\mathrm{A}}^{\max}$, $H = 0.180m$, $R^2 = 0.998$. d): fit up to $p_{\mathrm{A}}^{\max}$, $H = 0.179m$, $R^2 = 0.976$.

This "tail" issue is more noticeable in $45\mu m$ glass beads because the capillary pressure is even lower. Consequently, there will be less liquid that can penetrate into the porous media. In the example shown in figure 5.4, the total amount of liquid that entered the column is only 0.12g. In figure 5.4a, when the pressure differential reaches 2500Pa, the liquid penetration slows down and the scale is not able to capture the small changes in the liquid weight. This very last part of the experiment will not provide very useful data when estimating H, which is the reason we only fit the data up to $0.9p_{\mathrm{A}}^{\max}$.

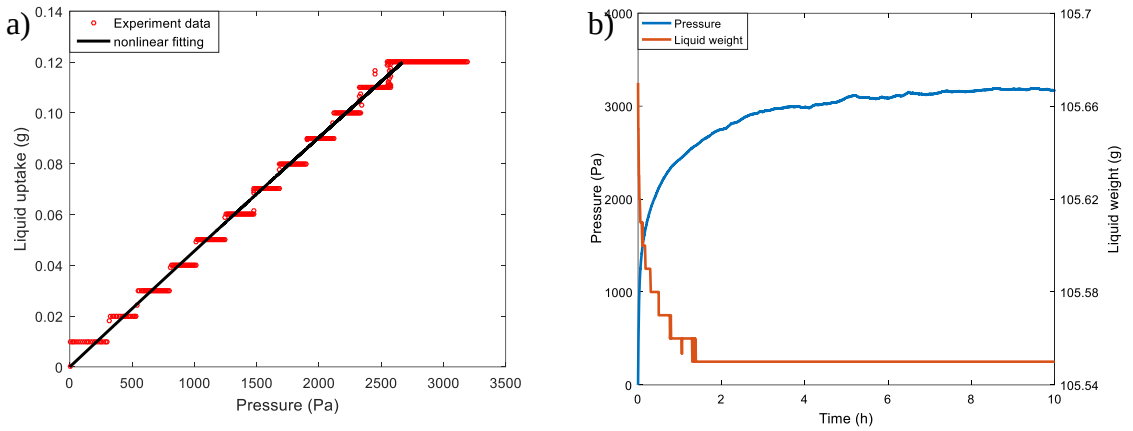

Figure 5.4 An experiment of 45μm glass beads with PDMS. a): The fitting of liquid uptake vs. pressure differential. b): The development of pressure and liquid over time during the imbibition. After p reaches 2500Pa, the liquid uptake is so small that the scale cannot measure, while the pressure differential still keeps increasing.

Comparing to the theoretical value H_{th} that is discussed in the previous section, the value of the effective height obtained by fitting experimental data is larger, with a difference of about 10-20%. This difference is expected. When calculating the empty space in the connector, we assume that the opening in the center is cylindrical, however, its inner diameter might not be consistent throughout the connector, the same goes for the column itself. In fact, we have noticed this issue with the columns and that is why we machined two connectors with slightly different outer diameter to secure a tight fit with different columns. In addition, the top of the connector has a tap drill so that it connects to the tubes. This drill part is assumed as a cylinder as the rest of the opening for simplicity. Besides, the empty space in the other connectors and valves are also neglected for simplicity. Accordingly, the estimated H_{th} is smaller than the actual empty space in the setup. In figure 5.5 we plot the experimental data, the fitting using equation 5.1, together with the prediction curve that uses H_{th} in equation 5.1. Since $H_{\mathrm{fitting}} > H_{\mathrm{th}}$, the curve predicted by H_{th} has a smaller slope in the plot. In the experiment presented in figure 5.5, the difference in H_{fitting} is 8%. In some experiments the difference between H_{fitting} and H_{th} is 20%. This

larger error cannot come from neglecting the small void space in the connectors. In those situations, there must other sources causing the error. We shall cover more details on this topic in the following section, discussing how overestimating H will affect the fittings. Before that, we shall consider the fitting using the linear approximation.

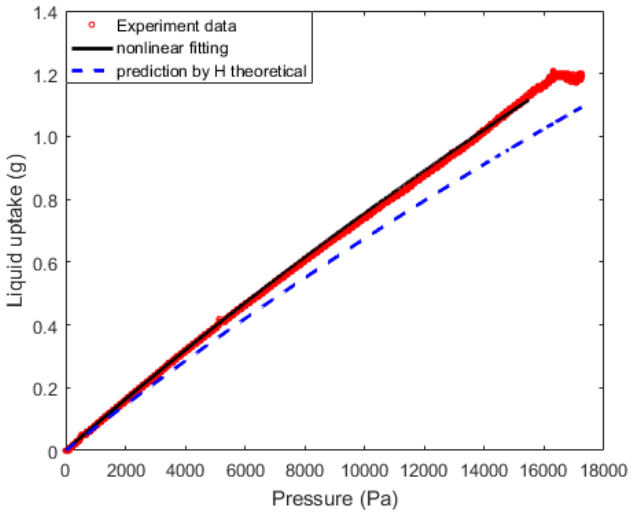

Figure 5.5 Plot of the liquid uptake vs. pressure differential for an experiment with 10 μm glass beads with PDMS. Red dots are the experimental data. The black curve is the fitting up to $0.9p_{\mathrm{A}}^{\max}$, using equation 5.1. The blue dashed line is the prediction using the H_{th} in equation 5.1.

In section 3.1 we introduced the linear approximation between m and p, which is valid when the pressure differential p is small compared to p_0.

$$\frac{m}{\rho S\varphi} = (H - \frac{m_0}{\rho S\varphi})\frac{p}{p + p_0} \tag{5.1}$$

Under the linear approximation, the factor $(H - m_0/\rho S\varphi)/(p_0 + p)$ in equation 5.1 is treated as a constant by neglecting p. Liquid uptake m can then be assumed to depend linearly on the pressure differential. Equation (5.1) now becomes $m = Kp$ where $K = \rho S\varphi(H - m_0/\rho S\varphi)/p_0$ is a constant. If we use this linear equation to fit experimental data in which the pressure differential becomes larger than $0.5p_0$, it will not accurately predict the trend. In figure 5.6 we present the plot of two experiments with $10\mu m$ glass beads. In

figure 5.6a the wetting liquid is PDMS, in figure 5.6b is DI water. The prediction of the linear fitting is obtained by fitting the experimental data for pressures smaller than $0.25p_{\mathrm{A}}^{\max}$ and then extrapolating the curve to the entire range of pressures, up to its maximum value $p_{\mathrm{A}}^{\max}$. When we extend the linear approximation to higher pressures, the curve deviates from the actual experimental data as p increases and the linear assumption is no longer valid. In the experiment with PDMS, the capillary pressure is lower (16kPa compared to 60kPa in the case of DI water), therefore, the deviation of the linear approximation is smaller. It is clear in figure 5.6a that the differences between the linear prediction and the experiments are smaller compared to the case with DI water in figure 5.6b. Given that DI water generate a higher pressure (up to 60kPa), using the linear assumption can lead to larger errors. The linear approximation can only be used in cases when the capillary pressure is small. Using the full pressure dependence (equation 5.1) instead of the linear approximation allows us to work with finer particles, which result in a higher capillary pressure. This is one of the benefits resulting from our work.

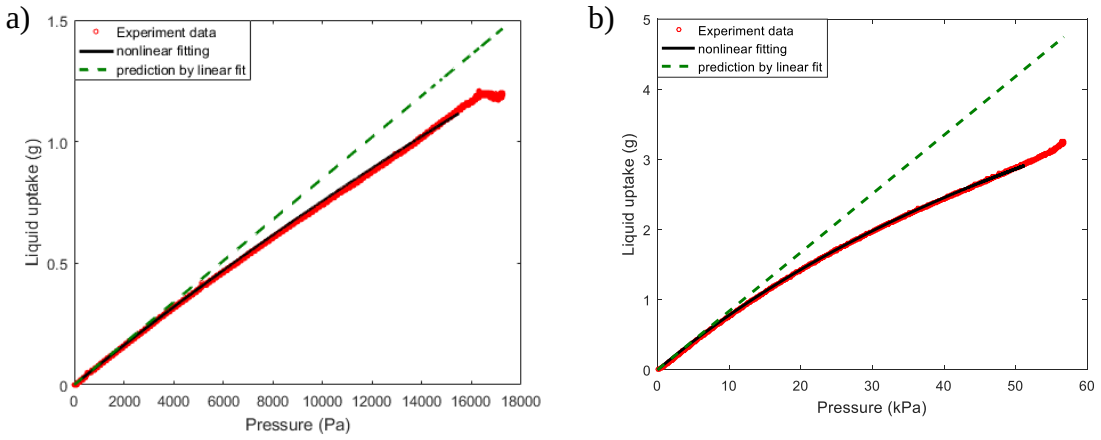

Figure 5.6 Plot of the liquid uptake vs. pressure differential. Red dots are the experimental data. The black curve is the fitting up to $0.9p_{\mathrm{A}}^{\max}$, using equation 5.1. The green dashed line is the prediction using the linear fit of the first $0.25p_{\mathrm{A}}^{\max}$. a): $10\mu m$ glass beads with PDMS, b): $10\mu m$ glass beads with DI water.

5.3.3 Possible sources for overestimating H

In section 5.3.2 we mentioned one of the possible reasons for the difference between H_{th} and H_{fitting}, that is the system error in neglecting small void space in the connectors and valves. However, in some experiments we observed a large error that cannot be caused by the system error alone, in this section we will consider more possible sources that lead to the error when estimating H.

In both theoretical and experimental estimations, we use the liquid uptake m and the porosity φ to calculate the liquid front h under the assumption that the liquid is fully saturating the pores inside the porous media. This assumption, however, might not be valid in cases when there is air trapped as liquid advances in the porous media. If the pressure inside the trapped air is different from the pressure on top of the porous media, the volume change when the air is compressed will be different from equation 5.1.

When using equation 5.1 to fit liquid uptake with the column pressure, we are also assuming that the liquid uptake is completely caused by the capillary rise. However, if the liquid is evaporating, or if there is a leak in the setup, it can also cause deviations from equation 5.1. In figure 5.7a the evaporation rate of PDMS is presented. It is measured by leaving PDMS in the container used in experiments. There is a round opening in the cover of the container. The evaporation rate is only 0.00018g/min. This rate is so small that it is considered negligible compared to the liquid uptake due to capillary rise or leakage. In some experiments, we observe the liquid weight is remarkably decreasing even when the pressure reaches equilibrium at advancing pressure. An example is shown in figure 5.7b. This weight change can be 10 times larger than the rate observed due to liquid evaporation, suggesting that air is leaking from the setup.

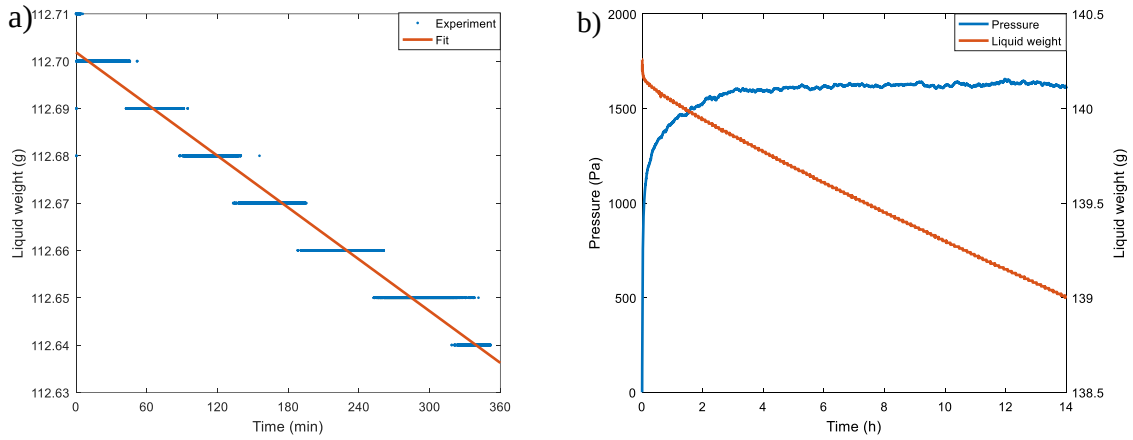

Figure 5.7 (a) Evaporation rate of PDMS measured by leaving PDMS in the container used in experiments, there is a circle opening on the cover of the container. The evaporation rate is 0.00018g/min. (b) An example of an experiment plot when there is a leak. After 4 hours, the liquid continues to enter the porous media without causing the pressure to increase.

When air is leaking from the system, the liquid will continue to fill in the porous media without causing any increase in the pressure. If we plot the pressure and liquid weight vs. time, we will see a stable pressure but a decrease in the weight of the liquid that remains in the container. In the example shown in Figure 5.7b, after 4 hours, the pressure stabilizes at 1620Pa while the liquid weight left in the container is still decreasing. This weight decrease rate is 0.00128g/min, it is 7 times faster than the evaporation rate of PDMS measured in Figure 5.7a (0.00018g/min), indicating that the weight decreases after 4 hours in Figure 5.7b is mostly due to a leak in the setup. During this time of the experiment, the liquid front was also seen moving up in the porous media while the pressure did not increase. This behavior indicates that the liquid was still entering because of the leak. After applying leak detector fluid around the connections of the setup, the leak was found in the connection between the tube and the column and it was fixed for future experiments by tightening the connectors.

If we use equation 5.1 to fit experiments when the system is leaking, we will overestimate the empty length H. For a given amount of liquid penetrating into the system, the resulting

pressure differential in the presence of a leak would be smaller than for an air-tight system. As a result, the slope will appear larger in the plot of weight vs pressure in the presence of a leak. Figure 5.8 is an experiment where there is a leak, the black line is obtained by fitting with equation 5.1, which gives an empty length of $H_{\text{fitting}} = 0.235m$. However, the $H_{\text{th}} = 0.176m$. It is smaller than H_{fitting} . Represented by the blue dots, it appears to have a lower slope in the plot. In a case like this when there is large error in H caused by the leak, we do not use data from this experiment for analysis.

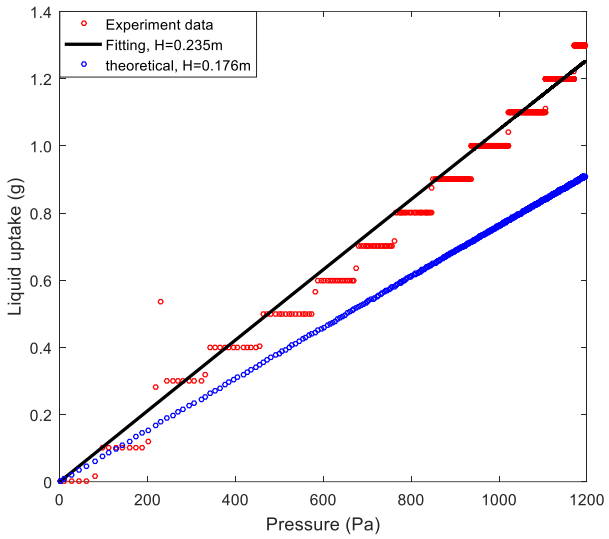

Figure 5.8 Plot of liquid uptake vs column pressure. When there is leak in the experiment (red dots), the slope of m vs. p (black line) will appear larger than theoretical (blue dots).

In the following section when we fit the experimental data to the analytical solutions, we will come back to this discussion and consider its impact on the permeability obtained by fitting. Based on the discussions in this section, we recommend using equation 5.1 to estimate the effective height. The data up to $0.9p_{\text{A}}^{\max}$ is suggested to be used in the fitting. The linear approximation is not recommended because it is not applicable for finer particles. After discarding the experiment when the difference between H_{fitting} and H_{th} is greater

than 20%, the difference between H_{fitting} and H_{th} in the other experiments are between 10% to 20% .

5.4 Dynamic Characterization: effective capillary pressure and permeability

5.4.1 Fitting with weight solution

In Section 3.3 we obtained the implicit solution for the imbibition process in terms of the liquid uptake mass m as a function of time:

$$-\left(\frac{A_1}{g}+B_1\right)m+\frac{A_1 m_1}{g}\ln\frac{m_1}{m_1-m}+(C_1+B_1 m_2)\ln\frac{m_2}{m_2-m}=\frac{\kappa\rho^2 S}{\mu}t \qquad (3.12)$$

In this solution, the permeability κ of the porous media and the capillary pressure p_{c} are unknown. Although we measure the advancing pressure in the experiments, it corresponds to the smaller pores due to the heterogeneity of the porous media as discussed in Section 5.1. Through fitting experiments with the analytical solutions, we can obtain an effective p_{c} that represents all the pores filled by the liquid.

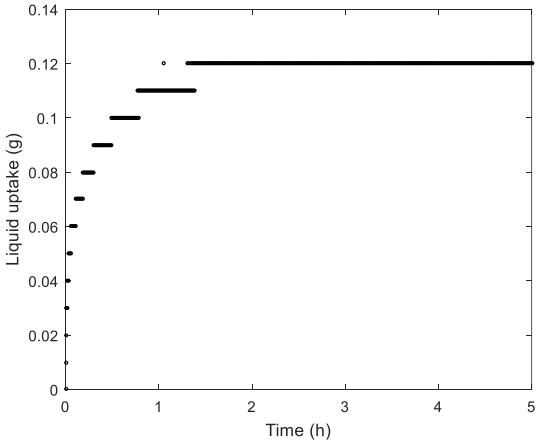

Figure 5.9 The liquid uptake over time in an experiment with 45 μm glass beads and PDMS.

The liquid uptake in 45μm glass beads is very small, as shown in figure 5.9, it is only 0.12g. We did not use these experiments to fit the weight solution because the resolution of the

scale is only 0.01g. For $10\mu m$ glass beads we fit the experiment up to a certain range of mass values, analogous to the fitting of the pressure as a function of mass discussed in Section 5.3.2. In figure 5.10a we fit up to $0.7p_{\mathrm{A}}^{\max}$while in 5.10b we fit up to $0.9p_{\mathrm{A}}^{\max}$. It is straightforward from the plot that the fitting obtained using the experimental data up to $0.7p_{\mathrm{A}}^{\max}$ is better than the fitting using experimental data up to $0.9p_{\mathrm{A}}^{\max}$, with a larger R^2 (0.999 for $0.7p_{\mathrm{A}}^{\max}$ and 0.994 for $0.9p_{\mathrm{A}}^{\max}$). From the fitting we can obtain the value for the capillary pressure and permeability. In the fitting shown in figure 5.10a we obtained the capillary pressure is 15500Pa and permeability is 0.022darcy. In the fitting shown in figure 5.10b we obtained the capillary pressure is 15200Pa and permeability is 0.026darcy. We will discuss more details about the fitting with solutions in section 5.4.3.

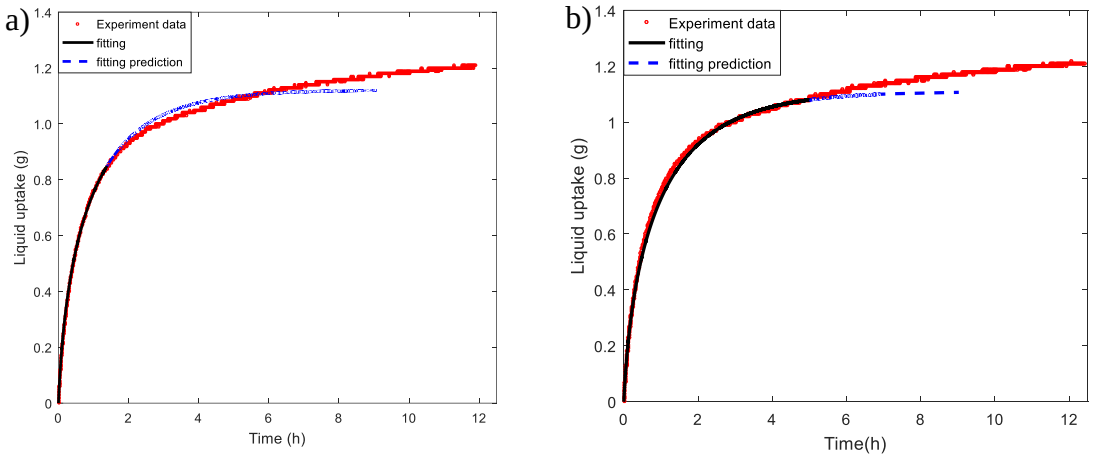

Figure 5.10 Fitting curves for 10μm glass beads and PDMS using the weight solution. Red dots are data collected from the experiment. Black line is the fitting curve using the derived solution (Equation 3.12). The blue dashed line represents the weight predicted by the fitting. a): fit up to $0.7p_{\mathrm{A}}^{\max}$, R^2=0.999. b) fit up to $0.9p_{\mathrm{A}}^{\max}$, R^2=0.994.

5.4.2 Fitting with pressure solution

Since there are limitations in the resolution of scale in cases when the liquid uptake is very small (less than 0.5g), we can use the pressure measurements for a better resolution. In Section 3.4 we obtained an implicit solution in terms of the pressure differential as a function of time for the capillary rise process in a closed column,

$$A_2 \ln\frac{p_0}{p_0+p} + \frac{A_2 p}{p_0+p} - C_2 p_1 \ln(1-\frac{p}{p_1}) + (C_2 p_2 + D_2)\ln(1-\frac{p}{p_2}) = \frac{\kappa}{\mu\varphi p_0 (H-h_0)} t \tag{3.21}$$

We can thus use this solution to fit the experimental data and determine the effective capillary pressure and the permeability. Figure 5.11 shows an example of the fittings for $10\mu m$ and $45\mu m$ glass beads with PDMS.

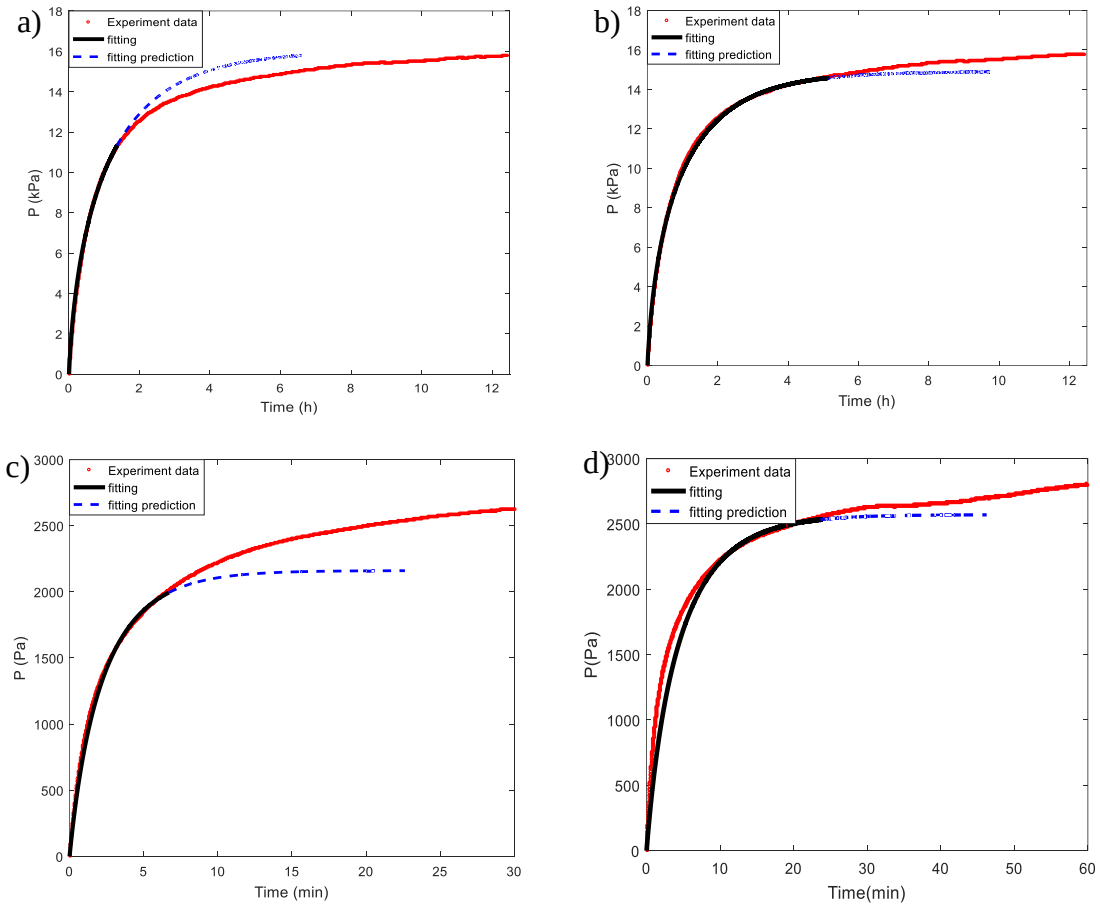

Figure 5.11 Fitting curves for 10μm and 45μm glass beads with PDMS using the pressure solution. Red dots are collected from the experiment. Black line is the fitting curve using the derived solution. The blue dash line represents the pressure predicted by the fitting. (a): $10\mu m$ glass beads, fit up to $0.7p_{\mathrm{A}}^{\max}$, R^2 =0.999 ; (b): $10\mu m$ glass beads, fit up to $0.9p_{\mathrm{A}}^{\max}$, R^2 =0.998; (c) $45\mu m$ glass beads, fit up to $0.7p_{\mathrm{A}}^{\max}$, R^2 =0.994; (d): $45\mu m$ glass beads, fit up to $0.9p_{\mathrm{A}}^{\max}$, R^2 =0.986.

Figure 5.11a and b present data from an experiment with $10\mu m$ glass beads, c and d correspond to an experiment with $45\mu m$ glass beads. We fit the experiment up to $0.7p_{\mathrm{A}}^{\max}$ and $0.9p_{\mathrm{A}}^{\max}$, same as we did with the fittings of weight solution. In 5.11b and d we fit up to $0.7p_{\mathrm{A}}^{\max}$, it is straightforward to see that the fit is in better agreement with the experiments than the fit up to $0.9p_{\mathrm{A}}^{\max}$ shown in figure 5.11a and c. This difference is more noticeable for $45\mu m$ glass beads. In addition, the fitting obtained in the experiments with $45\mu m$ glass beads are not as good as the fitting obtained with $10\mu m$ glass beads. We will discuss in the following section that a different range of pressures should be used for fitting with $45\mu m$ glass beads.

From the fitting we are able to determine the capillary pressure and the permeability with PDMS at $0.7p_{\mathrm{A}}^{\max}$ and $0.9p_{\mathrm{A}}^{\max}$. We first characterize $10\mu m$ glass beads, the results are summarized in Table 5.3. The value of the capillary pressure obtained by fitting up to $0.7p_{\mathrm{A}}^{\max}$ is slightly lower than that obtained by fitting up to $0.9p_{\mathrm{A}}^{\max}$. The capillary pressure value obtained at $0.9p_{\mathrm{A}}^{\max}$ is also lower than the advancing pressure $p_{\mathrm{A}}^{\max}$ measured in the experiments. This difference is again due to the heterogeneity of the porous media. During the advancing process, the larger pores with a smaller capillary pressure value have already been filled at a lower pressure, while the liquid is still filling up those smaller pores whose capillary pressure is higher. The advancing pressure measured in experiments is static, it represents the capillary pressure of these smaller pores. However, the capillary pressure obtained by fitting is an *effective pressure* $p_{\mathrm{c\_eff}}$ that represents pores of different sizes. From the effective capillary pressure, if we assume the $\cos(\theta_{\mathrm{PDMS}}) = 1$, we obtain an *effective radius* r_{eff} of the porous media from the Laplace equation. The results are summarized in Table 5.3. The effective radius is larger than the advancing radius obtained

by static measurements in Table 5.2. Specifically, the effective radius obtained by fitting the experimental data up to $0.7p_{\mathrm{A}}^{\max}$ is larger than that obtained by fitting up to $0.9p_{\mathrm{A}}^{\max}$, since at $0.9p_{\mathrm{A}}^{\max}$ the liquid is penetrating into those smaller pores.

Then we shall consider the permeability. Similar to the capillary pressure, the permeability obtained in the fitting is also an *effective permeability* κ_{eff}. The effective permeability obtained by fitting up to $0.7p_{\mathrm{A}}^{\max}$ is slightly higher than that obtained by fitting up to $0.9p_{\mathrm{A}}^{\max}$. As we discussed, the liquid is only filling the smaller spaces at $0.9p_{\mathrm{A}}^{\max}$, consequently, the effective permeability is lower.

Fitting range	$p_{\mathrm{c\ eff}}(Pa)$	$r_{\mathrm{eff}}(\mu m)$	κ_{eff} (darcy)
$0.7p_{\mathrm{A}}^{\max}$	15700 ± 500	2.6 ± 0.1	0.027 ± 0.006
$0.9p_{\mathrm{A}}^{\max}$	16000 ± 800	2.5 ± 0.1	0.022 ± 0.004
Static measurement	17000 ± 900	2.4 ± 0.1	NA

Table 5.3 The effective capillary pressure, the corresponding effective pore radius and the effective permeability obtained by fittings for PDMS with 10 μm glass beads using the pressure solution, fitting range: $0.7p_{\mathrm{A}}^{\max}$ and $0.9p_{\mathrm{A}}^{\max}$. The static measurements from the advancing process are listed for reference.

As of now we will not characterize that for $45\mu m$ glass beads because of the poor fit when fitting up to $0.7p_{\mathrm{A}}^{\max}$ and $0.9p_{\mathrm{A}}^{\max}$, as indicated in figure 5.11. Since the R^2 values are 0.994 and 0.984, respectively, the fit is not good enough. It would be misleading to use these poor fittings to obtain values for capillary pressure and permeability. They will be determined in the next section after we obtain an appropriate fitting range by considering the goodness of the fit over different pressure ranges and comparing early and intermediate stage solutions.

5.4.3 Pressure fitting at different imbibition stage

In the previous section, we observed that, the agreement obtained by fitting the experiments up to a pressure differential equal to $0.7p_{\mathrm{A}}^{\max}$ and $0.9p_{\mathrm{A}}^{\max}$ are not very good in $45\mu m$ glass beads. A greater heterogeneity in the porous media is believed to be responsible for the poor fit. While for porous media packed with $45\mu m$ glass beads, the dynamics when the pressure differential is equal to $0.7p_{\mathrm{A}}^{\max}$ and $0.9p_{\mathrm{A}}^{\max}$ is significantly different from the early and intermediate stage when the pressure is relatively low. A different pressure range should be used to obtain the effective capillary pressure and permeability. In this section, we will study the early and intermediate stage of the imbibition and compare them with the late stage.

We shall first look at the early stage of the imbibition process. In Section 3.5 we derived a modified Washburn solution for the initial part of the experiment,

$$\frac{h_0}{K}p + \frac{p^2}{2} = \frac{\kappa p_{\mathrm{c}}}{\mu\varphi K^2}t \tag{3.30}$$

We note that there were three assumptions made in order to obtain the modified Washburn solution: (1) the hydrostatic pressure is negligible; (2) p is negligible comparing to p_0 so the liquid front h depends linearly on the pressure differential p, $h = Kp$, where K is a constant $K = (H - h_0)/p_0$; and (3) the pressure differential is significantly small comparing to $p_{\mathrm{A}}^{\max}$. To ensure these three assumptions are valid, in the fittings we only use the data up to $0.1p_{\mathrm{A}}^{\max}$. Examples of the fitting using the $0.1p_{\mathrm{A}}^{\max}$ from experiments using $10\mu m$ and $45\mu m$ glass beads with PDMS are presented in figure 5.12a and 5.12b, respectively. It is clear in figure 5.12 that during this time, the experimental curve and the fitting using the modified Washburn solution are in good agreement.

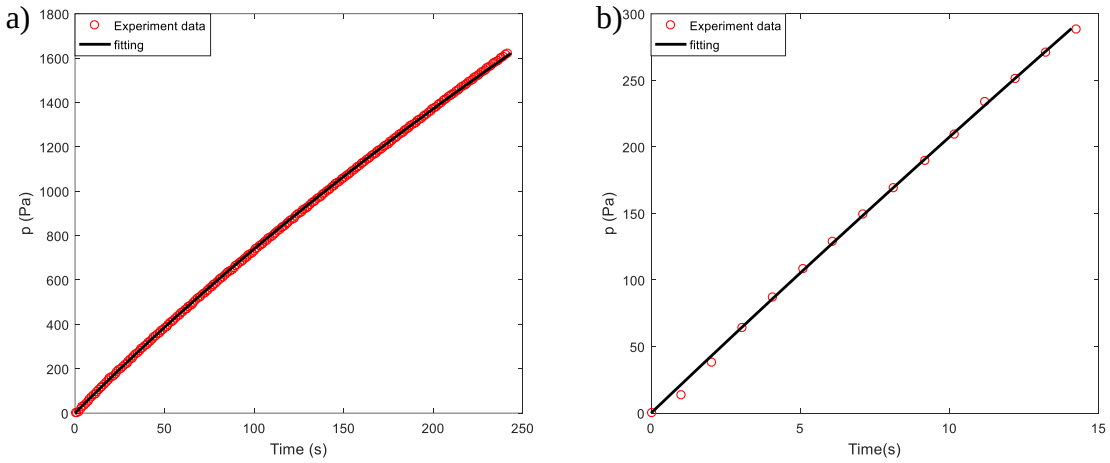

Figure 5.12 The fitting of pressure vs time using the modified Washburn solution for experiment with PDMS. (a): 10μm glass beads, (b): 45μm glass beads. Only the data before pressure reaches $0.1p_{\mathrm{A}}^{\max}$ were used. During this range, the pressure term $\left(\frac{h_0}{K}p+\frac{p^2}{2}\right)$ is proportional to the penetration time.

In the modified Washburn solution (equation 3.30), $K=(H-h_0)/p_0$ is a constant. The two unknown independent parameters, that is the permeability and the capillary pressure, act together as a single factor, which can be obtained from the slope $\frac{\kappa p_{\mathrm{c}}}{\mu\varphi K^2}$. We can only obtain the combination of them from the slope of the pressure differential as a function of penetration time. In order to estimate the permeability, we use the advancing pressure $p_{\mathrm{A}}^{\max}$ measured in experiments to obtain the permeability during the initial stage of the capillary rise from the Washburn slope, the values are summarized in Table 5.4.

Wetting liquid	10μm glass beads	45μm glass beads
PDMS $\kappa(darcy)$	0.021 ± 0.004	0.20 ± 0.10

Table 5.4 Permeability obtained by fitting the experimental data using the modified Washburn solution for PDMS with 10μm and 45μm glass beads.

We compare the permeability obtained from fitting the experimental data up to a pressure differential equal to $0.1p_{\mathrm{A}}^{\max}$ with that obtained using the full solution to fit up to $0.7p_{\mathrm{A}}^{\max}$ and $0.9p_{\mathrm{A}}^{\max}$ in Figure 5.13. We observe that in 10μm glass beads, the permeability obtained by modified Washburn solution is similar to that obtained with full solutions ($p>0.05$). Specifically, the permeability obtained using the modified Washburn solution is

closer to the value obtained by fitting experiments up to $0.9p_A^{max}$. As we discussed in section 5.2, because of the heterogeneity of the porous media, the capillary pressure obtained from fitting the experiments up to a pressure differential equal to $0.9p_A^{max}$ is closer to the advancing pressure p_A^{max}. This advancing pressure is also used to obtain the permeability from the Washburn fittings, which is why this permeability is closer to the permeability obtained by fitting up to $0.9p_A^{max}$. Again, for $45\mu m$ glass beads we will discuss the results after identifying an appropriate fitting range and using that range to obtain the effective permeability.

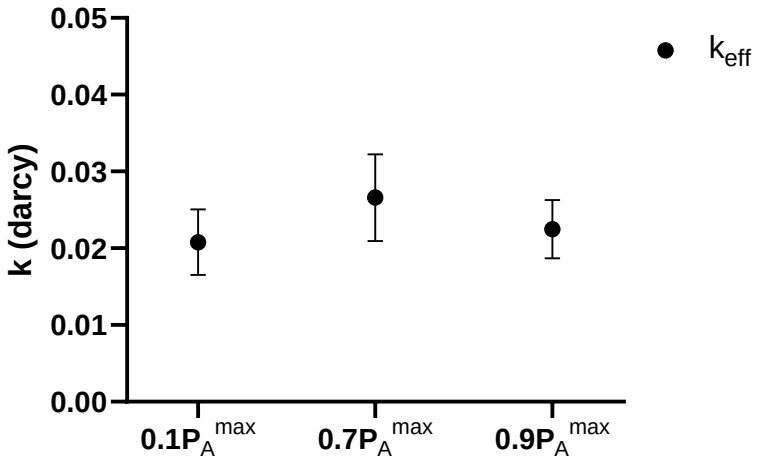

Figure 5.13 Permeability obtained by fitting with modified Washburn solution($0.1p_A^{max}$) and full pressure solution ($0.7p_A^{max}$ and $0.9p_A^{max}$) for experiments between $10\mu m$ glass beads with PDMS.

Since the limitation of using the initial imbibition stage is that the individual values of the effective permeability and capillary pressure cannot be determined, we focus on an intermediate stage. This intermediate imbibition region should therefore be a region where we can use the full solution to determine the permeability and the capillary pressure, but before the pressure is too large and the liquid only fills in the very small pores. In such region where we can distinguish the permeability and the capillary pressure in the fitting, the Washburn solution and the full solution must be different from each other. We shall

first determine this region for the case of $10\mu m$ glass beads and PDMS. In order to determine this region in figure 5.14 we present the Washburn solution that was obtained by fitting the experimental data up to $0.1p_{\mathrm{A}}^{\max}$, together with the full solution obtained by fitting the experiments up to $0.4p_{\mathrm{A}}^{\max}$. It will become clear later why the value of $0.4p_{\mathrm{A}}^{\max}$ was used. Note that although the fittings are performed using the data up to $0.1p_{\mathrm{A}}^{\max}$ and $0.4p_{\mathrm{A}}^{\max}$, we present the entire solution up to $p_{\mathrm{A}}^{\max}$.

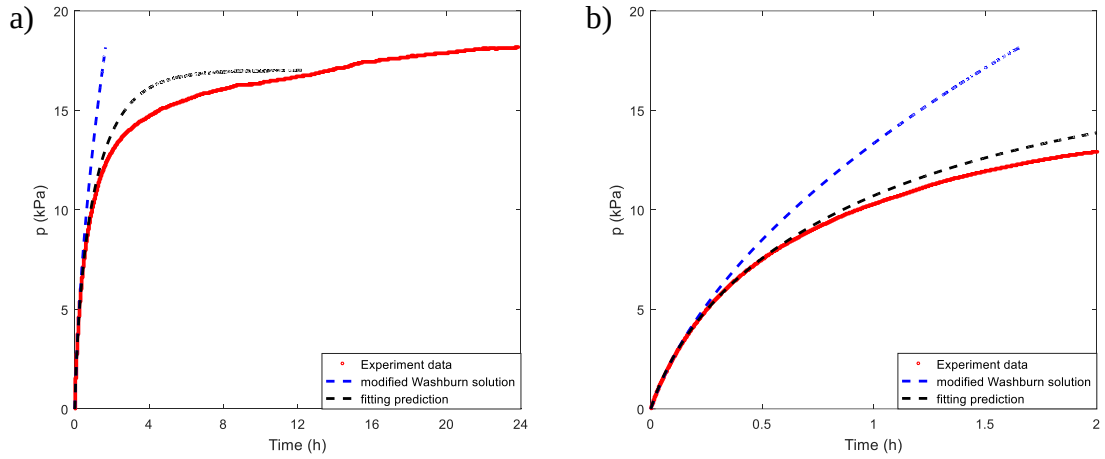

Figure 5.14 Plot of the pressure differential over time using fittings with different solutions. The red curve is data collected in an experiment between $10\mu m$ glass beads and PDMS. The blue dashed line is the pressure curve predicted by fitting with the modified Washburn solution. The black dashed line is the pressure predicted by the full solution. a) the entire experiment, b) a close up look of the first 2h of a).

In the experiment shown in figure 5.14, the advancing pressure is 18000Pa. From figure 5.14b we observe that up to 7000Pa, there is little difference between both solutions and the experiment, meaning that up to this pressure, it is not possible to accurately determine two independent parameters, κ and p_{c}, from the best fit to the experimental curve, as the full solution is similar to a Washburn solution with a single parameter. As a result, we are not able to determine the effective κ for pores filled at this region because the effective p_{c} is unknown. Similarly, we cannot determine the effective pressure in this range, because the permeability is not known from an independent measurement. However, for pressures

larger than 7000Pa, the Washburn solution starts to deviate from both the full solution and the experimental data. In this region when the pressure exceeds 7000Pa we are able to determine both κ and the p_c separately by fitting with the full solution. The full solution eventually deviates from the experimental curve because the effective capillary pressure obtained by fitting the experimental data up to $0.4p_A^{max}$ is 17000Pa, it is lower than the advancing pressure p_A^{max}=18000Pa.

We are interested in understanding and to be able to systematically determine this intermediate region where we can separate κ and p_c in the fitting for arbitrary experiments. When κ and p_c can be distinguished, the Washburn fitting will deviate from the experiments. In figure 5.15 we present a measure of this deviation obtained by fitting the experimental data up to a pressure differential equal to 0.1, 0.2, 0.3, 0.4, 0.5, 0.6, 0.7, 0.8, $0.9p_A^{max}$. The deviation is measured by the difference between the pressure predicted by the fitting and the experimental pressure differential,

$$\text{deviation}=\frac{1}{n}\sum_{i=1}^{n}\sqrt{\left(\pi_{\text{fit}}^{*}-\pi_{\text{exp}}^{*}\right)^{2}} \tag{5.2}$$

Here we use the normalized pressure $\pi^* = p/p_A^{max}$. Note that in chapter 4 the pressure is normalized by the capillary pressure p_c while here it is normalized by the maximum pressure p_A^{max} measured at the end of the advancing process.

The average value of this deviation obtained from fitting the experimental data up to a pressure differential ranging from $0.1p_A^{max}$ to $0.9p_A^{max}$ is presented in figure 5.15. In figure 5.15a the deviation is plotted in a linear scale while in figure 5.15b a logarithm scale is used to for convenience. The deviation obtained from fitting with the Washburn solution is marked in blue color and the deviation obtained by fitting with the full solution is marked

in red. We use this plot and a threshold value 0.01 to determine the lower and upper limits of the intermediate region. The lower limit can be determined from the fitting with the modified Washburn solution, marked in blue. It is clear from figure 5.15a that the error starts to increase significantly after $0.4p_{\mathrm{A}}^{\max}$ and the value is greater than the threshold 0.01. Prior to $0.4p_{\mathrm{A}}^{\max}$, the deviation of the fitting with modified Washburn solution is small, suggesting that the solution and the experiment agrees well. We call this region the Washburn region, or early imbibition and marked it grey in figure 5.15. Within this region, κ and p_{c} cannot be distinguished from the fitting. Only after reaching $0.4p_{\mathrm{A}}^{\max}$ we can use the full solution to fit with the experiments and obtain individual values for κ and p_{c}. In the experiment shown in figure 5.14, the advancing pressure is $p_{\mathrm{A}}^{\max}$ =18000Pa, accordingly, $0.4p_{\mathrm{A}}^{\max}$=7200Pa. In Figure 5.15b we observe that at around 7000Pa the deviation of the Washburn curve is very obvious. These two values are close, suggesting that choosing $0.4p_{\mathrm{A}}^{\max}$ as the starting point for the intermediate stage is reasonable.

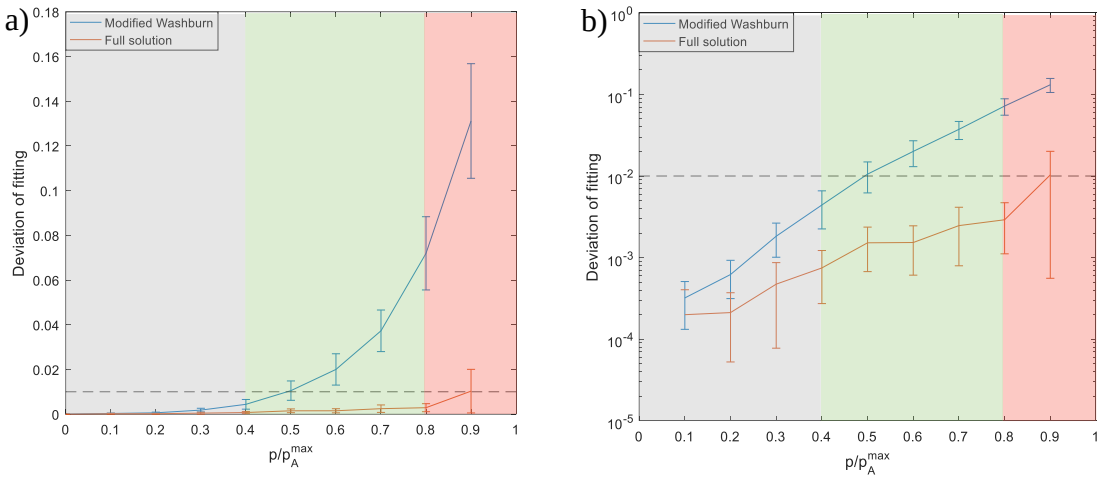

Figure 5.15 The deviation of the fitting from experiments using modified Washburn solution (blue) and the full solution (red) obtained at different pressure ranges for 10μm glass beads with PDMS. The deviation is calculated by Equation 5.2. The grey region is the Washburn region, the green region is the intermediate region and the red region is the final region. a): the deviation is presented in linear scale, b) the deviation is presented in logarithm scale. The dashed line is the threshold value (deviation =0.01).

The upper limit of the intermediate stage can be obtained from the deviation of the full solution, marked in red color. Using the same threshold 0.01 (dashed line) we found the upper limit is $0.8p_{\mathrm{A}}^{\max}$. In figure 5.15b where the deviation is plotted in logarithm scale, it is straightforward that the trend of how the deviation increases changes at $0.8p_{\mathrm{A}}^{\max}$. This is the upper limit of the intermediate region. After passing this region, the liquid only fills in the small pores and the dynamics will no longer follow the full solution. This is the reason why the deviation in the best fit of the experimental data obtained with the full solution increases significantly after $0.8p_{\mathrm{A}}^{\max}$. In figure 5.15b there is an obvious increase in the slope of the red curve for pressures higher than $0.8p_{\mathrm{A}}^{\max}$. We call this region the late imbibition region and marked it in red in figure 5.15. To sum up, in figure 5.15 we observe that the intermediate region for $10\mu m$ glass beads with PDMS is between $0.4p_{\mathrm{A}}^{\max}$ and $0.8p_{\mathrm{A}}^{\max}$. Within this range the full solution can be used to determine the effective value of κ and p_{c}. For pressures above $0.8p_{\mathrm{A}}^{\max}$, the experimental curve cannot be fitted well by the full solution. In this region, the dynamics is dominated by the heterogeneity of the porous media. In section 5.4.2 we obtain the effective values of κ and p_{c} by fitting the experimental data up to a pressure differential equal $0.7p_{\mathrm{A}}^{\max}$, this range falls within the intermediate region determined above.

We shall then determine the intermediate region for experiments between $45\mu m$ glass beads with PDMS. Figure 5.16 shows the plots of the deviation of the fitting using the modified Washburn solution (blue) and the full solution (red) at different pressure ranges. In figure 5.16a the deviation is presented in linear scale while in figure 5.16b it is presented in logarithm scale. Using the same threshold 0.01 (dashed line) on the deviation of the fitting using the Washburn solution we determine the lower limit of the intermediate region

is $0.2p_{\mathrm{A}}^{\max}$. From the deviation of the fitting using the full solution we obtain that the upper limit of the intermediate region is $0.4p_{\mathrm{A}}^{\max}$. It is straightforward in figure 5.16b that the slope of the red curve increases after reaching $0.4p_{\mathrm{A}}^{\max}$. The change in the slope suggests the deviation of the fitting with the full solution increases significantly. Combining the blue curve and the red curve, we obtain the intermediate region for experiments between $45\mu m$ glass beads with PDMS is between $0.2p_{\mathrm{A}}^{\max}$ and $0.4p_{\mathrm{A}}^{\max}$.

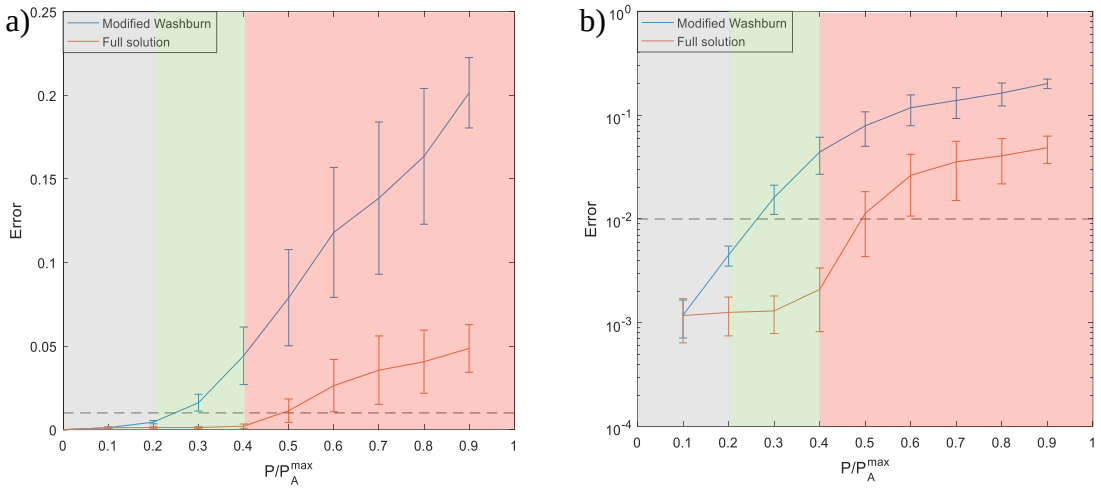

Figure 5.16 The development of the deviation of the fitting by modified Washburn solution (blue) and the full solution (red) obtained by fitting the experimental data up to pressure differential at 0.1, 0.2, 0.3, 0.4, 0.5, 0.6, 0.7, 0.8, $0.9p_{\mathrm{A}}^{\max}$ for $45\mu m$ glass beads with PDMS. The deviation is calculated by Equation 5.2. The grey region is the Washburn region, the green region is the intermediate region and the red region is the final region. a): the deviation is presented in linear scale, b) the deviation is presented in logarithm scale. The dashed line is the threshold value (deviation =0.01).

In figure 5.17 we present the average value of $p_{\mathrm{c\_eff}}$ and κ_{eff} obtained from the fitting with the full solution. The data obtained within the grey region is not included because they are significantly different from the others. As we mentioned before, within this region they are combined as one parameter and their individual values cannot be determined. For $45\mu m$ glass beads, the effective κ value obtained by fitting experimental data up to pressure differential equal to $0.3p_{\mathrm{A}}^{\max}$ is (0.48 ± 0.20)darcy. Recall from section 5.4.2 the effective value for the permeability of porous media packed with $10\mu m$ glass beads obtained by

fitting with the full solution for pressure differential up to $0.7p_{\mathrm{A}}^{\max}$ is (0.027 ± 0.006)darcy. The ratio between the permeability value of two porous media is (18 ± 8). According to the Kozeny Carman equation, this ratio is about 20. The result obtained from fitting experiments up to $0.3p_{\mathrm{A}}^{\max}$ for porous media packed with $45\mu m$ glass beads is more reasonable compared to the values obtained by fitting up to $0.7p_{\mathrm{A}}^{\max}$. It also suggests that choosing from $0.2p_{\mathrm{A}}^{\max}$ to $0.4p_{\mathrm{A}}^{\max}$ as the intermediate region is acceptable.

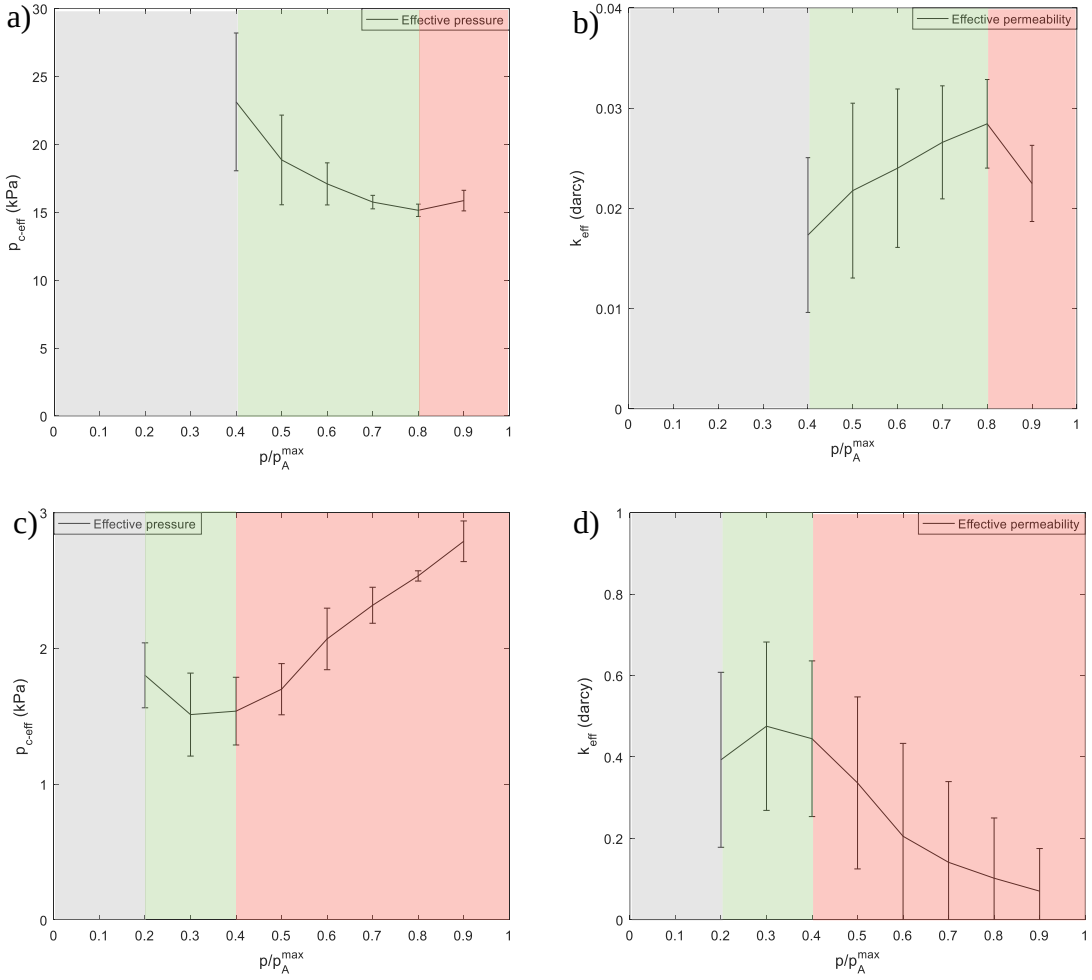

Figure 5.17 The average value of a) $p_{\mathrm{c\_eff}}$ for $10\mu m$ glass beads; b) κ_{eff} for $10\mu m$ glass beads; c) $p_{\mathrm{c\_eff}}$ for $45\mu m$ glass beads and d) κ_{eff} for $45\mu m$ glass beads. The results were obtained using the full solution to fit with experimental data at different pressure ranges.

Table 5.5 summarizes the effective values of the capillary pressure, the corresponding pore size and the permeability obtained within the intermediate region of the porous media. For

10 μm glass beads, we use the data up to a pressure differential equal to $0.7p_{\mathrm{A}}^{\max}$. For 45 μm glass beads, we use the data up to a pressure differential equal to $0.3p_{\mathrm{A}}^{\max}$. It should be pointed out that the ratio between the effective radius is about 10 times, although the particle size ratio is only 5 times. Additionally, in 45 μm glass beads, the effective capillary pressure obtained by fitting up to $0.3p_{\mathrm{A}}^{\max}$ is only half of the advancing pressure $p_{\mathrm{A}}^{\max}$ measured at the end of the advancing process. This large difference is due to the broader pore size distribution in 45 μm glass beads.

particle	$p_{\mathrm{c\ eff}}(Pa)$	$r_{\mathrm{eff}}(\mu m)$	κ_{eff} (darcy)
10 μm glass beads	15700 ± 500	2.6 ± 0.1	0.027 ± 0.006
45 μm glass beads	1500 ± 300	27 ± 5	0.48 ± 0.20

Table 5.5 The effective capillary pressure, pore size and permeability obtained by fitting the experimental data using the full solution for PDMS with 10μm and 45μm glass beads. The results with 10μm glass beads were obtained using the data up to $0.7p_{\mathrm{A}}^{\max}$, while for 10μm glass beads the results were obtained using the data up to $0.3p_{\mathrm{A}}^{\max}$.

During the initial and intermediate stage of the imbibition, all the large and small pores are filled. We call this region the *bulk imbibition*. The effective capillary pressure during this time represents an average value of these pores. While during the final stage, the connectivity between the pores changes. Only the very small pores can be filled and they correspond to the advancing pressure $p_{\mathrm{A}}^{\max}$ that is measured at the end of the advancing process. For a porous media with a wide pore size distribution, the size difference between the r_{eff} during the bulk imbibition and the r_{eff} during final imbibition is significant. Consequently, the $p_{\mathrm{A}}^{\max}$ will be significantly different from the effective capillary pressure in the intermediate region. In fact, in this case with the 45μm glass beads the $p_{\mathrm{A}}^{\max}$ is almost twice of the $p_{\mathrm{c\_eff}}$. In section 5.2 the ratio between the advancing radius obtained from the advancing pressure $p_{\mathrm{A}}^{\max}$ is 5.4 ± 0.3. This ratio is more similar to the ratio between the particle size. During this time the liquid fills in the very small pores in both 10μm and

$45\mu m$ glass beads. Considering the different pore size distribution, it is not surprising that the ratio between the pore radius obtained at $0.3p_{\mathrm{A}}^{\max}$ for $45\mu m$ glass beads and the pore radius obtained at $0.7p_{\mathrm{A}}^{\max}$ for $10\mu m$ glass beads is 10 times.

The broader pore distribution in $45\mu m$ glass beads is also the reason for the difference in the intermediate region. Since the value of the $p_{\mathrm{c\_eff}}$ obtained during this region is only half of the advancing pressure $p_{\mathrm{A}}^{\max}$. While in $10\mu m$ glass beads the $p_{\mathrm{c\_eff}}$ is very similar to $p_{\mathrm{A}}^{\max}$ because the pore size is more homogeneous. Accordingly, the value of the lower and upper limits for the intermediate region in $10\mu m$ glass beads is also twice of that in $45\mu m$ glass beads. It should be pointed out that this relation is only coincidental and it is not necessarily true for experiments with other materials.

5.5 Conclusions

In this chapter we presented the experimental results with the model system of glass beads and PDMS. We first presented the curves illustrating the development of the pressure and the liquid weight during the advancing and receding processes. From the "staircase-like" behavior of the pressure curve during the receding process, we concluded that the porous media is heterogeneous. At the beginning of the advancing process, the liquid is filling all the available pores. As it advances and the pressure reaches the advancing pressure for some larger pores, those large pores above them will not be filled when the liquid front keeps advancing. Only the smaller pores can be filled at high pressure. During the receding process, the liquid first recedes in the larger pores. The smaller pores are evacuated later. When more pores are emptied and they form a channel that connects the top of the porous

media to the bottom, air will percolate. We introduced three pressure terms to characterize the porous media: the advancing pressure $p_{\mathrm{A}}^{\max}$, the receding pressure $p_{\mathrm{R}}^{\min}$ and the bubbling pressure $p_{\mathrm{B}}^{\max}$. The static characterization is based on these pressures measured in the experiment. Since the contact angle for PDMS is zero, from the Laplace equation we can determine the corresponding advancing, receding and bubbling radii. There are two groups of glass beads used in the experiments: $10\mu m$ and $45\mu m$ glass beads. By comparing the ratio of the advancing, receding and bubbling radii between the two particle sizes we concluded that their pore size distribution is different. There are a larger portion of smaller pores in the porous media packed with $10\mu m$ glass beads.

Then, before presenting the dynamic characterization which uses the analytical solution derived in chapter 3 to fit the experimental results, we discussed the estimation of the effective column length H. We demonstrated that using the linear approximation to estimate H will lead to large error in cases where the capillary pressure reaches values as high as $0.5\,p_0$. Using the full pressure dependence to fit the data up to $0.9\,p_{\mathrm{A}}^{\max}$ is recommended to obtain the effective column height H.

In the dynamic characterization we used the analytical solutions derived in chapter 3 to fit the data from the experiments. We demonstrated that both the weight solution and the pressure solution fit the experiments. In cases where the liquid uptake is small, using the pressure solution provides better resolution. By comparing the fitting up to $0.7p_{\mathrm{A}}^{\max}$ and $0.9p_{\mathrm{A}}^{\max}$, we determine the effective capillary pressure, the corresponding effective radius and the permeability of the porous media during different stages of the imbibition for $10\mu m$ glass beads. The values are in accordance with the heterogeneous structure of the porous media. We did not characterize $45\mu m$ glass beads because the fit obtained using data up to

$0.7p_{\mathrm{A}}^{\max}$ and $0.9p_{\mathrm{A}}^{\max}$ was not good. Different pore filling dynamics caused by the greater heterogeneity in the porous media created with $45\mu m$ glass beads is believed to be the reason for the poor fitting obtained for experimental data including pressures up to $0.7p_{\mathrm{A}}^{\max}$ and $0.9p_{\mathrm{A}}^{\max}$. For highly heterogeneous porous media, we need to fit the experimental data in an earlier region to obtain accurate values for κ and p_{c}.

We studied the different stages of the imbibition. In the initial stage of the imbibition, we use the modified Washburn solution derived in section 3.4 to fit the experiments. In this solution, the permeability and the capillary pressure are combined as one parameter, and they cannot be independently determined by the fitting. Although using the advancing pressure $p_{\mathrm{A}}^{\max}$ can provide an estimated value for the permeability obtained from the Washburn fitting, this value is not reliable when the porous media is highly heterogeneous, as in the case of the $45\mu m$ glass beads. In this situation, it would be useful to determine an intermediate region. Within this region the permeability and capillary pressure can be determined independently, yet the liquid has not advanced to the region where it is only filling the smaller pores. To study the different regions of the imbibition process, we presented the deviation from the experiments for fittings using the modified Washburn solution and the full solution for different $p/p_{\mathrm{A}}^{\max}$ regions. We use 0.01 as the threshold to determine the lower and upper limit for the intermediate region. It is observed that for $10\mu m$ glass beads, $p/p_{\mathrm{A}}^{\max}$ <0.4 is the Washburn region where the modified Washburn solution fits nicely yet the κ and p_{c} cannot be determined separately. The pressure range $0.4< p/p_{\mathrm{A}}^{\max} <0.8$ is the intermediate region where the full solution can be used to determine κ and p_{c} individually. The final imbibition occurs when $p/p_{\mathrm{A}}^{\max}$ >0.8, where the liquid is only penetrating in the smaller pores and the dynamics do not follow the full

solution. For $45\mu m$ glass beads, the Washburn region is $p/p_{\mathrm{A}}^{\max} < 0.2$ and final region happens when $p/p_{\mathrm{A}}^{\max} > 0.4$. The broader pore size distribution in $45\mu m$ glass beads is believed to be the reason for this difference in the intermediate region for the two particle groups. After determining the intermediate region, we presented the effective values of the capillary pressure, pore size and permeability obtained within this region for $10\mu m$ and $45\mu m$ glass beads. In the experiments with $45\mu m$ glass beads, the effective capillary pressure obtained at $0.3\,p_{\mathrm{A}}^{\max}$ is only half of the advancing pressure $p_{\mathrm{A}}^{\max}$. This big difference is due to the broad pore distribution. Accordingly, the ratio between the effective pore radius is 10 times of the pore radius obtained at $0.7p_{\mathrm{A}}^{\max}$ in $10\mu m$ glass beads. Since $10\mu m$ glass beads are more homogeneous, the difference between the effective capillary pressure and the advancing pressure is small. This is also the reason for the difference in the intermediate range between the two particle groups. We also compared the ratio of the effective permeability obtained by fitting the full solution within the intermediate range between the two particle groups. The permeability of the porous media packed with $45\mu m$ glass beads is about 20 times greater than the $10\mu m$ glass beads, this is consistent with the Kozeny-Carman equation.

6. Experimental Results: comparison between test and reference liquids

In Chapter 5, the experiments with PDMS were presented and used for the characterization of the pore radius and permeability of columns filled with glass beads. In this chapter, we present complementary experiments in which DI water is the imbibing liquid. We will follow the same characterization methods used in the case of PDMS. First, we use the Laplace equation to study the static measurements. Then we use the pressure solution to characterize the imbibition process dynamically. We will also study the Washburn, intermediate and final stages. In addition to characterize the permeability and capillary pressure of the porous media, we will estimate the contact angle by using the results obtained with PDMS as reference.

6.1 Static characterization: Advancing, receding and bubbling pressure

In figure 6.1 we present the advancing and receding curves for experiments performed using columns filled with 10 and 45μm glass beads. The experimental procedures are the same as the experiments with PDMS. Moreover, the fit up to $0.7p_{\mathrm{A}}^{\max}$, R^2=0.999. The evolution of the pressure and the liquid weight are similar to the plots presented in figure 5.1 for PDMS. During the receding process, there is also the “staircase-like” trend in the pressure curve, suggesting the heterogeneity of the porous media. We have discussed the analogous results in detail in chapter 5, and we will therefore not repeat the same discussion here.

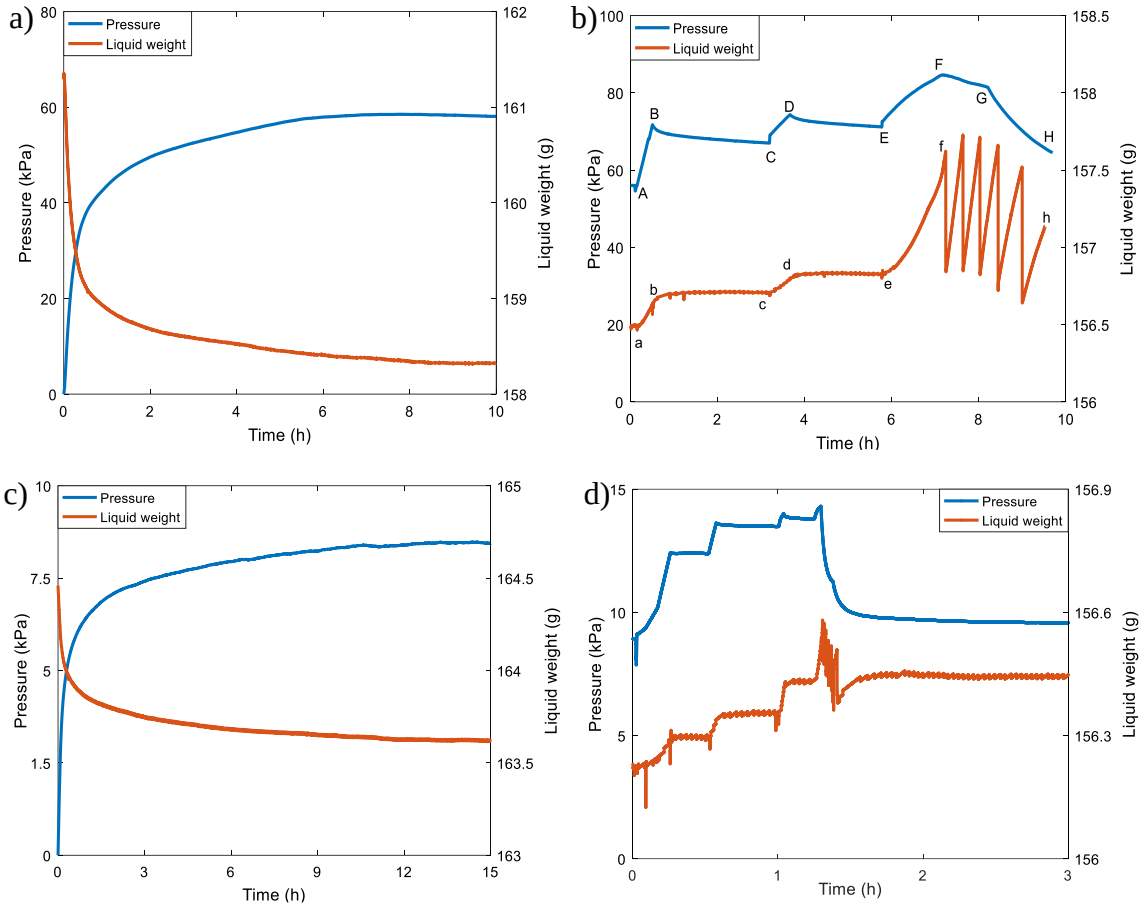

Figure 6.1 The development of the pressure and liquid weight over time for glass beads with DI water. The blue curve is the pressure differential in the column and the red curve is the mass of the liquid left in the bottom container. (a) advancing process of 10μm glass beads, (b) receding process of 10μm glass beads, (c) advancing process of 45μm glass beads, (d) receding process of 45μm glass beads.

From the values of the advancing, receding and bubbling pressure obtained with DI water, we can study the contact angle following the static characterization methods used in section 5.2. If we assume the pore sizes inside the column are the same, independent of the penetrating liquid (either PDMS or DI water in our case), together with the assumption $cos\theta_{\mathrm{PDMS}} = 1$we can obtain the value of the contact angle for DI water from the ratio of the static pressures between the two liquids $p_{\mathrm{DI\ water}}/p_{\mathrm{PDMS}}$. The average values of the static pressure measurements for 10 μm and 45 μm glass beads with DI water are summarized in table 6.1. The values of PDMS from table 5.1 are also listed in the same table for reference.

Solid-liquid	Advancing pressure (Pa)	Receding pressure (Pa)	Bubbling pressure
$10\mu m$ + DI	58600 ± 1200	66700 ± 5800	85700 ± 3700
$10\mu m$ + PDMS	17000 ± 900	18800 ± 1700	27700 ± 2500
$45\mu m$ + DI	7800 ± 1000	12000 ± 1000	14500 ± 500
$45\mu m$ + PDMS	3000 ± 300	3500 ± 400	4300 ± 100

Table 6.1 The advancing, receding and bubbling pressure of $10\mu m$ and $45\mu m$ glass beads with DI water and PDMS.

For $10\mu m$ glass beads, from the advancing pressure we obtain $\cos\theta_{\mathrm{w}}^{\mathrm{adv}} = 0.95 \pm 0.06$. This value suggests the $10\mu m$ glass beads are hydrophilic. From the receding pressure between PDMS and DI water we obtain the receding contact angle for DI water: $\cos\theta_{\mathrm{w}}^{\mathrm{rec}} = 0.94 \pm 0.15$. This value indicates that the $10\mu m$ glass beads are completely wetted by both PDMS and water, there is no hysteresis in contact angle. The capillary pressure hysteresis in DI water is nearly negligible, as the p value from obtained in the t-test for the advancing and receding pressure is greater than 0.05. Same as the case with PDMS, if any, the small capillary pressure hysteresis is a result of the heterogeneity in pore radius within the porous media.

For $45\mu m$ glass beads we obtain the advancing contact angle for DI water: $\cos\theta_{\mathrm{w}}^{\mathrm{adv}} = 0.70 \pm 0.20$. This contact angle is different from the $10\mu m$ glass beads. In addition, the variability for $45\mu m$ glass beads (15-30%) is also greater than that with $10\mu m$ glass beads (5-15%). As discussed in chapter 5, the porous media with $45\mu m$ glass beads is more heterogeneous than the $10\mu m$ glass beads, which leads to a greater variability. From the receding pressure between PDMS and DI water we obtain the receding contact angle for $45\mu m$ glass beads with DI water: $\cos\theta_{\mathrm{w}}^{\mathrm{rec}} = 0.95 \pm 0.10$. The receding angle is zero, same as the $10\mu m$ glass beads. However, the advancing angle is different. The capillary pressure hysteresis for $45\mu m$ glass beads with DI water is a result of both the hysteresis in the contact angle and the pore size distribution. The hysteresis is indicated by the ratio

between the receding pressure and the advancing pressure. For $45\mu m$ glass beads with DI water this ratio is $p_R/p_A = 1.5 \pm 0.2$. The hysteresis in $10\mu m$ glass beads is $p_R/p_A = 1.14 \pm 0.10$, it is smaller than for $45\mu m$ glass beads because it only comes from the heterogeneity of the porous media. Since these two sizes of glass beads come from two different suppliers, the manufacturing process are not the same. Accordingly, the hydrophilicity of the material might be different, leading to the differences in their contact angle with DI water.

Particle size (μm)	$\cos\theta_w^{adv}$	$\cos\theta_w^{rec}$
10	0.95 ± 0.06	0.94 ± 0.15
45	0.70 ± 0.20	0.95 ± 0.10

Table 6.2 The cos values of the advancing and receding contact angle for $10\mu m$ and $45\mu m$ glass beads with DI water. The values are obtained by assuming the same pore radius with PDMS experiments.

6.2 Dynamic Characterization: effective capillary pressure and permeability

6.2.1 Fitting with weight solution

In Figure 6.2 we present the fittings for $10\mu m$ glass beads using the weight solution (equation 3.12) derived in section 3.2. The experiments with $45\mu m$ glass beads are not fitted because the liquid uptake is small (less than 1g, the resolution of the scale is 0.01g). In figure 6.2a we fit the experimental data up to $0.7p_A^{max}$ and in figure 6.2b we fit up to $0.9p_A^{max}$. The fitting at $0.7p_A^{max}$ is better than $0.9p_A^{max}$, with a larger R^2 (0.999 for $0.7p_A^{max}$ and 0.983 for $0.9p_A^{max}$). This trend is analogous to that observed in the experiments performed with PDMS. Later in this chapter we will compare the fitting results obtained for the evolutions of the liquid uptake to those to those obtained for the evolution of the pressure differential.

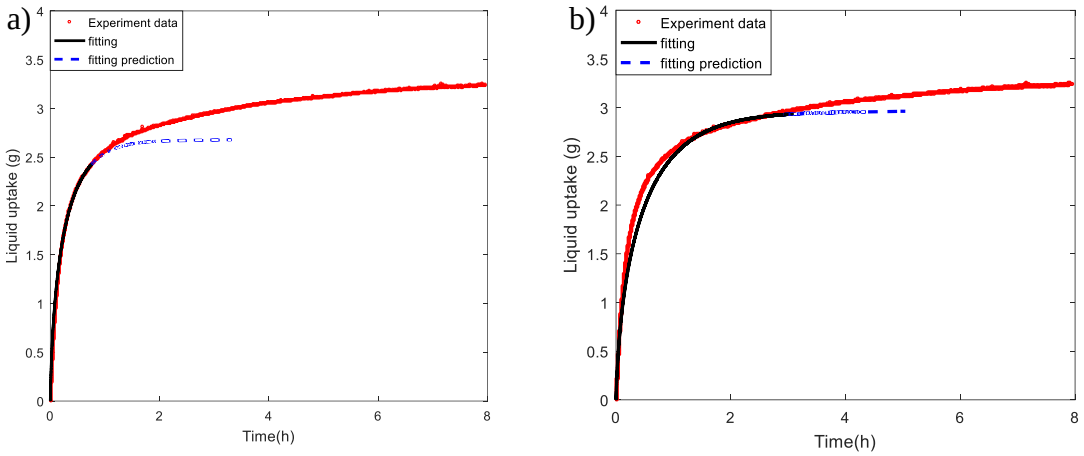

Figure 6.2 Fitting curves for 10μm glass beads with DI water using the weight solution. Red dots are data collected from the experiment. Black line is the fitting curve using the derived solution (Equation 3.12). The blue dashed line represents the weight predicted by the fitting. (a): fit up to $0.7p_{\max}$, R^2 =0. 999; (b): fit up to $0.9p_{\max}$, R^2 =0.983.

6.2.2 Fitting with pressure solution

Now we shall look at the fittings for $10\mu m$ and $45\mu m$ glass beads with DI water using the pressure solution (equation 3.21). The plots are presented in figure 6.3. In figure 6.3a and c we fit up to $0.7p_{\mathrm{A}}^{\max}$, it is obvious that the fit is better than that obtained by fitting up to $0.9p_{\mathrm{A}}^{\max}$ indicated in figure 6.3b and d. The value of R^2 also suggests the fit obtained by fitting up to $0.7p_{\mathrm{A}}^{\max}$ is better than $0.9p_{\mathrm{A}}^{\max}$. This difference is more noticeable for $45\mu m$ glass beads.

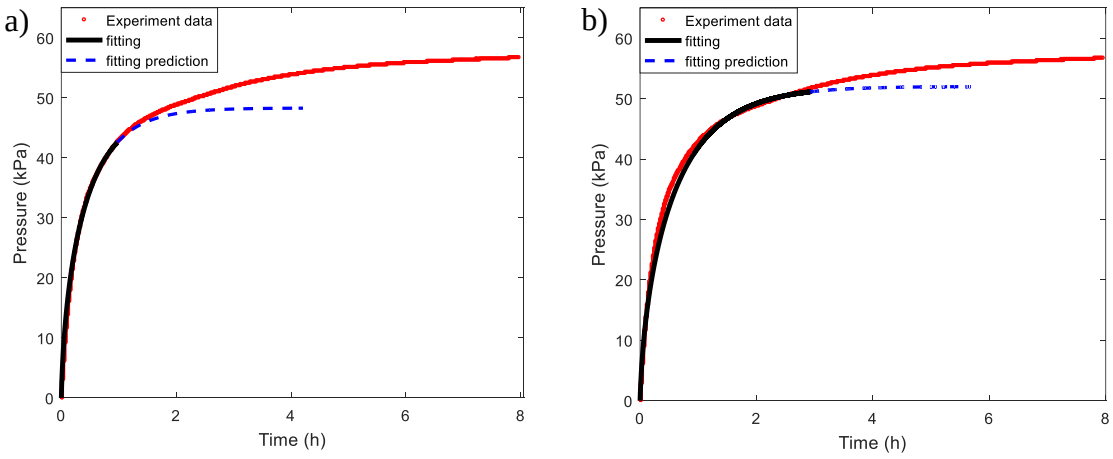

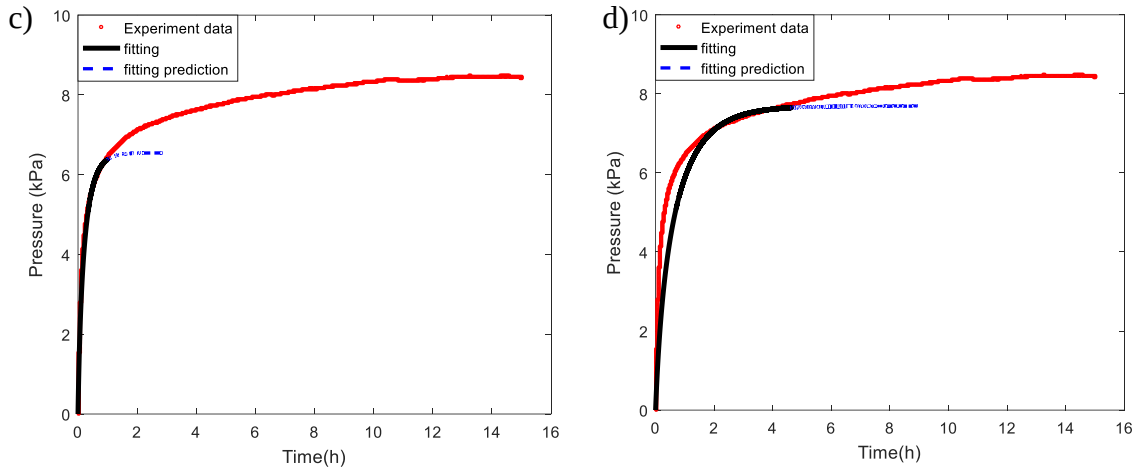

Figure 6.3 Fitting curves for 10μm and 45μm glass beads with DI water using the pressure solution. Red dots are collected from the experiment. Black line is the fitting curve using the derived solution. The blue dash line represents the pressure predicted by the fitting. (a): $10\mu m$ glass beads, fit up to $0.7p_{\mathrm{A}}^{\max}$, R^2 =0.999 ; (b): $10\mu m$ glass beads, fit up to $0.9p_{\mathrm{A}}^{\max}$, R^2 =0.994; (c): $45\mu m$ glass beads, fit up to $0.7p_{\mathrm{A}}^{\max}$, R^2 =0.996; (d): $45\mu m$ glass beads, fit up to $0.9p_{\mathrm{A}}^{\max}$, R^2 =0.956.

The values of the effective capillary pressure and the corresponding contact angle obtained for $10\mu m$ glass beads by the fittings are summarized in table 6.3. Analogous to the case with PDMS, the results of $45\mu m$ glass beads are not listed here because of the bad fit obtained when using the data up to $0.7\,p_{\mathrm{A}}^{\max}$ and $0.9\,p_{\mathrm{A}}^{\max}$. From table 6.3 it is straightforward that the effective p_{c} obtained by fitting up to $0.9p_{\mathrm{A}}^{\max}$ is closer to the advancing pressure $p_{\mathrm{A}}^{\max}$ compared to the effective p_{c} obtained by fitting up to $0.7p_{\mathrm{A}}^{\max}$. This behavior is similar to the case in PDMS, which can be explained by the pore size heterogeneity as in section 5.4.2. The effective $cos\theta$ obtained by fitting the experimental data up to $0.9p_{\mathrm{A}}^{\max}$ is also closer to the value obtained in the static characterization. The value obtained by fitting up to $0.7p_{\mathrm{A}}^{\max}$ is slightly different. When estimating $cos\theta$, it is assumed that the pore size is the same when PDMS and DI water penetrate into the porous media. However, the dynamics of liquid penetration might be different for the two liquids. It is possible when pressure differential equals $0.7p_{\mathrm{A}}^{\max}$, the effective pore radius when PDMS penetrates through is different from that of DI water. While when the pressure

differential equals $0.9p_{\mathrm{A}}^{\max}$, the liquid front is only filling in the small pores and the value of this effective pore radius between the two liquid becomes similar.

Fitting range	PDMS $p_{\mathrm{c\_eff}}(Pa)$	DI water $p_{\mathrm{c\_eff}}(Pa)$	$cos\theta_{\mathrm{w}}$
$0.7p_{\mathrm{A}}^{\max}$	15700 ± 500	46800 ± 2300	0.82 ± 0.05
$0.9p_{\mathrm{A}}^{\max}$	16000 ± 800	54000 ± 1000	0.93 ± 0.05

Table 6.3 The effective capillary pressure and the corresponding cosθ obtained by fittings experiments of $10\mu m$ glass beads with DI water using the pressure solution, fitting range is $0.7p_{\mathrm{A}}^{\max}$ and $0.9p_{\mathrm{A}}^{\max}$.

The effective permeability obtained in the fitting with pressure solution are summarized in table 6.4. Similar to the experiments with PDMS, the value of the effective permeability obtained by fitting the experimental data up to pressure differential equal to $0.7p_{\mathrm{A}}^{\max}$ is higher than the permeability obtained by fitting up to $0.9p_{\mathrm{A}}^{\max}$. But in the case with DI water, this difference is larger. The value of the effective permeability obtained by fitting experiments up to $0.9p_{\mathrm{A}}^{\max}$ is only half of that obtained by fitting up to $0.7p_{\mathrm{A}}^{\max}$. It will be discussed in the following section that $0.9p_{\mathrm{A}}^{\max}$ is the final imbibition region. At this time the liquid only fills in the very small pores, thus the effective permeability decreases.

Fitting range	$10\mu m$+ DI water	$10\mu m$ + PDMS
$0.7p_{\mathrm{A}}^{\max}$	0.018 ± 0.004	0.027 ± 0.006
$0.9p_{\mathrm{A}}^{\max}$	0.009 ± 0.001	0.022 ± 0.004

Table 6.4 . Effective permeability obtained by fittings for DI water and PDMS with $10\mu m$ glass beads using the pressure solution, the fittings are performed using the experimental data up to pressure differential equal to $0.7p_{\mathrm{A}}^{\max}$ and $0.9p_{\mathrm{A}}^{\max}$. The unit for the permeability value is in darcy.

It is worth noticing that the difference between the permeability in DI water and PDMS is also large, especially in the values obtained by fitting the experimental data up to $0.9p_{\mathrm{A}}^{\max}$. When measuring the permeability of a porous media that was saturated by DI water or PDMS, the values are similar in both liquids and they are larger than the effective permeability obtained by fitting. In principle, the permeability is a property of the porous media and is independent of the liquid penetrates through. However, in the capillary rise experiments, as water advances faster in the porous media, there could be more air trapped

when water penetrates through. The trapped air can contribute to the low permeability. However, there is no sufficient data to support this assumption yet.

In figure 6.4 we compare the fitting results obtained by the weight solution (circles) with the pressure solution (squares) for $10\mu m$ glass beads and DI water. In figure 6.4 it is obvious there is no significant difference between the effective capillary pressure and permeability obtained by fitting with weight solution and the pressure solution. We also performed t-test on the values obtained using the two solutions, all the p-value are larger than 0.05 and there is no statistically significant difference between the fitting results obtained by these two solutions. Considering the resolutions of the measurement, the values obtained by pressure solution are preferred.

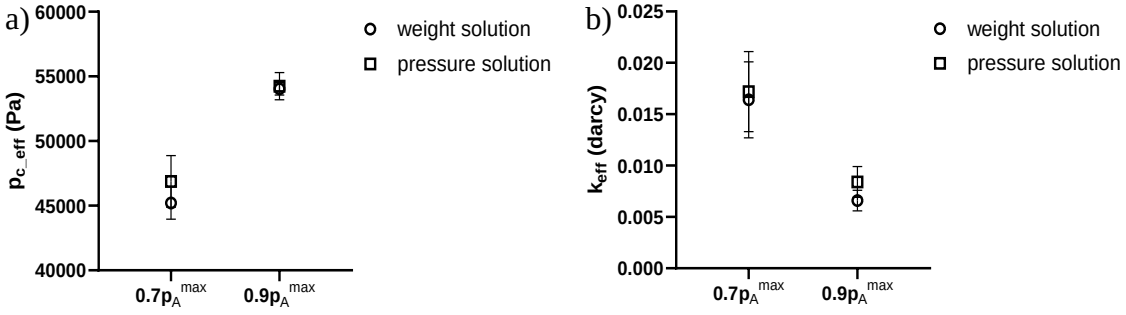

Figure 6.4 The effective p_c and κ obtained by fitting with weight solution and the pressure solution for $10\mu m$ glass beads and DI water. a) effective capillary pressure b) effective permeability.

In general, in the dynamic characterization method for experiments with $10\mu m$ glass beads and DI water, fitting the experimental data up to a pressure differential equal to $0.7p_A^{max}$ using the full pressure solution is recommended to obtain the effective permeability. Indeed, in the next section, we will use the same approach as in chapter 5 to show that the suitable range to fit the experimental data for $10\mu m$ glass beads is up to between $0.6p_A^{max}$ and $0.8p_A^{max}$. The same approach will also be used with $45\mu m$ glass beads.

6.2.3 Pressure fitting at early and intermediate stage

In section 5.4.3 we discussed the fitting with modified Washburn solution for experiments with PDMS to study the early stage of the imbibition. For DI water we can also use this solution to obtain the contact angle value during the beginning of the imbibition. Recall that with the modified Washburn solution we are not able to determine the individual values for the permeability and the capillary pressure through the fittings. We can only obtain the combination of them from the slope of the fitting. Then, by comparing the slope of PDMS and DI water and assuming the same permeability when both liquids penetrate through, we obtain the contact angle for DI water using $cos\theta_{\mathrm{PDMS}} = 1$. Using this method, we obtained a very small value for $cos\theta_{\mathrm{w}}$ in both particle groups. For $10\mu m$ glass beads, $cos\theta_{\mathrm{w}} = 0.27 \pm 0.13$, it is only $1/3$ of that obtained by the fitting with the full solution up to $0.7p_{\mathrm{A}}^{\mathrm{max}}$. For $45\mu m$ glass beads, the difference is even greater, $cos\theta_{\mathrm{w}} = 0.027 \pm 0.02$, it is only $1/25$ of that obtained by the static characterization. At this contact angle value the glass beads would be almost hydrophobic. Yet it is in disagreement with what we observe in the experiments since DI water can easily penetrate into the porous media. This "apparent" contact angle is obtained under the assumption that the permeability is the same for PDMS and DI water. However, this assumption is not true and the permeability is actually different for the two liquids in the initial stage. This is one of the major findings in this work. In some previous works, only the dynamic contact angle was considered as the reason for the disagreement with the Washburn equation [93]. The different effective permeability value depending on the liquid may also contribute to the discrepancy.

To estimate a more realistic contact angle by fitting with the modified Washburn solution, we use the permeability obtained by the fittings with full solution to calculate a "corrected"

contact angle from the slope of the modified Washburn fittings for 10μm glass beads. This "corrected angle" is $cos\theta_{\mathrm{w}} = 0.87 \pm 0.06$, it is similar to the contact angle obtained from the fitting with full solution, where the permeability and the capillary pressure are determined individually. It is worth noticing that, this value may not be the actual permeability either, since the permeability may not be constant throughout the imbibition process. This value will not exceed the permeability when the porous media is fully saturated. From the permeability value of a fully saturated porous media, we can estimate a boundary value for the dynamic contact angle. For 10μm glass beads, this boundary value is $cos\theta_{\mathrm{w}}$>0.4. The measurement of the permeability is in the Appendices.

As we discussed in section 5.4.3, the permeability value obtained using the Washburn solution to fit the experimental data in the initial stage is not very reliable because the value of the corresponding p_{c} is unknown. Similar to the case with PDMS, it is necessary to identify the region of the Washburn, intermediate and final imbibition and use the intermediate region to estimate the effective permeability of the experiments with DI water. Following the same methods used in section 5.4.3, we plot the deviation of the fitting using the modified Washburn and the full solution at different pressure ranges. The deviation is calculated using equation 5.2. We first present the case of 10μm glass beads with DI water in figure 6.5. In figure 6.5a we present the values of the deviation in linear scale and in figure 6.5b we present it in logarithm scale. Each point is obtained by a fitting that uses the experimental data up to a pressure differential p such that $p/p_{\mathrm{A}}^{\max} =$ 0.1,0.2,0.3,0.4,0.5,0.6,0.7,0.8 and 0.9. The deviation obtained by fitting with the modified Washburn solution is used to determine the lower limit of the intermediate region. Here we use 0.02 (dashed line in figure 6.5a and 6.5b) as the threshold value for the deviation and

obtain the lower limit of $10\mu m$ glass beads with DI water is $0.6p_A^{max}$. We use a different threshold value because from figure 6.5b, the slope of the deviation increase in the Washburn solution changes significantly after $0.6p_A^{max}$. If using the same threshold value of 0.01, the lower limit of the intermediate region would be $0.1p_A^{max}$. However, the values of the deviation between $0.1p_A^{max}$ and $0.6p_A^{max}$ are only slightly larger than 0.01.

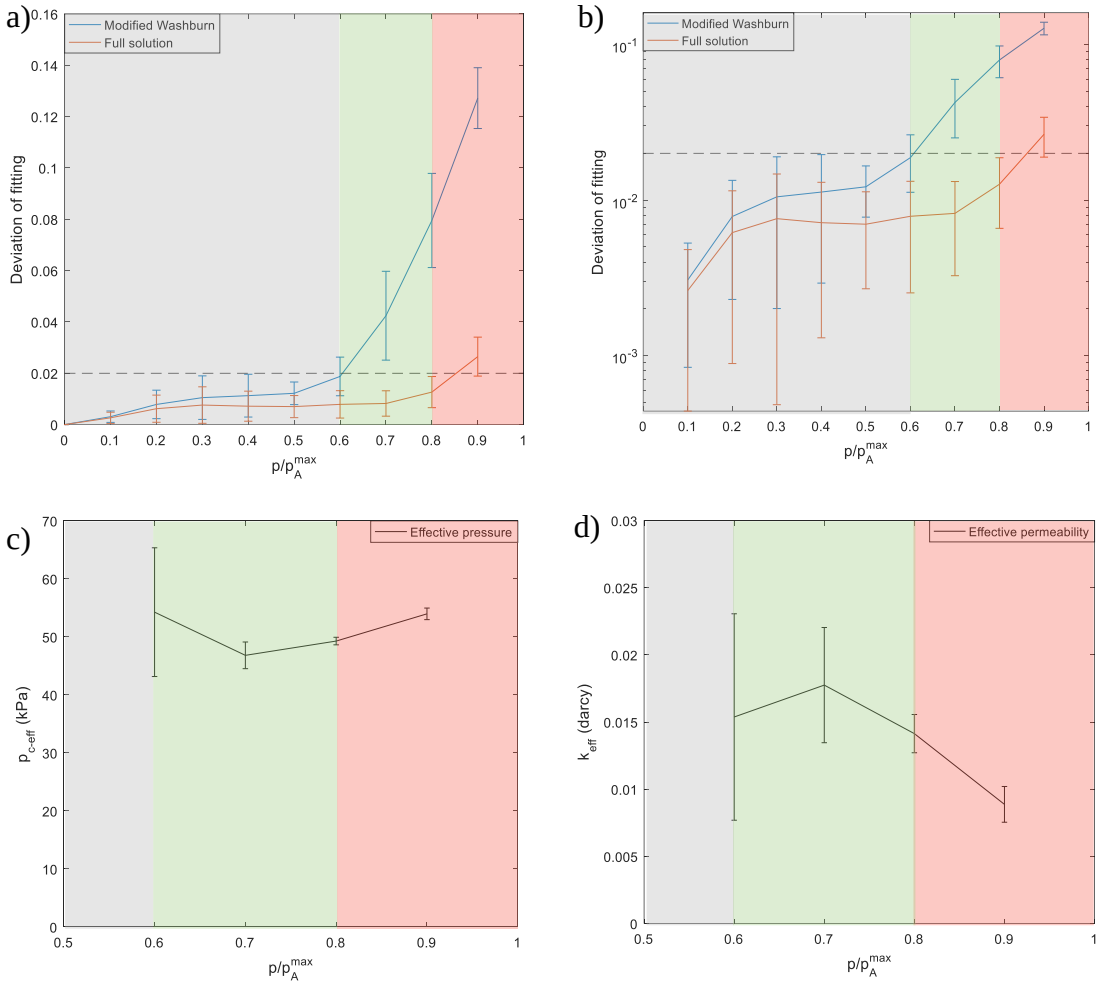

Figure 6.5 The deviation of the fitting from experiments using modified Washburn solution (blue) and the full solution (red) obtained at different pressure ranges for $10\mu m$ glass beads with DI water. The deviation is calculated by equation 5.2. The grey region is the Washburn region, the green region is the intermediate region and the red region is the final region. a) the deviation is presented in linear scale, b) the deviation is presented in logarithm scale. The dashed line is the threshold value (deviation =0.02). c) the average value of p_{c_eff} obtained and d) the average value of κ_{eff} obtained using the full solution.

Using the same threshold value 0.02 for the deviation of the full solution, we obtain the upper boundary of the intermediate range is $0.8p_{\mathrm{A}}^{\max}$. For the experiments with $10\mu m$ glass beads and DI water, the intermediate region is between $0.6p_{\mathrm{A}}^{\max}$ and $0.8p_{\mathrm{A}}^{\max}$. This is the recommended region to use the full solution to determine the effective values of κ and p_{c}. In figure 6.5c and d we present the average value of $p_{\mathrm{c\_eff}}$ and κ_{eff} obtained within the intermediate and late imbibition region from the fitting with the full solution. The data obtained within the Washburn region is not included because the values are not useful. In the previous section, we recommended fitting the experimental data up to $0.7p_{\mathrm{A}}^{\max}$, it falls within the intermediate region. The fitting results are $\kappa_{\mathrm{eff}} = (0.018 \pm 0.004)$darcy and $p_{\mathrm{c_eff}} = (46800 \pm 2300)$Pa.

In Figure 6.6 the values of the deviation of the fitting using the modified Washburn solution and the full solution for experiments with $45\mu m$ glass beads with DI water were presented. Figure 6.6a presents the deviation in linear scale and figure 6.6b uses the logarithm scale. Each point is obtained by a fitting that uses the data up to a pressure differential p such that $p/p_{\mathrm{A}}^{\max} = 0.1,0.2,0.3,0.4,0.5,0.6,0.7,0.8$ and 0.9. Same with the case of $10\mu m$ glass beads with DI water, we use threshold value 0.02 to determine the limits for the intermediate region. From the deviation curve of the Washburn fitting, we determine the lower limit is $0.5p_{\mathrm{A}}^{\max}$ for $45\mu m$ glass beads with DI water. Similarly, the upper limit is obtained as $0.7\,p_{\mathrm{A}}^{\max}$ by applying the threshold value 0.02 on the deviation of the full solution. Therefore, the intermediate region is between $0.5p_{\mathrm{A}}^{\max}$ and $0.7p_{\mathrm{A}}^{\max}$ for the experiments between $45\mu m$ glass beads and DI water. The values of the lower and upper limit are in agreement with the change of the slope on the curve in figure 6.6b, suggesting choosing 0.02 as the threshold value is reasonable. Comparing to the case with $10\mu m$ glass beads,

the intermediate region takes place at an earlier stage of the imbibition in 45μm glass beads. A similar trend is also seen in chapter 5 when the imbibition liquid is PDMS. For porous media with a wider pore distribution and thus more heterogeneous, the intermediate region takes places earlier than homogeneous media, the details are already discussed in section 5.4.3.

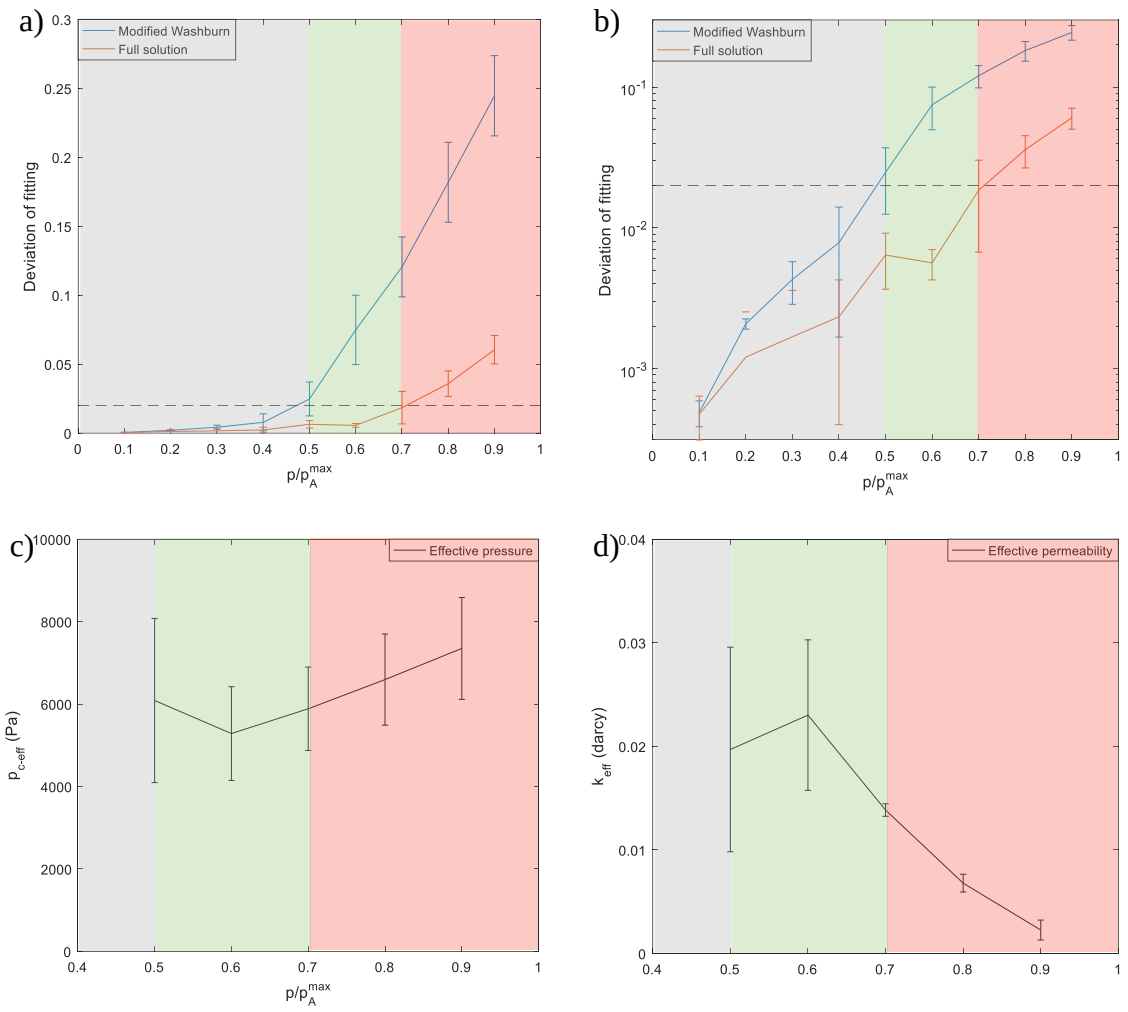

Figure 6.6 The deviation of the fitting from experiments using modified Washburn solution (blue) and the full solution (red) obtained at different pressure ranges for 45μm glass beads with DI water. The deviation is calculated by equation 5.2. The grey region is the Washburn region, the green region is the intermediate region and the red region is the final region. a) the deviation is presented in linear scale, b) the deviation is presented in logarithm scale. c) the average value of $p_{\mathrm{c\_eff}}$ obtained and d) the average value of κ_{eff} obtained using the full solution.

In figure 6.6c and d we present the average value of $p_{\mathrm{c\_eff}}$ and κ_{eff} obtained within the intermediate and late imbibition region from the fitting with the full solution. The data obtained within the Washburn region is not presented because the values are not valuable. For the experiments of $45\mu m$ glass beads with DI water, we recommended fitting the experimental data up to $0.6p_{\mathrm{A}}^{\mathrm{max}}$ to obtain the effective values of the capillary pressure and permeability. The fitting results are $\kappa_{\mathrm{eff}} = (0.023 \pm 0.007)$darcy and $p_{\mathrm{c_eff}} = (5300 \pm 1100)$Pa.

The effective values of the capillary pressure and permeability obtained within the intermediate region are summarized in table 6.5. For 10 μm glass beads, the values are obtained by fitting the experimental data up to $0.7p_{\mathrm{A}}^{\mathrm{max}}$. For 45 μm glass beads, the values are obtained by fitting the experimental data up to $0.6p_{\mathrm{A}}^{\mathrm{max}}$. By comparing the effective capillary pressure between PDMS and DI water, we also obtain the DI water contact angle. For 10 μm glass beads, $cos\theta_{\mathrm{w}} = 0.82 \pm 0.05$ and for $45\mu m$ glass beads, $cos\theta_{\mathrm{w}} = 1.0 \pm 0.3$. The variation in the effective capillary pressure obtained for 45 μm glass beads is larger. Thus the value of $cos\theta_{\mathrm{w}}$ also has larger variance. In general, the system with 45 μm glass beads is more heterogeneous and there is also large variability between each experiment. The large system-to-system variability may be a result of surface contamination. Since the glass beads are cleaned and then reused for the experiments, it is possible they were not cleaned completely and there was some oil left on the surface. The contact angle value in 45 μm glass beads is greater than zero and the glass beads are less hydrophilic compared to 10 μm glass beads. Similar results were obtained in the static characterization in section 6.1. In addition, when comparing the permeability between the two particle groups, it is surprising that the permeability is extremely low for 45 μm glass

beads. Besides the greater heterogeneity of 45 μm glass beads, the hydrophilicity is also responsible for the low permeability in DI water. Since the 45 μm glass beads are less hydrophilic, the porous media is not saturated as it is in the 10 μm glass beads. The less saturated porous media can attribute to the low permeability in 45 μm glass beads.

particle	$p_{\mathrm{c\_eff}}(Pa)$	$cos\theta_{\mathrm{w}}$	κ_{eff} (darcy)
10 μm glass beads	46800 ± 2300	0.82 ± 0.05	0.018 ± 0.004
45 μm glass beads	5300 ± 1100	1.0 ± 0.3	0.023 ± 0.007

Table 6.5 The effective capillary pressure $cos\theta_{\mathrm{DI\,water}}$ and permeability obtained by fitting the experimental data using the full solution for DI water with $10\mu m$ and $45\mu m$ glass beads. The results with $10\mu m$ glass beads were obtained using the data up to $0.7p_{\mathrm{A}}^{\mathrm{max}}$, while for $45\mu m$ glass beads the results were obtained using the data up to $0.5p_{\mathrm{A}}^{\mathrm{max}}$.

6.3 Conclusions

In this chapter we presented the experimental results from the glass beads and DI water. The pressure and liquid weight behavior during the advancing and receding processes are similar to the case with PDMS. We performed both static and dynamic characterizations on the porous media, with a focus on the contact angle and the permeability. The contact angle value for $10\mu m$ glass beads is almost zero, indicating that the glass beads are hydrophilic. The contact angle value for $45\mu m$ glass beads is greater than zero thus they are less hydrophilic. Since the two size of glass beads were produced by different manufactures, the material properties might not be the same. For the experiments with DI water we observed a smaller permeability value compared with PDMS. Air trapping is a possible reason for the low permeability. However, there is not sufficient evidence to support this idea.

We study the different regions during the imbibition of DI water in glass beads following the same approach we used in chapter 5 for imbibition of PDMS. In the beginning of the

imbibition, we use the modified Washburn solution derived in section 3.4 to fit with the experiments. However, the value of permeability and the capillary pressure cannot be determined individually during this time. We then use the deviation of the fitting with the modified Washburn solution and the full solution to determine the lower and upper boundary for the intermediate region. We used a different threshold value 0.02. This value is not arbitrary, it is chosen based on the trend of the deviation increase presented in the logarithm plot. For $10\mu m$ glass beads the intermediate region is from $0.6p_{\mathrm{A}}^{\max}$ to $0.8p_{\mathrm{A}}^{\max}$. For $45\mu m$ glass beads the intermediate region is between $0.5p_{\mathrm{A}}^{\max}$ and $0.7p_{\mathrm{A}}^{\max}$. The intermediate region takes place at an earlier stage of the imbibition for $45\mu m$ glass beads because the porous media is more heterogeneous. This behavior is similar when the wetting liquid is PDMS. Additionally, we compare the effective values obtained during the intermediate region for both particles. For $10\mu m$ glass beads, the effective permeability in DI water is smaller than that in PDMS and air trapping could be responsible for this difference. For $45\mu m$ glass beads, the effective permeability with DI water is extremely low. Instead of being 20 times larger than that in $10\mu m$ glass beads, it is only 30% larger than the permeability obtained in $10\mu m$ glass beads with DI water that is already small. The reason for such low permeability could be a combination of the large heterogeneity and less hydrophilicity in the $45\mu m$ glass beads. Additionally, there is large variance in the effective capillary pressure and the corresponding contact angle values, which is a result of the large variability between each experiment. In general, the large system-to-system variability, together with the heterogeneity for the system with $45\mu m$ glass beads and DI water makes it challenging to characterize with confidence using our method. This system is in the limit of this characterization method.

7. Preliminary results with pharmaceutical powders

7.1 Introduction: characterization protocol

In Chapter 5 and 6 we presented the experimental results and methodology used to characterize a model system, i. e. glass beads packed inside a closed column. Based on these experiments, we developed a *recommended* characterization protocols for any given granular materials. During the experiments we measure the static pressures at specific points in the process, i. e. the advancing, receding and bubbling pressure. Using the static pressures obtained in the experiments performed with PDMS, which was chosen as the reference liquid because it completely wets most solid surfaces, and the Laplace equation, we obtain the corresponding radius for the advancing, receding and bubbling pressure. Then, using the static pressures obtained in the experiments performed with DI water, and assuming that the porous media has the same characteristic pore radius as in the case of PDMS, we determine the $cos\theta_{\mathrm{w}}$ from Laplace equation.

In the dynamic characterization, we fit the experiments using the analytic solutions to obtain values of the effective permeability and capillary pressure. We first characterize the column, determining the effective column height by fitting the liquid mass as a function of the pressure differential using equation 5.1. This effective column height is then compared with the theoretical value H_{th} to determine if it is reliable. When the difference between H_{fitting} and H_{th} is greater than 20%, the experiment is discarded because there is leaking in the system. Otherwise, the experimental data up to an intermediate pressure range is fitted with the pressure solution to obtain an effective permeability and capillary pressure. It is not recommended to use the entire data set up to the maximum advancing pressure

$p_{\mathrm{A}}^{\max}$ in the fitting, because the liquid only fills in the smaller pores at high pressure and the connectivity of the pores as well as the local permeability decreases. On the other hand, the initial imbibition stage is also not recommended to obtain the effective values, because fitting the initial part of the pressure evolution using the modified Washburn solution cannot provide independent values of the permeability and capillary pressure. Therefore, it is recommended to use an intermediate range, where the permeability and capillary pressure can be determined independently by fitting with the full solution, but before reaching the final stage where the liquid is only filling in the smaller pores and the permeability is reduced. This intermediate stage is determined by the deviation of the two fittings from experimental data, one is obtained using the modified Washburn solution and the other is obtained using the full solution. After obtaining the effective values of capillary pressure and permeability, we determine the corresponding effective pore radii from the results of PDMS. Then, with the results obtained for DI water, we calculate the corresponding contact angle.

After characterizing the model system, in this chapter, we are interested in some pharmaceutical powders that are irregularly shaped and thus lead to a more complicated process during wetting. Lactose is used to study the case when the sample is soluble in water and Microcrystalline cellulose (MCC) is used as an example for swelling materials. Alumina is chosen because its particle size is different from all the other particles used. All of them are commonly used in pharmaceutical industry as excipients. We will follow the characterization methods used in Chapter 5 and 6 and summarized above. In addition, we present preliminary results investigating the effects on the dynamic process when different porosities or different effective column heights are used.

7.2 Soluble material: Lactose

In pharmaceutical industry, lactose is often used as a filler or diluent in tablet compaction and capsule filling. The particle size distribution of the lactose powder used in this study is presented in section 2.2. Since lactose is soluble in water, a saturated solution will be used as the testing wetting liquid, to avoid dissolution of the powder during the imbibition process. Another property of lactose powder is that the individual lactose particles have irregular shape. When preparing the column by tapping, following the procedure described in section 2.3, we obtained a large value of the porosity φ~0.44. This value is significantly greater than the porosity achieved with glass beads, φ~0.37. However, a porosity similar to the one measured for glass beads can also be obtained using lactose powder by compressing the powder with a cylindrical rod. We will compare the results obtained in both cases to discuss an important feature of heterogeneous systems not seen in the previous experiments described in chapters 5 and 6. Then, we will characterize the system with the smallest porosity following the methodology described in 7.1.

7.2.1 Effect of pore size heterogeneity by varying media porosity: Lactose

It is not easy to vary the porosity of the porous media when the particles are spherical and with a narrow size distribution. However, this can be accomplished with particles of a different shape, as is the case with lactose. In figure 7.1 we present the plots from the imbibition process of two experiments of PDMS and lactose in packed columns with different porosity. In figure 7.1a the porosity of the packed column is $\varphi = 0.435$ while in 7.1b the porosity is $\varphi = 0.355$. In the case of a large porosity ($\varphi = 0.435$), we observe that there are a lot of fluctuations in the pressure curve. These fluctuations correspond to bubbles forming and detaching from the bottom of the column while the liquid front is still

advancing in the porous media. In this case, the advancing, receding and bubbling processes are happening spontaneously and probably simultaneously, but through pores of different sizes. The underlying pore structure that could lead to this situation is discussed in chapter 1. Briefly, when the porous media is highly heterogeneous, the receding pressure for the large pores can be lower than the advancing pressure of the small pores. Therefore, the liquid is evacuating the large pores while it is still filling some of the small pores. When the emptied pores connect with each other and form a channel from the top of the porous media to the bottom, air percolates through, and bubbling happens. Because of the percolation, the pressure differential cannot increase anymore. Therefore, the maximum pressure $p_{\max}$ measured in the experiment is not the same as the advancing pressure $p_{\mathrm{A}}^{\max}$ defined in chapter 5 and 6. This advancing pressure which corresponds to the smaller pores cannot be determined by the static measurements in the experiments. In this case, the maximum pressure $p_{\max}$ represents the bubbling pressure $p_{\mathrm{B}}^{\max}$ at which the emptied large pores form a channel in that porous media. The average value of this maximum pressure for the packed column with large porosity is $p_{\mathrm{B}}^{\max}$=(2500 ± 600)Pa. In the case of a packed column with a smaller porosity, a spontaneous pressure drop was also observed, but less dramatically compared to experiments with large porosity porous media. In the example presented in figure 7.1b, the pressure decreased spontaneously at 5 hours. It is possible that a small bubble was slowly formed and released during this time. Since the porous media is less heterogeneous than the large porosity porous media, the bubbling process is less dramatic. However, it is still more heterogeneous than the cases with glass beads because the lactose particles have irregular shape. We estimate that the large heterogeneity is responsible for the spontaneous bubbling observed. In the case of a smaller

porosity, the maximum pressure $p_{\max}$ also represents the bubbling pressure $p_{\mathrm{B}}^{\max}$. The average value of this pressure for the small porosity lactose media is $p_{\mathrm{B}}^{\max}$=(5200 $\pm$ 1200)Pa, which is clearly larger than the maximum pressure $p_{\max}$ in the experiments with a packed column with large porosity.

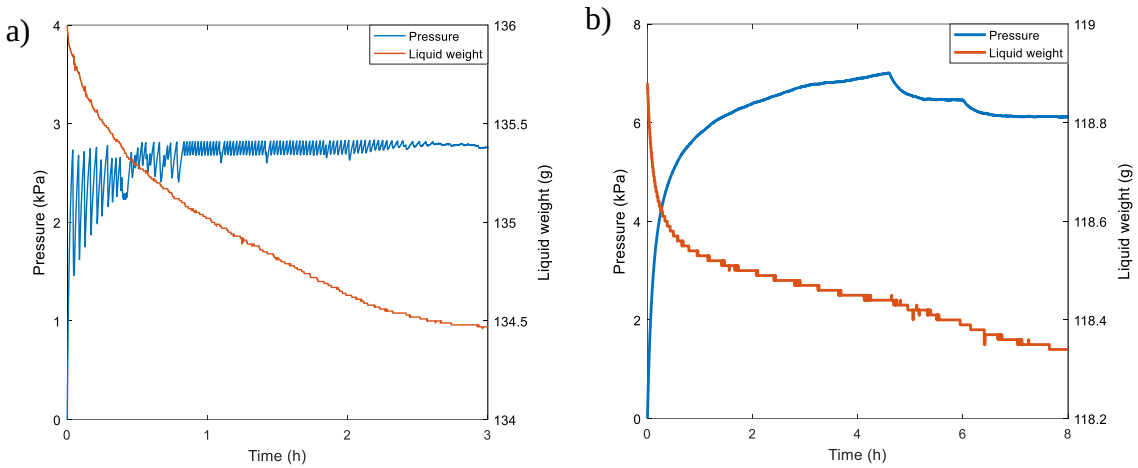

Figure 7.1 The evolution of the pressure and liquid weight during the imbibition process of PDMS in lactose. a): φ=0.435, b): φ=0.355.

For porous media with large pore size heterogeneity, the advancing pressure cannot be measured in the experiments. Only the effective capillary pressure can be estimated using the dynamic characterization method. In figure 7.2 we present an example of the fitting, using the experimental data up to a pressure differential equal to at $0.7p_{\mathrm{B}}^{\max}$ and $0.9p_{\mathrm{B}}^{\max}$. The solution fits very well the experiments in both cases, with R^2 =0.999. The results are also similar in both cases. Therefore, we will use the results obtained by fitting up to $0.9p_{\mathrm{B}}^{\max}$ because it contains more data. The effective pressure (3700Pa) obtained in the fittings is larger than the maximum pressure reached in experiments (2800Pa). This effective capillary pressure provides us information about the smaller pores of the porous media, which cannot be obtained from the static measurements in experiments.

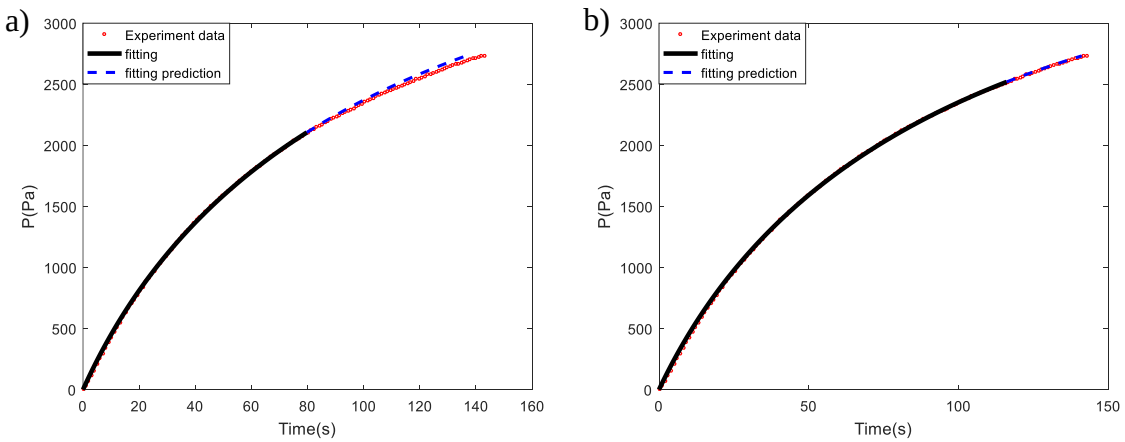

Figure 7.2 Fitting curves for lactose at large porosity (φ=0.435) with PDMS using the pressure solution. Red dots the experimental data. Black line is the fitting curve using the full solution. The blue dash line represents the pressure predicted by the fitting. (a): fit up to $0.7p_{\mathrm{B}}^{\max}$, $p_{\mathrm{c\_eff}}$ =3900Pa, R^2 =0.999; (b) fit up to $0.9p_{\mathrm{B}}^{\max}$, $p_{\mathrm{c\_eff}}$ =3700Pa, R^2 =0.999.

We studied the different regions of imbibition for lactose and PDMS, following the same approach used for glass beads and described in section 7.1. In figure 7.3 the deviation of the fitting using the modified Washburn solution and the full solution at different ranges are presented. Using the same threshold value of 0.01 together with a change in the trend observed for the deviation increase, as shown in figure 7.3b, we obtain that the lower limit of the intermediate region is $0.5p_{\mathrm{B}}^{\max}$. Specifically, at this value of the fitting range we observe a sharp increase in the deviation of the modified Washburn solution fitting. From the deviation of the full solution fitting we determine that the upper limit of the intermediate region is $0.9p_{\mathrm{B}}^{\max}$. Therefore, the intermediate region for experiments of large porosity lactose and PDMS is between $0.5p_{\mathrm{B}}^{\max}$ and $0.9p_{\mathrm{B}}^{\max}$.

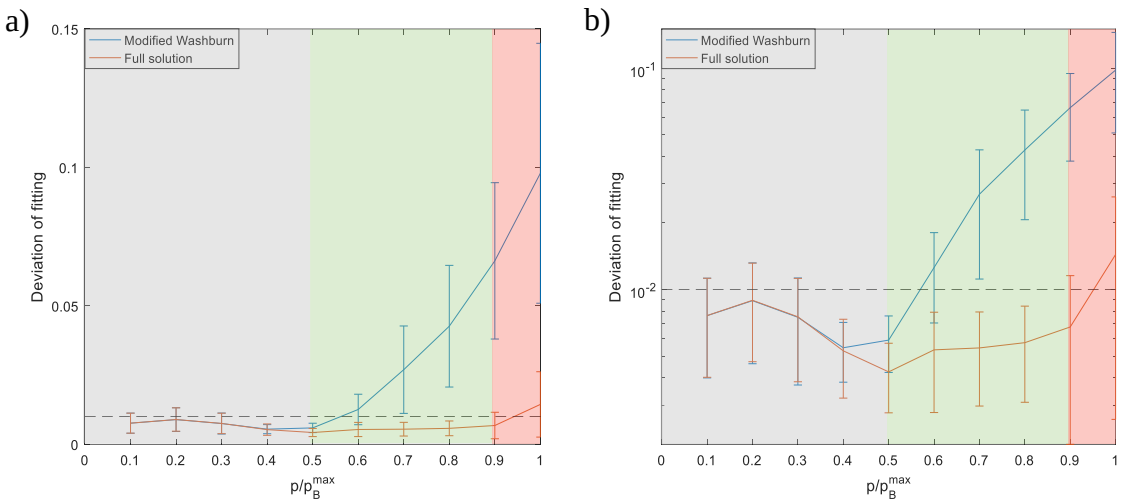

Figure 7.3 The development of the deviation of the fitting by modified Washburn solution (blue) and the full solution (red) obtained by fitting the experimental data up to pressure differential at p/p_B^{max}= 0.1, 0.2, 0.3, 0.4, 0.5, 0.6, 0.7, 0.8, 0.9 and 1 for large porosity lactose with PDMS. The deviation is calculated by equation 5.2. The grey region is the Washburn region, the green region is the intermediate region and the red region is the final region. a): the deviation is presented in linear scale, b) the deviation is presented in logarithm scale. The dashed line is the threshold value (deviation =0.01).

In figure 7.4 we present the fitting for an experiment with a packed column presenting a small porosity (φ =0.355). This case is similar to the fittings with glass beads in chapter 5. The effective pressure obtained by fitting is smaller than the maximum pressure p_B^{max} reached in experiments. The fitting obtained using the experimental data up to $0.7p_B^{max}$ is better, with R^2 =0.998. The effective capillary pressure is lower than that obtained using the experimental data up to $0.9p_B^{max}$ because up to $0.7p_B^{max}$, the liquid is still filling in both large and small pores. For this case of a low porosity of the packed column, we will use the fitting results obtained at $0.7p_B^{max}$, analogous to the analysis of the system with $10\mu m$ glass beads.

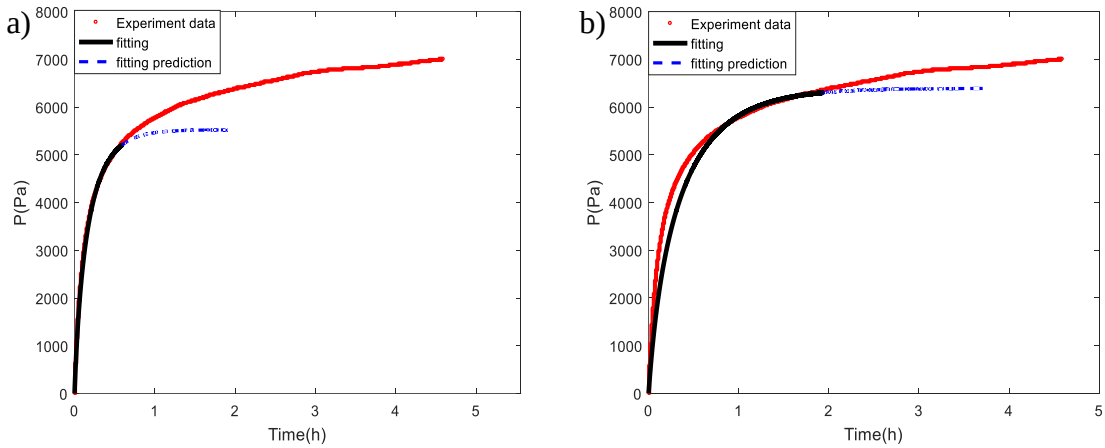

Figure 7.4 Fitting curves for lactose at small porosity (φ=0.355) with PDMS using the pressure solution. Red dots the experimental data. Black line is the fitting curve using the full solution. The blue dash line represents the pressure predicted by the fitting. (a): fit up to $0.7p_{\mathrm{B}}^{\max}$, $p_{\mathrm{c\_eff}}$ =5600Pa, R^2 =0.998; (b) fit up to $0.9p_{\mathrm{B}}^{\max}$, $p_{\mathrm{c\_eff}}$ =6500Pa, R^2 =0.981.

The different imbibition regions for experiments with small porosity lactose and PDMS is presented in figure 7.5. Using the threshold value 0.01 together with the trend of the deviation increase as shown in figure 7.5b, the intermediate region is determined to be from $0.4p_{\mathrm{B}}^{\max}$ to $0.8p_{\mathrm{B}}^{\max}$. The intermediate regions for experiments with lactose and PDMS are similar to the intermediate region for $10\mu m$ glass beads and wider than $45\mu m$ glass beads, even though lactose is more heterogeneous. For experiments with lactose, the bubbling pressure $p_{\mathrm{B}}^{\max}$ is used to determine the imbibition regions, this bubbling pressure is lower than the advancing pressure. However, in glass beads the advancing pressure $p_{\mathrm{A}}^{\max}$ is used. This is why the intermediate region is wider in a more heterogeneous media with lactose.

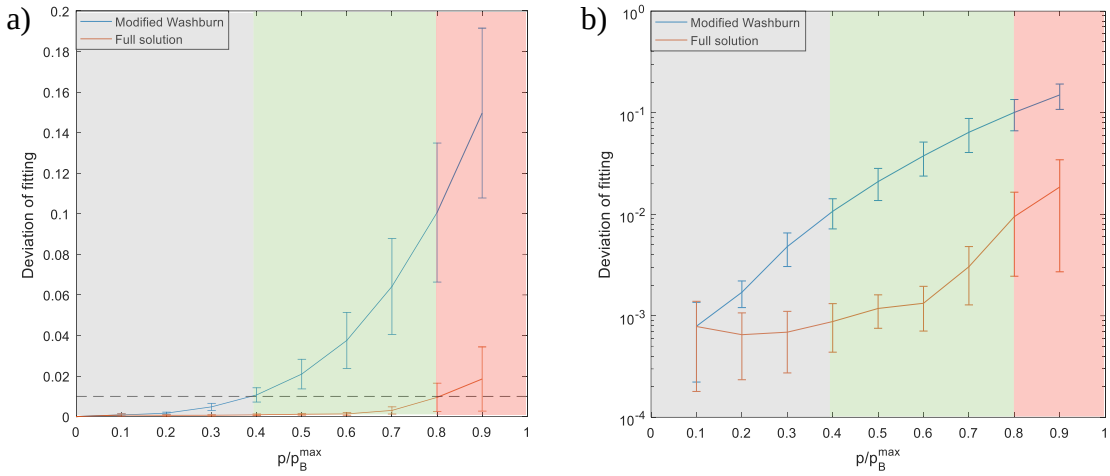

Figure 7.5 The development of the deviation of the fitting by modified Washburn solution (blue) and the full solution (red) obtained by fitting the experimental data up to pressure differential at $p/p_{\mathrm{B}}^{\max}$= 0.1, 0.2, 0.3, 0.4, 0.5, 0.6, 0.7, 0.8, 0.9 and 1 for small porosity lactose with PDMS. The deviation is calculated by equation 5.2. The grey region is the Washburn region, the green region is the intermediate region and the red region is the final region. a): the deviation is presented in linear scale, b) the deviation is presented in logarithm scale. The dashed line is the threshold value (deviation =0.01).

The fitting results obtained within the intermediate region for the columns with two different porosities are summarized in Table 7.1. For experiments with large porosity, the fitting uses the experimental data up to $0.9p_{\mathrm{B}}^{\max}$. For small porosity, the experimental data up to $0.7p_{\mathrm{B}}^{\max}$ is used in fittings. The effective pressure for large porosity is smaller while the permeability is larger, as expected. The ratio of the effective radius is 1.5 ± 0.4. For permeability this ratio is 4.6 ± 3.8.

φ	$p_{\mathrm{c\_eff}}(Pa)$	$r_{\mathrm{eff}}(\mu m)$	$\kappa_{\mathrm{eff}}(darcy)$
0.44	3100 ± 550	13.0 ± 2.3	0.70 ± 0.40
0.37	4500 ± 750	9.0 ± 1.5	0.14 ± 0.07

Table 7.1 The average value of effective capillary pressure, pore radius and permeability obtained by fitting with pressure solution. The experiments are between lactose and PDMS at different porosity. For φ=0.44, the results are obtained by fitting the experimental data up to $0.9p_{\mathrm{B}}^{\max}$. For φ=0.37, the results are obtained by fitting the experimental data up to $0.7p_{\mathrm{B}}^{\max}$.

7.2.2 Lactose with saturated solutions: different column height H

The experiment with DI water is more complicated because lactose is soluble in water. For this reason, we use saturated solution of lactose in DI water as the wetting liquid. Based on

the experiments with PDMS, large porosity systems result in experiment that are more complicated to interpret and analyze. Therefore, we prepare the porous media columns with a low porosity, $\varphi \sim 0.37$. During the initial experiments we noticed that, approximately 20min after we start, there was a crack that appeared in the middle of the porous media, shown in figure 7.6a. After the crack was formed, liquid stopped advancing and the pressure was slowly decreasing (shown in figure 7.6b). The maximum pressure reached during the experiment was the pressure before the crack appeared. At this point, it is not clear if the advancing pressure is reached. We can thus use the fittings to estimate an effective capillary pressure.

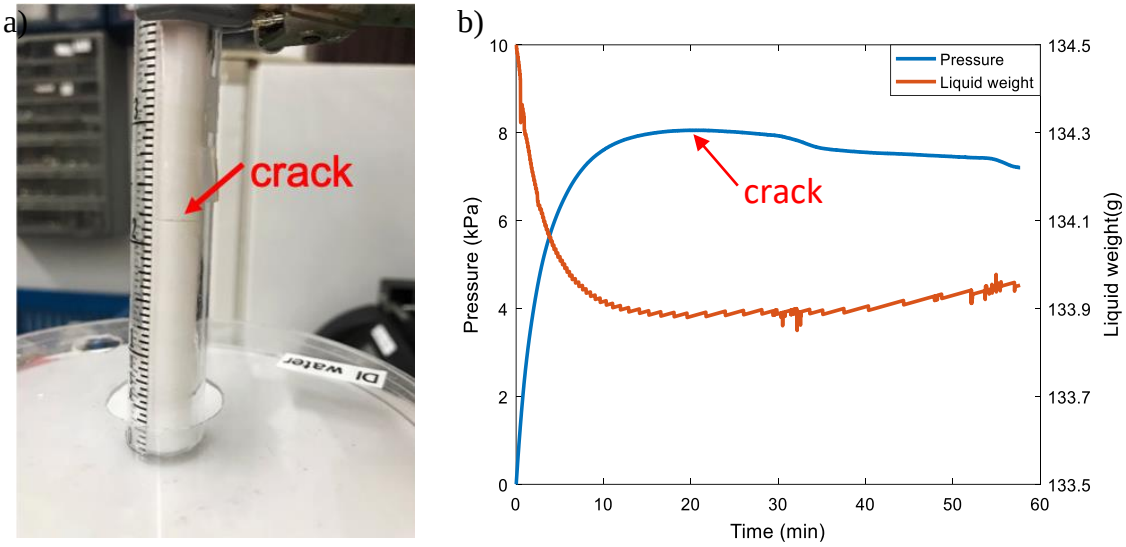

Figure 7.6 a): The crack appeared in the experiment. b): The pressure and liquid weight evolution over time during an experiment with lactose and saturated solution. The pressure reached the maximum at 20min when a crack was formed and then slowly decreased.

In figure 7.7 we present the fitting for the experiment with saturated solution. This is the experiment mentioned above where a crack formed in the porous media and liquid stopped advancing. Therefore, the advancing pressure was unknown. The effective capillary pressure obtained in figure 7.7a and 7.7b are 8500Pa and 9000Pa, they were obtained by fitting the experimental data up to $0.7p_{\max}$ and $0.9p_{\max}$, respectively. Both values are

higher than the maximum pressure reached in the experiment (8000Pa). The value suggests that the crack occurred when the system was close to reach the advancing pressure. On the other hand, the reason why the crack appears and how it is formed is not very clear. A possible reason is that lactose dissolved due to the long duration of the experiments.

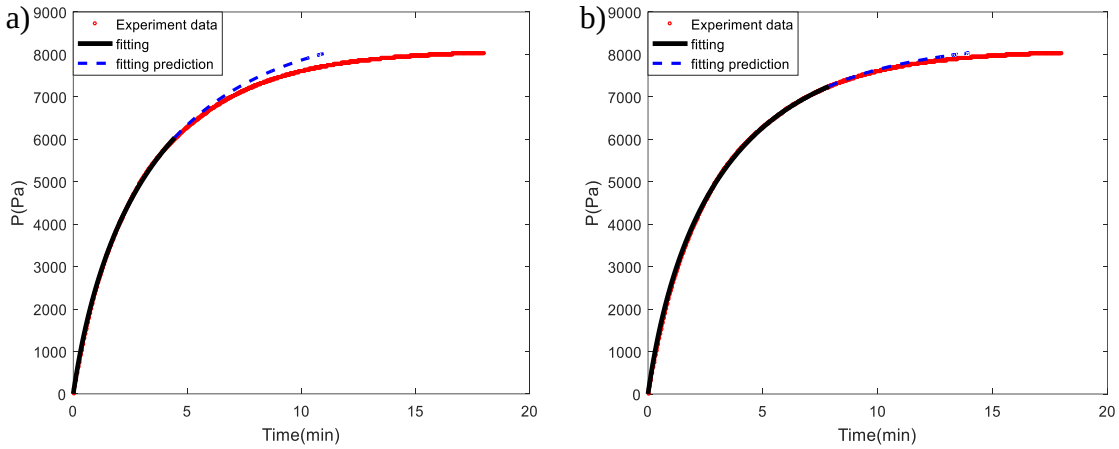

Figure 7.7 Fitting curves for lactose at small porosity (φ=0.373) with saturated solution using the pressure solution. Red dots the experimental data. Black line is the fitting curve using the full solution. The blue dash line represents the pressure predicted by the fitting. (a): fit up to $0.7p_{\max}$, $p_{c_eff} = 9000$Pa, R^2 =0.999; (b)fit up to $0.9p_{\max}$, p_{c_eff} =8500Pa, R^2 =0.999.

To avoid the formation of a crack at such long times, we prepared another porous media but using a shorter column (1.5 inch), to reduce the saturation time as suggested in chapter 4. For a shorter column, it is expected to reach the advancing pressure in a shorter time such that the crack is yet to form. However, the column we used was so short that the advancing pressure was not reached even though the liquid reached the top of the porous media. We fitted the experiments with solutions to estimate the capillary pressure, similar to the case of large porosity porous media, the effective pressure is larger than the maximum pressure reached in experiments. The data up to $0.9p_{\max}$ was used in the fittings and the results are summarized in Table 7.2. Similar to the experiments with $10\mu m$ glass beads, the effective permeability measured when the saturated solution penetrates through the system is smaller than the permeability obtained from the liquid penetration with PDMS.

Comparing the effective capillary pressure obtained by fitting up to $0.7p_{\mathrm{B}}^{\max}$ in experiments of small porosity lactose with PDMS and assuming same pore size for both liquids, we obtain the value of $cos\theta$ for saturated solution $cos\theta = 0.67 \pm 0.18$. Kiesvaara and Yilruusi [94] studied the contact angle of lactose using the Washburn method on a horizontal column. They obtained $\theta = 61.7° \pm 0.7°$ ($cos\theta = 0.46 \pm 0.01$) for saturated solution and compared this value to the contact angle obtained using the sessile drop method on lactose tablets, which is 10° [94] ($cos\theta = 0.98$). The results in our experiments are closer to that obtained using the Washburn column method since both are dynamic methods and the powder samples are packed in a column.

Liquid	$p_{\mathrm{c\_eff}}(Pa)$	$cos\theta$	$\kappa_{\mathrm{eff}}(darcy)$
Saturated solution	11000 ± 2400	0.67 ± 0.18	0.048 ± 0.010
PDMS	4500 ± 750	1	0.14 ± 0.07

Table 7.2 The average value of effective capillary pressure, $cos\theta$ and permeability obtained by fitting with pressure solution. The experiments are between lactose and saturated solution with φ=0.37, the small porosity PDMS results are listed as reference. The results are obtained by fitting the experimental data up to $0.9p_{\max}$ for saturated solution. For PDMS, the data up to $0.7p_{\mathrm{B}}^{\max}$ was used in the fitting.

Despite not reaching the equilibrium of the advancing process in our experiments with lactose and saturated solution, we noticed that the pressure increases faster in a shorter column. In figure 7.8 we present the time to reach $0.5p_{\max}$, $0.75p_{\max}$ and $0.9p_{\max}$ for three experiments with different column height H= 9.6cm, 14.5cm and 17.6cm. The maximum pressure $p_{\max}$ is the highest pressure measured in the experiment, it is not the advancing pressure because the advancing pressure is unknown. The effective column height is estimated by the fitting between m and p, as discussed in section 5.3.2. It is obvious in figure 7.8 that using a shorter column reduces the time to reach a certain completion fraction. However, the advancing pressure might not be achieved in a short column. It

would be critical to choose a column height that has enough empty space for the liquid to compress to reach the advancing pressure, but not too long that may cause cracks.

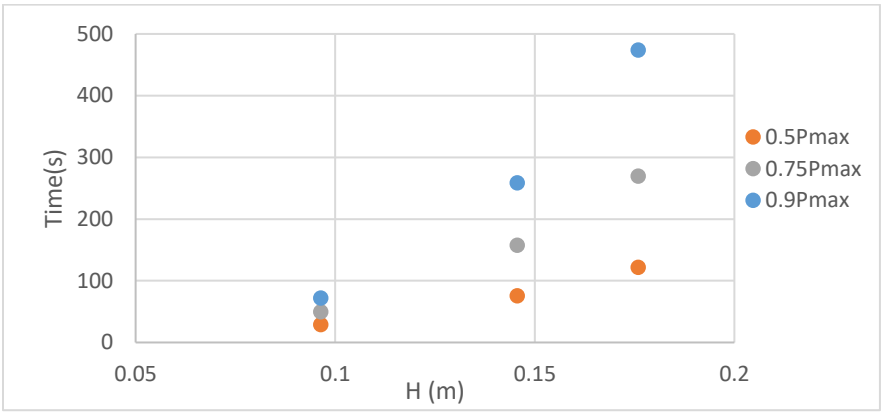

Figure 7.8 Time to reach $0.5p_{\max}$, $0.75p_{\max}$ and $0.9p_{\max}$ vs. effective column height for three experiments between lactose and saturated solution

7.3 Swelling material: Microcrystalline Cellulose (MCC)

Microcrystalline cellulose is one of the most important filler/binder in direct compression of tablets [95], [96]. Because of its relatively low bulk density, only very small amount of MCC is needed to bind other materials [97]. The porous media packed by MCC has an extremely large porosity of around 0.72, compared to lactose and glass beads. The intraparticle porosity is very high, almost 90-95% of the surface area is internal [98]. In figure 7.9 we present the advancing process of an experiment with MCC and PDMS. There were a lot of fluctuations in the pressure curve in figure 7.7a. The fluctuations are a result of the bubbling phenomena. In figure 7.7b it is clear that the first bubble appeared at 1.5min, when the pressure was $p_{\max}$=1600Pa. After that, the liquid was still penetrating in the column while the bubbles keep forming and detaching at the bottom of the column. The bubbling phenomena is not surprising given that the porosity is extremely large.

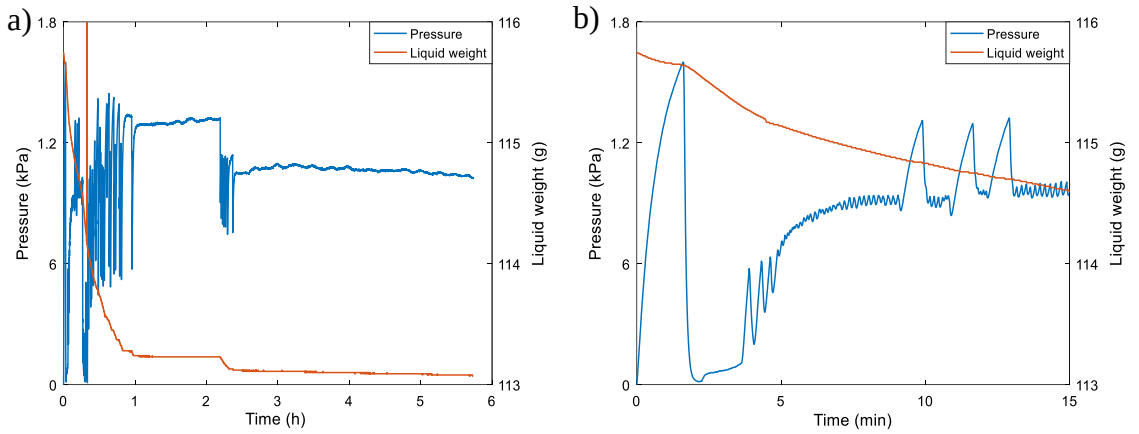

Figure 7.9 The evolution of pressure and liquid weight over time during the imbibition of PDMS in MCC. a): The entire imbibition process; b): The first 15min of a).

Using the pressure data collected during the first 1.5min to fit with pressure solution (equation 3.21) we obtain the effective capillary pressure $p_{\mathrm{c\_eff}}$ =1900Pa and the effective permeability κ_{eff} =0.44darcy. The fitting plot is presented in figure 7.10. The effective pressure is larger than the maximum pressure reached in imbibition $p_{\max}$ =1600Pa. Assuming $\cos(\theta_{\mathrm{PDMS}}) = 1$, the corresponding effective radius is 21.1μm. The MCC used in the experiment is Avicel 101, with an average particle diameter of 50μm. The particle size distribution is presented in section 2.2.2.

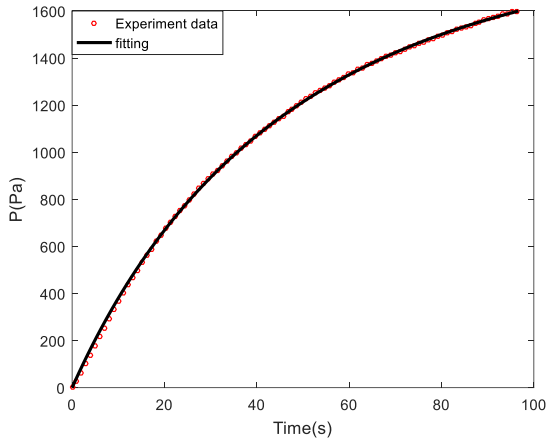

Figure 7.10 Fitting curves for experiment of MCC with PDMS using the pressure solution. $p_{\mathrm{c\_eff}}$ =1900Pa, κ_{eff} =0.44darcy and R^2 =0.999.

The experiments between MCC and DI water are more complicated, since the material swells when wetted by water. During the experiments there were bubbles leaving the column, creating a lot of disturbances in the reading of the liquid weight, shown by the red curve in figure 7.11. The disturbances making it difficult to estimate the effective column height by fitting. Without knowing the effective height we cannot fit the experiment with the analytic solutions.

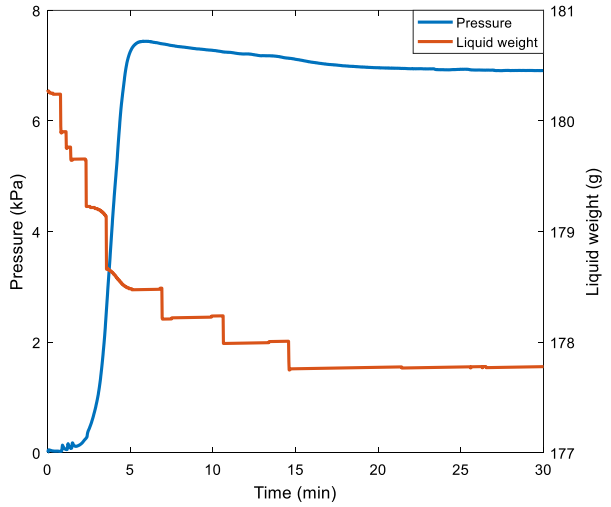

Figure 7.11 The evolution of pressure and liquid weight over time during the advancing process of DI water in MCC. There were a lot of "jumps" the liquid weight caused by bubbling.

7.4 Aluminum Oxide

Alumina, also called aluminum oxide, is an important material used in dental ceramics [99]. Its wettability is a critical parameter in the manufacturing of metal-ceramic composite materials, as well as the corrosion and wear protection [100]–[103]. We studied the imbibition of PDMS and DI water in columns packed with $20\mu m$ alumina powders. We only performed one experiment for each liquid to see the preliminary results. The plots from the advancing process are presented in figure 7.12. Figure 7.12a shows an experiment with PDMS and figure 7.12b show an experiment with DI water. From the static

measurements, the advancing pressure for DI water is 27800Pa and for PDMS it is 7400Pa. Since the contact angle for PDMS is zero, by assuming the same pore size between PDMS and DI water we obtained the DI water contact angle with alumina $cos\theta_{\mathrm{w}}^{\mathrm{adv}} = 1.0$. The value suggests these alumina particles are hydrophilic.

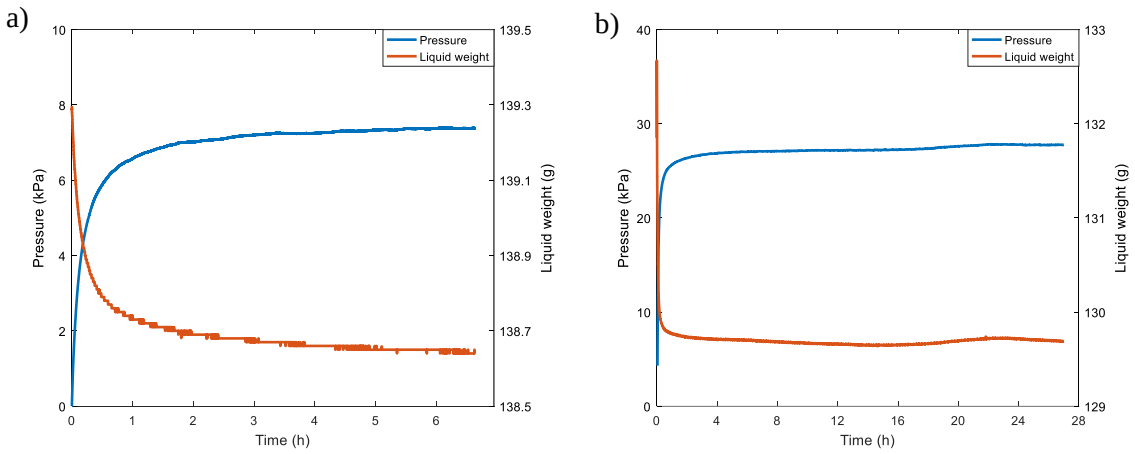

Figure 7.12 The evolution of pressure and liquid weight over time during the advancing process of a): PDMS in alumina; b): DI water in alumina.

In the dynamic characterization, the experimental data up to $0.7p_{\mathrm{A}}^{\mathrm{max}}$ is used to fit with the full solution. The effective values of capillary pressure and permeability obtained by the fittings are listed in table 7.3. Similar to the case with glass beads, the effective capillary pressure is smaller than the advancing pressure because they present different pore sizes. From the ratio of the effective pressure we also obtain the contact angle for DI water is zero, with $cos\theta_{\mathrm{w}}^{\mathrm{adv}} = 1.0$. The effective permeability is 0.098darcy for PDMS and 0.056darcy for DI water. The ratio between the permeability is also similar to the case with $10\mu m$ glass beads.

Wetting liquid	$p_{\mathrm{A}}^{\mathrm{max}}$	$p_{\mathrm{c\ eff}}$ (Pa)	κ_{eff} (darcy)
PDMS	7400	6700	0.098
DI water	27800	23500	0.056

Table 7.3 The advancing pressure, effective capillary pressure and permeability of experiments with alumina and PDMS, DI water. The effective values were obtained by fitting the experimental data up to $0.7p_{\mathrm{A}}^{\mathrm{max}}$.

In this chapter we summarized the characterization protocol and applied it on three pharmaceutical powder materials: lactose, MCC and alumina. In the case of lactose, we studied two cases depending of the porosity of the packed column. At large porosity (0.44), spontaneous bubbling takes place while the liquid is still advancing in the smaller pores, thus the advancing pressure cannot be measured experimentally. At small porosity (0.37), the spontaneous bubbling process is less dramatic, but the advancing pressure is still unknown. Only the effective capillary pressure can be estimated by fitting experimental data to the pressure solutions obtained in chapter 3. This effective pressure can be either higher or lower than the maximum pressure $p_{\max}$ reached in experiments. In the experiments with large porosity, the effective pressure is higher than $p_{\max}$ because the system is more heterogeneous, the maximum pressure is the bubbling pressure of the large pores while the effective pressure corresponds to a pore radius that is an average of large and small pores. The different regions of PDMS imbibition in lactose is studied following the same approach used for glass beads. For large porosity experiments, the intermediate region is between $0.5p_{\mathrm{B}}^{\max}$ and $0.9p_{\mathrm{B}}^{\max}$. For small porosity experiments this region is from $0.4p_{\mathrm{B}}^{\max}$ to $0.8p_{\mathrm{B}}^{\max}$. In the case of lactose with saturated solution, the experiments were performed using columns with various lengths. When the column is too long, there will be cracks formed in the porous media during imbibition. If the column is too short, it will not reach the advancing pressure because there is not enough space for the liquid to compress. Although not reaching the advancing pressure during the preliminary experiments, we can estimate the effective capillary pressure using the fittings and use the ratio of effective pressure to estimate the contact angle. Another finding during the experiments with lactose

and saturated solution is that the time to reach a certain completion fraction is reduced by using a shorter column.

For experiments with MCC the porosity of the porous media is even larger, $\varphi \sim 0.72$. At such extreme heterogeneity, the spontaneous bubbling happens soon after the liquid enters the porous media. Especially when the wetting liquid is DI water, bubbles caused disturbances in the reading of the scale. The disturbances make it difficult to estimate the effective column length. Accordingly, we are not able to fit with the solutions. In any case, the solutions obtained in this thesis do not apply to swelling media.

In the experiments with alumina we obtained results similar to the experiments with $10\mu m$ glass beads. The contact angle with DI water is zero. The results with these pharmaceutical granular materials suggest that our characterization method can be applied to practical powders. However, because they are usually irregular in shape and more heterogeneous, we need to pay extra attention in the design of the experiments, for example making sure that the porosity of the packed column is not high. In addition, in the case of soluble materials, it may be important to reduce the column length. The analytical solutions are very useful when estimating the effective capillary pressure and contact angle in cases when the advancing pressure cannot be measured directly from experiments.

8. Conclusions

The objective of this thesis is to develop and demonstrate a methodology able to characterize the properties of powder in contact with liquids, including wettability, using a closed column packed with the powder material of interest. In addition, using a packed column that is closed at the top, enables the study of both the advancing and receding processes. Analytical solutions describing the liquid uptake and pressure differential are obtained for the dynamics during the capillary rise in a close column. The wetting experiments are initially performed with a model system using glass beads and PDMS as the reference liquid. This system is characterized by static as well as dynamic methods. In the static method, the static capillary pressure and its corresponding pore radius is obtained for different specific moments in the experiments, that is, at the end of the advancing process, at the beginning of the receding process and at the threshold pressure leading to bubbling. In the dynamic method, the experimental results are fitted with two different analytical solutions, the modified Washburn solution and the full solution, to obtain the effective capillary pressure and permeability of the packed column. We also analyze the early stages of the penetration process using a modified Washburn solution. Based on the comparison between the fittings with the modified Washburn and the full solutions, different regions of the imbibition process are determined and a general methodology is proposed to analyze the advancing process. After validating the proposed characterization method with the model system, this method is then used to characterize other systems including glass beads and DI water, as well as pharmaceutical powders with PDMS and DI water. The conclusions from each chapter are summarized below:

In chapter one we provided an overview of the wetting in porous media. We introduced the basic concepts related to wettability and discussed cases of capillary hysteresis in different pore geometries. The capillary hysteresis in porous media is a combination result of the contact angle hysteresis, pore size heterogeneity and pore connectivity.

Chapter two introduced the experimental system and the improvements compared to previous works. Using the proposed experimental setup, we are able to study both the advancing and the receding processes of powders and even force the receding process up to bubbling. In addition, this system also allows us to investigate the dynamics of capillary rise.

In chapter three, the analytical solutions of the capillary rise in the porous media are obtained. The solutions describe the evolution of both the liquid mass and the pressure differential during the imbibition inside a closed column. Compared to the existing solutions, our solutions consider the hydrostatic effects and the non-linear pressure dependence on the liquid penetration height. Therefore, it is a more general solution and can be used with a wide range of capillary pressures. A simplified solution called Modified Washburn solution for imbibition during the initial stages is also obtained to compare with the general solution.

In chapter four we considered the analytical solutions in dimensionless forms. Two independent dimensionless parameters that control the liquid penetration were identified. One is the normalized initial pressure in the closed system and the other is the normalized capillary pressure that drives the imbibition. Then, two different scenarios are considered based on the two dimensionless parameters. In one scenario only the capillary pressure changes, the equilibrium height and pressure increase with the capillary pressure. The non-

dimensional equilibrium time is not monotonic with the non-dimensional capillary pressure. At small capillary pressures, the equilibrium time increases faster with the capillary pressure. Then at large capillary pressures, the non-dimensional equilibrium time asymptotically approaches a finite value. In the other scenario, the capillary pressure is fixed while the initial pressure and the effective height changes. In this case, the equilibrium height decreases with the initial pressure and the effective column height. While the equilibrium pressure follows the opposite trend. The equilibrium time is reduced when the initial pressure increases or the column height is reduced.

The experiments of the model system, glass beads and PDMS are discussed in chapter 5. The pressure and liquid mass curves during the advancing and receding processes are presented. From the "staircase-like" shape of the receding curves we learned that the porous media is heterogeneous. Three pressure definitions, the advancing pressure $p_{\mathrm{A}}^{\max}$, the receding pressure $p_{\mathrm{R}}^{\min}$, the bubbling pressure $p_{\mathrm{B}}^{\max}$ and their corresponding radii are introduced to characterize the porous media in a static way. In order to perform the dynamic characterization using the analytical solutions, the effective column height H needs to be determined. We provided two methods to determine it, through theoretical estimation and fitting with the equation relating h and p. The fitting estimation is preferred because the theoretical value neglected some small volumes which are difficult to measure. However, the theoretical value provides a reference to check if the system is leaking. After obtaining a reliable value for H, we fit the experimental data with the analytical solutions to a certain pressure range to determine the effective capillary pressure and permeability. The solution in terms of pressure is preferred over mass because of a higher resolution provided by the pressure sensor. In the fitting with experimental data up to different pressure ranges (0.1,

0.2, 0.3, 0.4, 0.5, 0.6, 0.7, 0.8, 0.9$p_{\mathrm{A}}^{\max}$), we noticed there are different stages in the imbibition. We use the deviation of the fittings and a threshold value 0.01 to determine the imbibition regions. Based on the results obtained using the modified Washburn solution and the general solution, the imbibition is divided into three different regions, the early/Washburn imbibition, the intermediate imbibition and the late imbibition. The early imbibition is when the pressure differential is small and the experimental data agrees well with the modified Washburn solution. During this region, the capillary pressure and the permeability are combined as one parameter and cannot be determined individually. Within the intermediate region, the Washburn solution deviates from both the experimental data and the general solution. The capillary pressure and the permeability can be obtained by fitting with the general solution as two independent parameters. The intermediate stage is where we obtain the effective pressure and permeability values. In the late imbibition stage, the pressure differential is large and the liquid only fills in the very small pores. Therefore, the dynamics no longer follow the general solution. We did not include data from this region in the fittings. For 10μm glass beads, the intermediate region is 0.4$< p/p_{\mathrm{A}}^{\max} <$0.8. For 45$\mu m$ glass beads, this region is 0.2$< p/p_{\mathrm{A}}^{\max} <$0.4. The difference in the intermediate region is due to a greater heterogeneity in 45μm glass beads. Finally, we compare the ratio of the effective radii and permeability obtained within the intermediate region. The ratio of the effective radii is 10 times, this is twice of the particle ratio. However, the 10 times ratio is not so surprising considering the large heterogeneity in 45μm glass beads. Since the effective capillary pressure obtained within the intermediate is only half of the advancing pressure. The ratio of the effective permeability between 10 and 45 micron spheres is about 20 times and is consistent with the Kozeny-Carman equation.

In chapter six, the results from experiments with glass beads and DI water are presented. We followed the static and dynamic characterization method used in chapter 5. By assuming zero contact angle for PDMS, the contact angle with DI water is obtained from the ratio of the capillary pressures. For $10\mu m$ glass beads, the contact angle is zero, indicating that the glass beads are hydrophilic. For $45\mu m$ glass beads, the contact angle is greater than zero and they are less hydrophilic. Different manufacturing procedures from two different supplies is believed to cause the difference in their contact angle. Different imbibition regions in DI water experiments are also obtained following the same approach. It is $0.6< p/p_{\mathrm{A}}^{\max} <0.8$ in $10\mu m$ glass beads and $0.4< p/p_{\mathrm{A}}^{\max} <0.6$ in $45\mu m$ glass beads. Similar to the case with PDMS, the intermediate region occurs at an earlier stage in $45\mu m$ glass beads because of a greater heterogeneity. Finally we considered the effective capillary pressure and permeability. The contact angle obtained from the effective capillary pressure is different from that obtained in the static measurement, especially for $45\mu m$ glass beads, where there was a great variance. The difference is believed to be the different filling dynamics between PDMS and DI water. For both $10\mu m$ and $45\mu m$ glass beads, the effective permeability in DI water is smaller than that in PDMS, but this difference is more significant in $45\mu m$ glass beads. Air trapping when DI water penetrates through is believed to be a reason for the low permeability in $10\mu m$ glass beads, but needs further validation. For the extremely low DI water permeability in $45\mu m$ glass beads, the reason is a combination of the large heterogeneity and less hydrophilicity. The variance in the effective capillary pressure and the corresponding contact angle is also very large, as a result of the large variability in the system with $45\mu m$ glass beads. This system is believed

to be a limit of this characterization method because of its large heterogeneity and variability.

In chapter seven we applied the characterization method on more complicated systems. We studied three pharmaceutical powders, lactose, MCC and alumina. In lactose we used two porosity values, 0.44 and 0.37. In the large porosity case, the porous media is highly heterogeneous and the spontaneous bubbling process happens while liquid is still advancing. Therefore, the advancing pressure cannot be measured. The effective capillary pressure is obtained by fitting with the analytical solutions and the value is higher than the maximum pressure measured in experiments. The maximum pressure reached in experiments is a bubbling pressure corresponds to the large pores. The effective pressure represents the average value of both large and small pores, which is why it is higher than the bubbling pressure. For the small porosity case, we also observed spontaneous bubbling phenomena but it is not as dramatic and the large porosity case. In the experiments with DI water, different column heights are used in order to obtain an appropriate height, such that the advancing pressure can be reached while a crack will not form in the long time. Although we did not obtain the appropriate column height yet, we noticed that the time it takes to reach a certain completion factor is reduced by using a shorter column. This is consistent with the conclusion in chapter four. The experiments with MCC also experienced spontaneous bubbling problems, at a more dramatic level such that the readings from the scale are disturbed constantly. For this reason, we did not fit the experimental data with the solutions. Finally, we studied the alumina powders. They behave very similar to the $10\mu m$ glass beads. The contact angle with DI water is zero. The ratio of the effective permeability between PDMS and DI water is also similar to $10\mu m$

glass beads. The results with pharmaceutical powders suggest that our characterization method is applicable to practical powders. Estimating the effective capillary pressure through the fittings provides useful information in some cases when the spontaneous bubbling disturbs the measurements. Extra attention is needed when dealing with practical powders since they are usually more complicated due to their irregular shapes and greater heterogeneity.

As we pointed out in chapter 6, the reason why the permeability in DI water is lower than PDMS is yet not fully understood. It would be helpful to investigate possible causes such as air trapping that may contribute to the low permeability in DI water. There were large variability in the experiments with the $45\mu m$ glass beads and the surface contamination is believed to be a possible reason. More experiments can be done between $45\mu m$ glass beads and DI water after thoroughly cleaning the glass beads. Moreover, the experiments of lactose and its saturated solution need to be completed after finding the right column length that avoids the formation of cracks. Different column lengths can also be used on experiments with other pharmaceutical powders to finish the characterization within a targeted time.

Appendix: Permeability measurement for fully saturated porous media

The permeability of a fully saturated porous media is measured using $10\mu m$ glass beads with PDMS and DI water. The column containing the porous media is first opened to ambient pressure and the liquid spontaneously penetrats into the porous media by capillary rise. After the porous media is saturated, a small amount of liquid is added to the top and the column is then closed by the o-ring seal plug. A syringe is connected to the system and is used to increase the pressure differential inside the column by injecting air. Liquid is forced to leave the porous media. The amount of liquid that leaves of the porous media is measured by the scale. The pressure differential is monitored by the pressure sensor. PDMS and DI water are used in the experiments. The measurement of the pressure differential and liquid weight is presented in figure A.

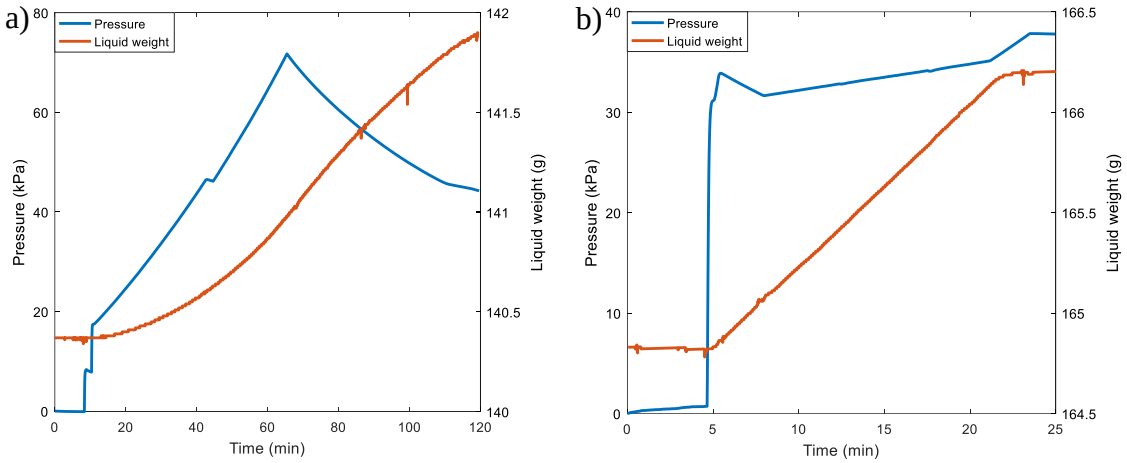

Figure A The pressure differential and liquid weight change during the permeability measurement of saturated porous media with $10\mu m$ glass beads. The liquid used is a) PDMS, b) DI water

According to Darcy's law, when the liquid passing through the porous media, the pressure drop Δp over a certain distance h is proportional to the flow discharge:

$$\varphi \frac{dh}{dt} = \frac{\kappa}{\eta} \frac{\Delta p}{h} \tag{A1}$$

Multiply by the density ρ of the fluid and the cross section area S of the cylindrical column on both sides of equation A1:

$$\rho S \varphi \frac{dh}{dt} = \rho S \frac{\kappa}{\eta} \frac{\Delta p}{h} \tag{A2}$$

Integrate both sides of equation A2 over time:

$$m_1 - m_0 = \frac{\rho S \kappa}{\eta h} \int_{t0}^{t1} p dt \tag{A3}$$

The LHS of equation A3 is the amount of liquid passing through the porous media from t_0 to t_1. The integrate of pressure over time can be obtained in figure A. η is the viscosity of the fluid and h is the height or length of the porous media. In our measurements, the permeability when PDMS going through was 0.033darcy and for DI water it was 0.032darcy. There is no significant difference between the measurements for the two fluids. Since the porous media is fully saturated, the permeability is not dependent on the fluid. However, in the imbibition process, the porous media may not be fully saturated for some fluids. Therefore, the effective permeability is dependent on the fluid passing through. The effective permeability obtained in fittings are smaller than the permeability measured for a fully saturated porous media.

Bibliography

[1] M. Li, G. Callegari, and G. Drazer, “Capillary rise in a closed column: Application to the characterization of powders,” *Colloids and Surfaces A: Physicochemical and Engineering Aspects*, vol. 602, p. 124822, Oct. 2020, doi: 10.1016/j.colsurfa.2020.124822.

[2] J. I. Wells and C. V. Walker, “The influence of granulating fluids upon granule and tablet properties: the role of secondary binding,” *International Journal of Pharmaceutics*, vol. 15, no. 1, pp. 97–111, May 1983, doi: https://doi.org/10.1016/0378-5173(83)90070-4.

[3] A. Roman-Gutierrez, J. Sabathier, S. Guilbert, L. Galet, and B. Cuq, “Characterization of the surface hydration properties of wheat flours and flour components by the measurement of contact angle,” *Powder Technology*, vol. 129, no. 1, pp. 37–45, Jan. 2003, doi: 10.1016/S0032-5910(02)00154-7.

[4] B. Cuq, E. Rondet, and J. Abecassis, “Food powders engineering, between knowhow and science: Constraints, stakes and opportunities,” *Powder Technology*, vol. 208, no. 2, pp. 244–251, Mar. 2011, doi: 10.1016/j.powtec.2010.08.012.

[5] J. Letey, J. Osborn, and R. E. Pelishek, “The influence of the water-solid contact angle on water movement in soil,” *International Association of Scientific Hydrology. Bulletin*, vol. 7, no. 3, pp. 75–81, Sep. 1962, doi: 10.1080/02626666209493272.

[6] D. A. L. Leelamanie, J. Karube, and A. Yoshida, “Characterizing water repellency indices: Contact angle and water drop penetration time of hydrophobized sand,” *Soil Science and Plant Nutrition*, vol. 54, no. 2, pp. 179–187, Apr. 2008, doi: 10.1111/j.1747-0765.2007.00232.x.

[7] Z. Liu, X. (Bill) Yu, and L. Wan, “Influence of Contact Angle on Soil–Water Characteristic Curve with Modified Capillary Rise Method,” *Transportation Research Record*, vol. 2349, no. 1, pp. 32–40, Jan. 2013, doi: 10.3141/2349-05.

[8] T. T. Chau, “A review of techniques for measurement of contact angles and their applicability on mineral surfaces,” *Minerals Engineering*, vol. 22, no. 3, pp. 213–219, Feb. 2009, doi: 10.1016/j.mineng.2008.07.009.

[9] K. Tang, S. Xuan, W. Lv, X. Lv, and C. Bai, “Contact Angle of Iron Ore Particles with Water: Measurements and Influencing Factors,” in *Characterization of Minerals, Metals, and Materials 2017*, Cham, 2017, pp. 321–328.

[10] Y. Chen, G. Xu, J. Huang, J. Eksteen, X. Liu, and Z. Zhao, “Characterization of coal particles wettability in surfactant solution by using four laboratory static tests,” *Colloids and Surfaces A: Physicochemical and Engineering Aspects*, vol. 567, pp. 304–312, Apr. 2019, doi: 10.1016/j.colsurfa.2019.01.068.

[11] C. F. Lerk, A. J. M. Schoonen, and J. T. Fell, “Contact angles and wetting of pharmaceutical powders,” *Journal of Pharmaceutical Sciences*, vol. 65, no. 6, pp. 843–847, Jun. 1976, doi: 10.1002/jps.2600650611.

[12] S. Oka *et al.*, “The effects of improper mixing and preferential wetting of active and excipient ingredients on content uniformity in high shear wet granulation,” *Powder Technology*, vol. 278, pp. 266–277, Jul. 2015, doi: 10.1016/j.powtec.2015.03.018.

[13] K. Pingali, R. Mendez, D. Lewis, B. Michniak-Kohn, A. Cuitiño, and F. Muzzio, “Evaluation of strain-induced hydrophobicity of pharmaceutical blends and its effect on drug release rate under multiple compression conditions,” *Drug Development and Industrial Pharmacy*, vol. 37, no. 4, pp. 428–435, Apr. 2011, doi: 10.3109/03639045.2010.521160.

[14] A. W. Adamson, *Physical Chemistry of Surfaces*. New York: Wiley, 1967.

[15] R. Defay and I. Prigogine, *Surface tension and adsorption*. New York: Wiley, 1966.

[16] J. Israelachvili, “Intermolecular and Surface Forces,” in *Intermolecular and Surface Forces*, Elsevier, 2011, p. iii.

[17] J. N. Israelachvili, "Adhesion and Wetting Phenomena," in *Intermolecular and Surface Forces*, Elsevier, 2011, pp. 415–467.
[18] D. E. Packham, "Work of adhesion: contact angles and contact mechanics," *International Journal of Adhesion and Adhesives*, vol. 16, no. 2, pp. 121–128, May 1996, doi: 10.1016/0143-7496(95)00034-8.
[19] N. K. Adam, "The Chemical Structure of Solid Surfaces as Deduced from Contact Angles," in *Contact Angle, Wettability, and Adhesion*, vol. 43, F. M. Fowkes, Ed. WASHINGTON, D.C.: AMERICAN CHEMICAL SOCIETY, 1964, pp. 52–56.
[20] T. Young, "An Essay on the Cohesion of Fluids.," *Proceedings of the Royal Society of London*, vol. 1, no. 0, pp. 171–172, Jan. 1800, doi: 10.1098/rspl.1800.0095.
[21] *The scientific papers.* New York: Dover Publications.
[22] L. Boruvka and A. W. Neumann, "Generalization of the classical theory of capillarity," *The Journal of Chemical Physics*, vol. 66, no. 12, pp. 5464–5476, Jun. 1977, doi: 10.1063/1.433866.
[23] P.-G. de Gennes, F. Brochard-Wyart, and D. Quéré, *Capillarity and Wetting Phenomena*. New York, NY: Springer New York, 2004.
[24] de G. P. G., "Wetting: statics and dynamics," *Rev. Mod. Phys.*, vol. 57, no. 3, pp. 827–863, 1985July, doi: 10.1103/RevModPhys.57.827.
[25] Jacob Bear, *Dynamics of fluids in porous media*. New York: Dover Publications, 1988.
[26] F. E. Bartell and J. W. Shepard, "The Effect of Surface Roughness on Apparent Contact Angles and on Contact Angle Hysteresis. I. The system Paraffin–Water–Air," *J. Phys. Chem.*, vol. 57, no. 2, pp. 211–215, Feb. 1953, doi: 10.1021/j150503a017.
[27] R. E. Johnson and R. H. Dettre, "Contact Angle Hysteresis: I. Study of an Idealized Rough Surface," in *Contact Angle, Wettability, and Adhesion*, vol. 43, F. M. Fowkes, Ed. WASHINGTON, D.C.: AMERICAN CHEMICAL SOCIETY, 1964, pp. 112–135.
[28] C. Huh and S. G. Mason, "Effects of surface roughness on wetting (theoretical)," *Journal of Colloid and Interface Science*, vol. 60, no. 1, pp. 11–38, Jun. 1977, doi: 10.1016/0021-9797(77)90251-X.
[29] J. F. Oliver and S. G. Mason, "Liquid spreading on rough metal surfaces," *Journal of Materials Science*, vol. 15, no. 2, pp. 431–437, 1980, doi: 10.1007/PL00020077.
[30] J. P. Oliver, C. Huh, and S. G. Mason, "An experimental study of some effects of solid surface roughness on wetting," *Colloids and Surfaces*, vol. 1, no. 1, pp. 79–104, 1980, doi: 10.1016/0166-6622(80)80039-4.
[31] R. H. Dettre and R. E. Johnson, "Contact Angle Hysteresis. IV. Contact Angle Measurements on Heterogeneous Surfaces [1]," *J. Phys. Chem.*, vol. 69, no. 5, pp. 1507–1515, May 1965, doi: 10.1021/j100889a012.
[32] L. W. Schwartz and S. Garoff, "Contact Angle Hysteresis on Heterogeneous Surfaces," *Langmuir*, vol. 1, no. 2, pp. 219–230, 1985, doi: 10.1021/la00062a007.
[33] Y. Pomeau and J. Vannimenus, "Contact angle on heterogeneous surfaces: Weak heterogeneities," *Journal of Colloid and Interface Science*, vol. 104, no. 2, pp. 477–488, Apr. 1985, doi: 10.1016/0021-9797(85)90055-4.
[34] A. W. Neumann and R. J. Good, "Thermodynamics of contact angles. I. Heterogeneous solid surfaces," *Journal of Colloid And Interface Science*, vol. 38, no. 2, pp. 341–358, 1972, doi: 10.1016/0021-9797(72)90251-2.
[35] A. Marmur, "Contact Angle Hysteresis on Heterogeneous Smooth Surfaces," *Journal of Colloid And Interface Science*, vol. 168, no. 1, pp. 40–46, 1994, doi: 10.1006/jcis.1994.1391.
[36] E. L. Decker and S. Garoff, "Using vibrational noise to probe energy barriers producing contact angle hysteresis," *Langmuir*, vol. 12, no. 8, pp. 2100–2110, 1996.
[37] E. L. Decker and S. Garoff, "Contact line structure and dynamics on surfaces with contact angle hysteresis," *Langmuir*, vol. 13, no. 23, pp. 6321–6328, 1997.

[38] C. N. C. Lam *et al.*, "Dynamic Cycling Contact Angle Measurements: Study of Advancing and Receding Contact Angles," *Journal of Colloid and Interface Science*, vol. 243, no. 1, pp. 208–218, Nov. 2001, doi: 10.1006/jcis.2001.7840.

[39] C. N. C. Lam, N. Kim, D. Hui, D. Y. Kwok, M. L. Hair, and A. W. Neumann, "The effect of liquid properties to contact angle hysteresis," *Colloids and Surfaces A: Physicochemical and Engineering Aspects*, vol. 189, no. 1, pp. 265–278, Sep. 2001, doi: 10.1016/S0927-7757(01)00589-1.

[40] C. N. C. Lam, R. Wu, D. Li, M. L. Hair, and A. W. Neumann, "Study of the advancing and receding contact angles: liquid sorption as a cause of contact angle hysteresis," *Advances in Colloid and Interface Science*, vol. 96, no. 1, pp. 169–191, Feb. 2002, doi: 10.1016/S0001-8686(01)00080-X.

[41] L. R. White, "The contact angle on an elastic substrate. 1. The role of disjoining pressure in the surface mechanics," *Journal of Colloid and Interface Science*, vol. 258, no. 1, pp. 82–96, Feb. 2003, doi: 10.1016/S0021-9797(02)00090-5.

[42] V. Starov, "Static contact angle hysteresis on smooth, homogeneous solid substrates," *Colloid and Polymer Science*, vol. 291, no. 2, pp. 261–270, Feb. 2013, doi: 10.1007/s00396-012-2840-6.

[43] O. Arjmandi-Tash, N. M. Kovalchuk, A. Trybala, I. V. Kuchin, and V. Starov, "Kinetics of Wetting and Spreading of Droplets over Various Substrates," *Langmuir*, vol. 33, no. 18, pp. 4367–4385, May 2017, doi: 10.1021/acs.langmuir.6b04094.

[44] R. L. Hoffman, "A Study of the Advancing Interface," *Journal of Colloid and Interface Science*, vol. 50, no. 2, p. 14, 1975.

[45] C. Neto, D. R. Evans, E. Bonaccurso, H.-J. Butt, and V. S. J. Craig, "Boundary slip in Newtonian liquids: a review of experimental studies," *Rep. Prog. Phys.*, vol. 68, no. 12, pp. 2859–2897, Dec. 2005, doi: 10.1088/0034-4885/68/12/R05.

[46] T. D. Blake and J. M. Haynes, "Kinetics of liquid liquid displacement," *Journal of Colloid and Interface Science*, vol. 30, no. 3, pp. 421–423, Jul. 1969, doi: 10.1016/0021-9797(69)90411-1.

[47] L. H. Tanner, "The spreading of silicone oil drops on horizontal surfaces," *Journal of Physics D: Applied Physics*, vol. 12, no. 9, pp. 1473–1484, Sep. 1979, doi: 10.1088/0022-3727/12/9/009.

[48] O. V. Voinov, "Hydrodynamics of wetting," *Fluid Dynamics*, vol. 11, no. 5, pp. 714–721, Sep. 1976, doi: 10.1007/BF01012963.

[49] R. G. Cox, "The dynamics of the spreading of liquids on a solid surface. Part 1. Viscous flow," *Journal of Fluid Mechanics*, vol. 168, pp. 169–194, 1986, doi: 10.1017/S0022112086000332.

[50] E. B. Dussan, "On the Spreading of Liquids on Solid Surfaces: Static and Dynamic Contact Lines," *Annu. Rev. Fluid Mech.*, vol. 11, no. 1, pp. 371–400, Jan. 1979, doi: 10.1146/annurev.fl.11.010179.002103.

[51] Q. Chen, E. Ramé, and S. Garoff, "The breakdown of asymptotic hydrodynamic models of liquid spreading at increasing capillary number," *Physics of Fluids*, vol. 7, no. 11, pp. 2631–2639, Nov. 1995, doi: 10.1063/1.868711.

[52] R. Lenormand, "Liquids in porous media," *J. Phys.: Condens. Matter*, vol. 2, no. S, pp. SA79–SA88, Dec. 1990, doi: 10.1088/0953-8984/2/S/008.

[53] R. E. Johnson, R. H. Dettre, and D. A. Brandreth, "Dynamic contact angles and contact angle hysteresis," *Journal of Colloid and Interface Science*, vol. 62, no. 2, pp. 205–212, Nov. 1977, doi: 10.1016/0021-9797(77)90114-X.

[54] K. Katoh, T. Wakimoto, Y. Yamamoto, and T. Ito, "Dynamic wetting behavior of a triple-phase contact line in several experimental systems," *Experimental Thermal and Fluid Science*, vol. 60, pp. 354–360, Jan. 2015, doi: 10.1016/j.expthermflusci.2014.05.006.

[55] F. A. L. Dullien and V. K. Batra, "Determination of the Structure of Porous Media," *Ind. Eng. Chem.*, vol. 62, no. 10, pp. 25–53, Oct. 1970, doi: 10.1021/ie50730a004.

[56] T. H. Muster and C. A. Prestidge, "Water Adsorption Kinetics and Contact Angles of Pharmaceutical Powders," *Journal of Pharmaceutical Sciences*, vol. 94, no. 4, pp. 861–872, Apr. 2005, doi: 10.1002/jps.20296.

[57] A. Chawla, G. Buckton, K. M. G. Taylor, J. M. Newton, and M. C. R. Johnson, "Wilhelmy plate contact angle data on powder compacts: considerations of plate perimeter," *European Journal of Pharmaceutical Sciences*, vol. 2, no. 3, pp. 253–258, Oct. 1994, doi: 10.1016/0928-0987(94)90030-2.

[58] G. Buckton and J. M. Newton, "Assessment of the wettability of powders by use of compressed powder discs," *Powder Technology*, vol. 46, no. 2, pp. 201–208, Apr. 1986, doi: 10.1016/0032-5910(86)80027-4.

[59] J. Jurin, "An account of some experiments shown before the Royal Society; with an enquiry into the cause of the ascent and suspension of water in capillary tubes.," *Philosophical Transactions of the Royal Society of London*, vol. 30, no. 355, pp. 739–747, Jan. 1719, doi: https://doi.org/10.1098/rstl.1717.0026.

[60] E. W. Washburn, "The Dynamics of Capillary Flow," *Physical Review*, vol. 17, no. 3, pp. 273–283, Mar. 1921, doi: 10.1103/PhysRev.17.273.

[61] P. Joos, P. Van Remoortere, and M. Bracke, "The kinetics of wetting in a capillary," *Journal of Colloid and Interface Science*, vol. 136, no. 1, pp. 189–197, Apr. 1990, doi: 10.1016/0021-9797(90)90089-7.

[62] N. Ichikawa and Y. Satoda, "Interface Dynamics of Capillary Flow in a Tube under Negligible Gravity Condition," *Journal of Colloid and Interface Science*, vol. 162, no. 2, pp. 350–355, Feb. 1994, doi: 10.1006/jcis.1994.1049.

[63] A. Hamraoui, K. Thuresson, T. Nylander, and V. Yaminsky, "Can a Dynamic Contact Angle Be Understood in Terms of a Friction Coefficient?," *Journal of Colloid and Interface Science*, vol. 226, no. 2, pp. 199–204, Jun. 2000, doi: 10.1006/jcis.2000.6830.

[64] A. Siebold, M. Nardin, J. Schultz, A. Walliser, and M. Oppliger, "Effect of dynamic contact angle on capillary rise phenomena," *Colloids and Surfaces A: Physicochemical and Engineering Aspects*, vol. 161, no. 1, pp. 81–87, Jan. 2000, doi: 10.1016/S0927-7757(99)00327-1.

[65] B. V. Zhmud, F. Tiberg, and K. Hallstensson, "Dynamics of Capillary Rise," *Journal of Colloid and Interface Science*, vol. 228, no. 2, pp. 263–269, Aug. 2000, doi: 10.1006/jcis.2000.6951.

[66] H. J. Barraza and S. Kunapuli, "Advancing Contact Angles of Newtonian Fluids During 'High' Velocity, Transient, Capillary-Driven Flow in a Parallel Plate Geometry," *J. Phys. Chem. B*, vol. 106, no. 19, pp. 4979–4987, May 2002, doi: 10.1021/jp013849q.

[67] M. Dreyer, A. Delgado, and H. J. Rath, "Fluid motion in capillary vanes under reduced gravity," *Microgravity Science and Technology*, vol. 5, no. 4, pp. 203–210, Feb. 1993.

[68] M. Dreyer, A. Delgado, and H.-J. Path, "Capillary Rise of Liquid between Parallel Plates under Microgravity," *Journal of Colloid and Interface Science*, vol. 163, no. 1, pp. 158–168, Mar. 1994, doi: 10.1006/jcis.1994.1092.

[69] F. E. Bartell and H. J. Osterhof, "Determination of the Wettability of a Solid by a Liquid," *Ind. Eng. Chem.*, vol. 19, no. 11, pp. 1277–1280, Nov. 1927, doi: 10.1021/ie50215a026.

[70] F. E. Bartell and E. J. Merrill, "Determination of Adhesion Tension of Liquids against Solids. A Microscopic Method for the Measurement of Interfacial Contact Angles," *J. Phys. Chem.*, vol. 36, no. 4, pp. 1178–1190, Apr. 1932, doi: 10.1021/j150334a010.

[71] D. Dunstan and L. R. White, "A capillary pressure method for measurement of contact angles in powders and porous media," *Journal of Colloid and Interface Science*, vol. 111, no. 1, pp. 60–64, May 1986, doi: 10.1016/0021-9797(86)90007-X.

[72] N. Stevens, J. Ralston, and R. Sedev, "The uniform capillary model for packed beds and particle wettability," *Journal of Colloid and Interface Science*, vol. 337, no. 1, pp. 162–169, Sep. 2009, doi: 10.1016/j.jcis.2009.04.086.

[73] A. Depalo and A. C. Santomaso, “Wetting dynamics and contact angles of powders studied through capillary rise experiments,” *Colloids and Surfaces A: Physicochemical and Engineering Aspects*, vol. 436, pp. 371–379, Sep. 2013, doi: 10.1016/j.colsurfa.2013.06.040.
[74] S. M. Iveson, S. Holt, and S. Biggs, “Contact angle measurements of iron ore powders,” *Colloids and Surfaces A: Physicochemical and Engineering Aspects*, vol. 166, no. 1–3, pp. 203–214, Jun. 2000, doi: 10.1016/S0927-7757(99)00455-0.
[75] H. Darcy, *Les Fontaines publiques de la ville de Dijon*. Paris: DALMONT, 1856.
[76] J. Kozeny, “Ueber kapillare Leitung des Wassers im Boden,” *Versickerung und Anwendung auf die Bewasserung*, vol. 136, no. 2a, pp. 271–306, 1927.
[77] P. C. CARMAN, “Fluid Flow through Granular Beds,” *Trans. Inst. Chem. Eng.*, vol. 15, pp. 150–166, 1937.
[78] P. C. Carman, *Flow of gases through porous media*. London: Butterworths scientific publications, 1956.
[79] N. Fries and M. Dreyer, “Dimensionless scaling methods for capillary rise,” *Journal of Colloid and Interface Science*, vol. 338, no. 2, pp. 514–518, Oct. 2009, doi: 10.1016/j.jcis.2009.06.036.
[80] C. H. Bosanquet, “LV. On the flow of liquids into capillary tubes,” *The London, Edinburgh, and Dublin Philosophical Magazine and Journal of Science*, vol. 45, no. 267, pp. 525–531, Mar. 1923, doi: 10.1080/14786442308634144.
[81] G. Lu, X.-D. Wang, and Y.-Y. Duan, “Study on initial stage of capillary rise dynamics,” *Colloids and Surfaces A: Physicochemical and Engineering Aspects*, vol. 433, pp. 95–103, Sep. 2013, doi: 10.1016/j.colsurfa.2013.05.004.
[82] W. Heber Green and G. A. Ampt, “Studies on Soil Phyics.,” *J. Agric. Sci.*, vol. 4, no. 1, pp. 1–24, May 1911, doi: 10.1017/S0021859600001441.
[83] M. Hilpert, “Explicit analytical solutions for liquid infiltration into capillary tubes: Dynamic and constant contact angle,” *Journal of Colloid and Interface Science*, vol. 344, no. 1, pp. 198–208, Apr. 2010, doi: 10.1016/j.jcis.2009.12.024.
[84] S.-Y. Hsu, V. Huang, S. Woo Park, and M. Hilpert, “Water infiltration into prewetted porous media: Dynamic capillary pressure and Green-Ampt modeling,” *Advances in Water Resources*, vol. 106, pp. 60–67, Aug. 2017, doi: 10.1016/j.advwatres.2017.02.017.
[85] R. H. Perry and D. W. Green, *Perry’s chemical engineers’ handbook.* New York: McGraw-Hill, 2008.
[86] B. Wei, Q. Chang, and C. Yan, “Wettability determined by capillary rise with pressure increase and hydrostatic effects,” *Journal of Colloid and Interface Science*, vol. 376, no. 1, pp. 307–311, Jun. 2012, doi: 10.1016/j.jcis.2012.02.072.
[87] D. A. Barry, J.-Y. Parlange, G. C. Sander, and M. Sivaplan, “A class of exact solutions for Richards’ equation,” *Journal of Hydrology*, vol. 142, no. 1–4, pp. 29–46, Feb. 1993, doi: 10.1016/0022-1694(93)90003-R.
[88] D. A. Barry, L. Wissmeier, J.-Y. Parlange, G. C. Sander, and D. A. Lockington, “Comment on ‘An analytic solution of capillary rise restrained by gravity’ by N. Fries and M. Dreyer,” *Journal of Colloid and Interface Science*, vol. 338, no. 1, pp. 293–295, Oct. 2009, doi: 10.1016/j.jcis.2009.06.015.
[89] N. Fries and M. Dreyer, “An analytic solution of capillary rise restrained by gravity,” *Journal of Colloid and Interface Science*, vol. 320, no. 1, pp. 259–263, Apr. 2008, doi: 10.1016/j.jcis.2008.01.009.
[90] R. M. Corless, G. H. Gonnet, D. E. G. Hare, D. J. Jeffrey, and D. E. Knuth, “On the LambertW function,” *Adv Comput Math*, vol. 5, no. 1, pp. 329–359, Dec. 1996, doi: 10.1007/BF02124750.
[91] V. K. S. Shante and S. Kirkpatrick, “An introduction to percolation theory,” *Advances in Physics*, vol. 20, no. 85, pp. 325–357, May 1971, doi: 10.1080/00018737100101261.
[92] S. Kirkpatrick, “The nature of percolation ‘channels,’” *Solid State Communications*, vol. 12, no. 12, pp. 1279–1283, Jun. 1973, doi: 10.1016/0038-1098(73)90865-X.

[93] D. Quéré, “Inertial capillarity,” *Europhys. Lett.*, vol. 39, no. 5, pp. 533–538, Sep. 1997, doi: 10.1209/epl/i1997-00389-2.
[94] J. Kiesvaara and J. Yliruusi, “The effect of compression pressure and compression time on the surface free energy of tablets,” *Acta Pharmaceutica Nordica*, vol. 3, no. 3, pp. 171–177, 1991.
[95] N. K. Patel, A. H. Upadhyay, J. S. Bergum, and G. E. Reier, “An evaluation of microcrystalline cellulose and lactose excipients using an instrumented single station tablet press,” *International Journal of Pharmaceutics*, vol. 110, no. 3, pp. 203–210, Sep. 1994, doi: 10.1016/0378-5173(94)90242-9.
[96] G. Thoorens, F. Krier, B. Leclercq, B. Carlin, and B. Evrard, “Microcrystalline cellulose, a direct compression binder in a quality by design environment—A review,” *International Journal of Pharmaceutics*, vol. 473, no. 1–2, pp. 64–72, Oct. 2014, doi: 10.1016/j.ijpharm.2014.06.055.
[97] G. K. Bolhuis and N. Anthony Armstrong, “Excipients for Direct Compaction—an Update,” *Pharmaceutical Development and Technology*, vol. 11, no. 1, pp. 111–124, Jan. 2006, doi: 10.1080/10837450500464255.
[98] E. Doelker, “Comparative compaction properties of various Microcrystalline Cellulose types and Generic Products,” *Drug Development and Industrial Pharmacy*, vol. 19, no. 17–18, pp. 2399–2471, Jan. 1993, doi: 10.3109/03639049309047196.
[99] F. A. Al-Sanabani, A. A. Madfa, and N. H. Al-Qudaimi, “Alumina ceramic for dental applications: A review article,” p. 10.
[100] P. Shen, L. Zhang, and Y. Wang, “Influence of Oxidation on Contact Angle between Liquid Aluminum and Al2O3,” in *Light Metals 2016*, E. Williams, Ed. Cham: Springer International Publishing, 2016, pp. 827–832.
[101] A. J. Klinter, G. Mendoza-Suarez, and R. A. L. Drew, “Wetting of pure aluminum and selected alloys on polycrystalline alumina and sapphire,” *Materials Science and Engineering: A*, vol. 495, no. 1, pp. 147–152, Nov. 2008, doi: 10.1016/j.msea.2007.10.113.
[102] H. John and H. Hausner, “Influence of oxygen partial pressure on the wetting behaviour in the system Al/Al2O3,” *Journal of Materials Science Letters*, vol. 5, no. 5, pp. 549–551, May 1986, doi: 10.1007/BF01728687.
[103] Q. Zhang, T. Çağın, A. van Duin, W. A. Goddard, Y. Qi, and L. G. Hector, “Adhesion and nonwetting-wetting transition in the Al/α−Al2O3 interface,” *Phys. Rev. B*, vol. 69, no. 4, p. 045423, Jan. 2004, doi: 10.1103/PhysRevB.69.045423.